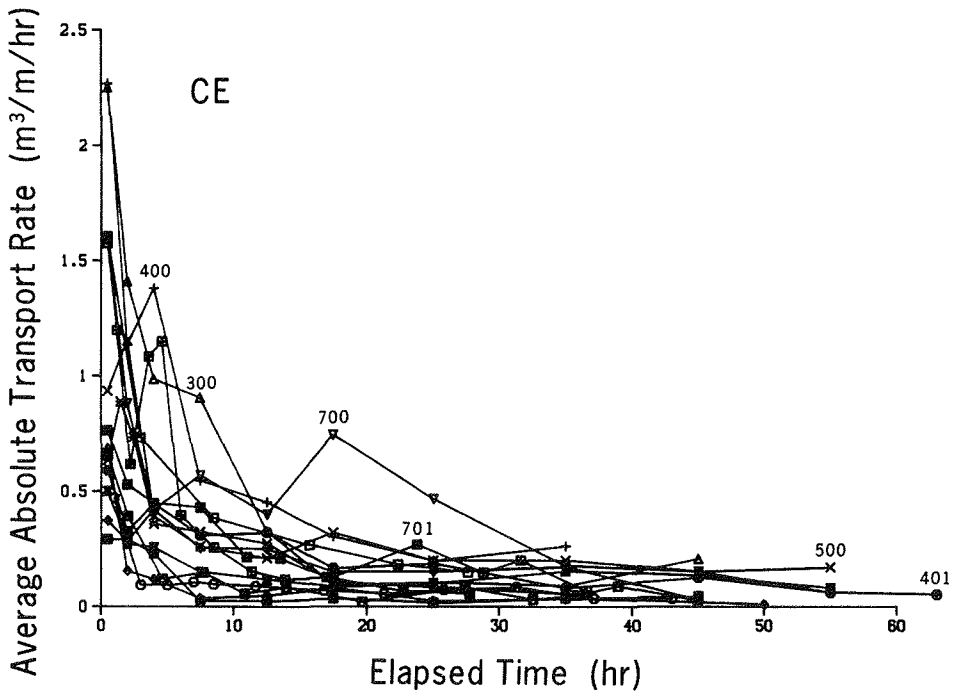

a. CE data, 16 cases

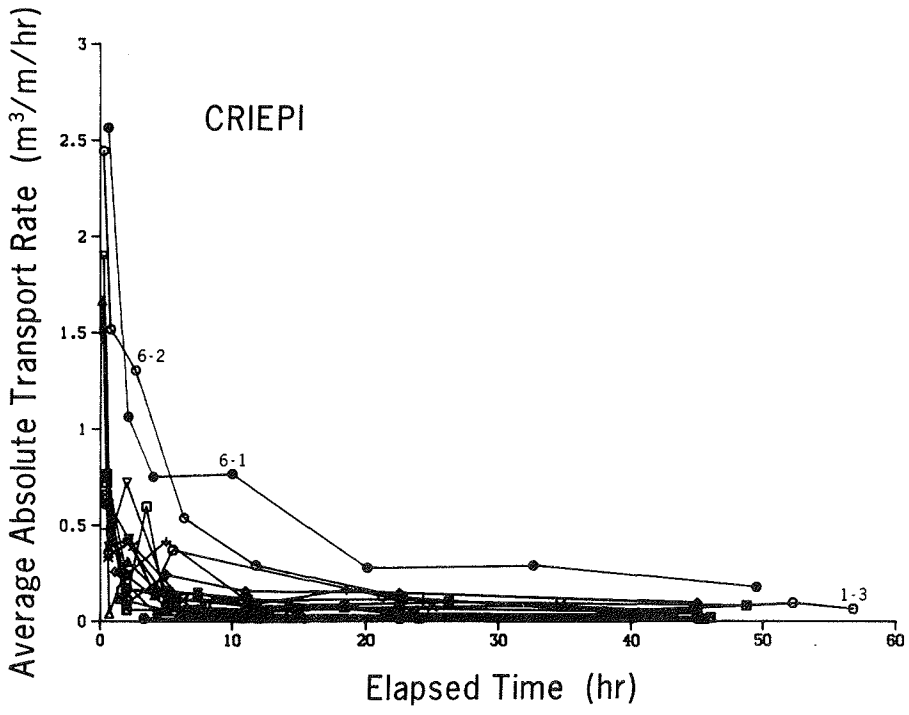

b. CRIEPI data, 17 cases

Figure 38. Decay of net cross-shore sand transport rate

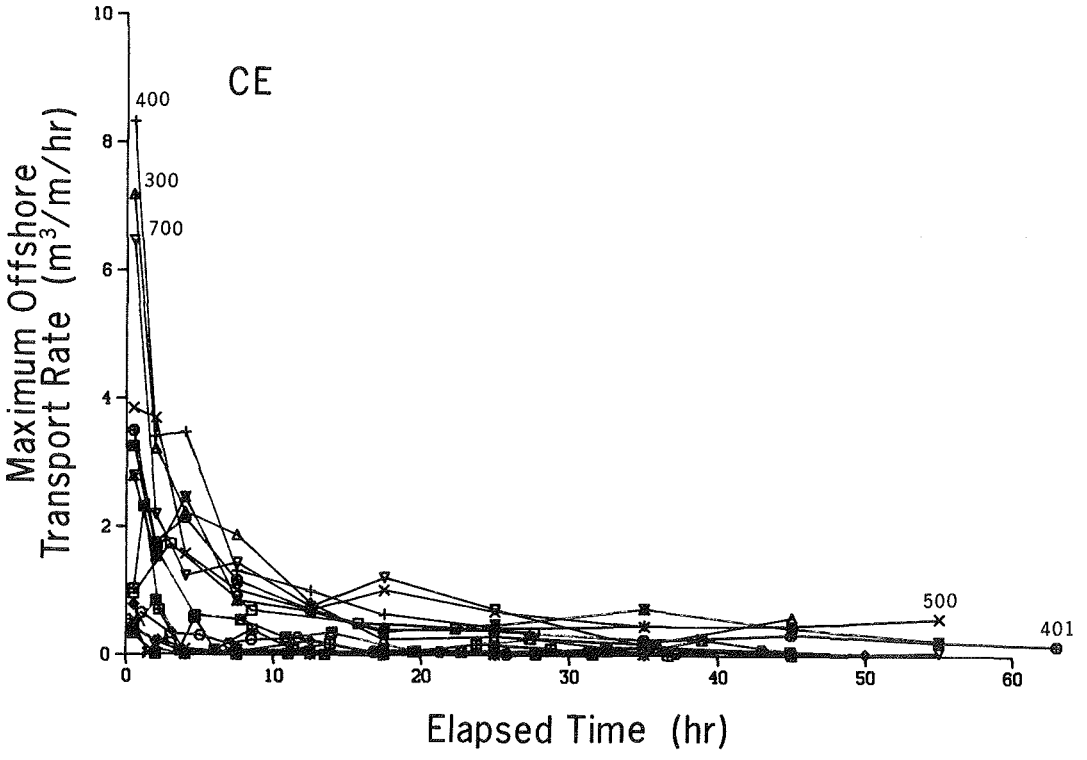

Figure 39. Evolution of peak offshore net sand transport rate for 16 CE cases

peak offshore transport rate was usually small or sometimes even zero through most of the run (see Figure 35).

326. Various trial empirical expressions to describe time decay of the peak offshore transport rate were least-squares fitted for cases having strong offshore transport in the combined CE and CRIEPI data set (12 cases). The best general agreement was obtained with an inverse dependence of the maximum transport rate on time according to

$$q_m = \frac{q_{mo}}{1 + \alpha t} \tag{20}$$

where

q_m = peak transport rate

q_{mo} = peak transport rate at time $t = 0$

α = rate coefficient of decay of peak transport rate

The rate coefficient α controls the time rate of decay of the peak offshore transport rate.

327. Figure 40 displays the peak offshore transport rates from Case 300 and the least-squares fitted line according to Equation 20 (solid line). The agreement is very good and the regression equation explained over 90 percent of the total variation.

328. The average value of α was 0.91 hr^{-1}, and the standard deviation was 0.48 hr^{-1} for the 12 cases. To relate the decay coefficient to wave and sand properties, a correlation analysis was carried out, although the data set was small. The decay coefficient showed the strongest correlation to wave period ($r = 0.60$) and the initial maximum transport rate ($r = 0.65$); that is, a longer wave period or a larger initial peak offshore transport rate (profile far from equilibrium shape) resulted in faster decay in the peak offshore transport rate. Correlation with grain size (or fall speed) was very weak, and no dependence on wave height could be found. Furthermore, it was not possible to arrive at a regression equation with an acceptable coefficient of determination by using any wave or sand parameters.

329. Among the trial functions examined was also an exponential decay with time, but this expression gave an inferior fit compared to Equation 20, especially at longer elapsed times, as there was a tendency for the peak offshore transport rate to have a small but still significant value at the end of a case. The exponential decay function approached zero too fast to accurately reproduce this feature. Kajima et al. (1983a, b) developed a conceptual model of beach profile change assuming that the peaks in the transport rate distribution decayed exponentially with time. Sawaragi and Deguchi (1981) also used an exponential decay to derive a time-dependent transport relationship.

330. An exponential decay is expected on general theoretical grounds, since the response of the profile should be proportional to the departure from equilibrium. However, microscale processes and, possibly, nonconstant forcing conditions evidently alter the time decay to a more gradual approach to equilibrium, causing a deviation of the profile response from the expected exponential idealization based on linear concepts.

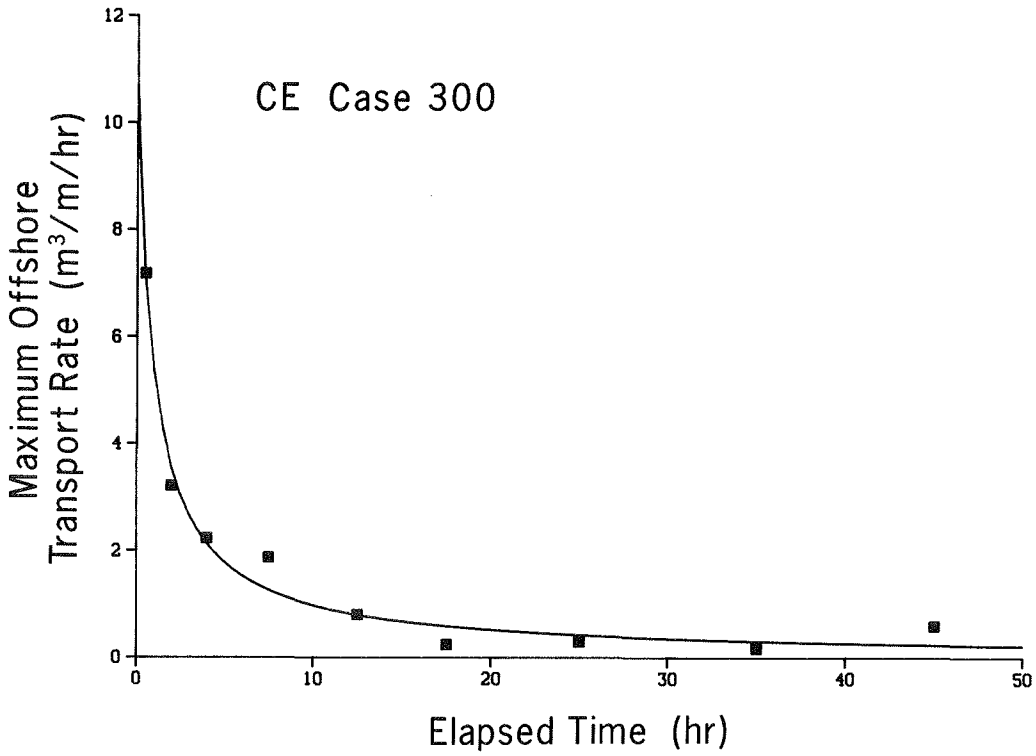

Figure 40. Decay of peak offshore sand transport rate and a best-fit empirical predictive expression

Peak onshore transport

331. The same analysis as for the peak offshore transport rate was carried out for the peak onshore rate, which encompassed 13 cases with strong onshore transport conditions. Figure 41 shows time decay of the peak onshore transport rate for the CE experiments. Similar to the behavior of the peak offshore rate, the initial peak onshore transport rate decayed rapidly, when the profile was far from its equilibrium shape, and then more slowly at the end of the run. Equation 20 was used to obtain an empirical expression to describe the decay with time by least-squares fitting. Figure 42 shows the agreement for a typical case (Case 101) between the peak onshore transport rate calculated from the profile surveys and Equation 20 (solid line). In this case also the regression equation explained over 90 percent of the total variation.

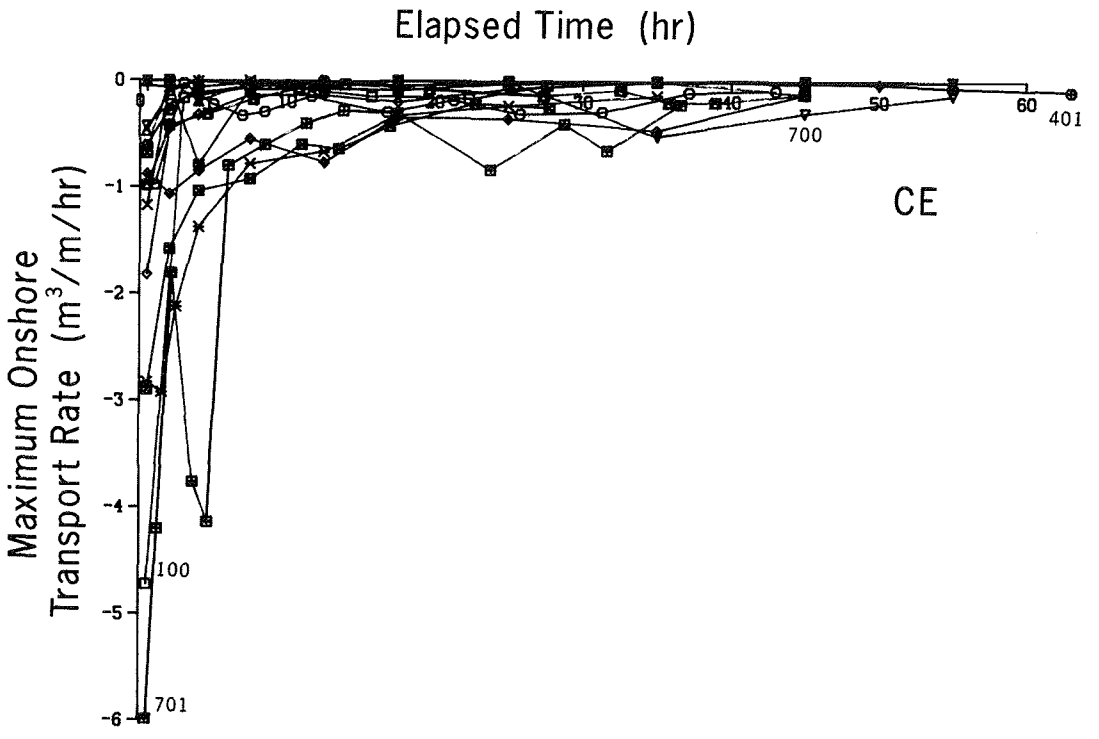

Figure 41. Evolution of peak onshore net sand transport rate for 16 CE cases

332. The average temporal rate coefficient in Equation 20 was α = 1.42 hr^{-1} for the studied cases, with standard deviation of 2.50 hr^{-1}. Thus, decay in the peak onshore transport rate was more rapid than for the peak offshore rate. This finding is in agreement with observations made by Sawaragi and Deguchi (1981) from laboratory experiments in which they noted that the onshore transport decayed faster with time than the offshore transport. It is hypothesized here that the peak onshore transport rate decays more rapidly than the peak offshore rate because of the retarding force of gravity on onshore sand motion on a sloping beach.

333. Also, in the present case, there is a wider range in values of the rate coefficient for the peak onshore transport rate compared to the peak offshore rate, as illustrated by the larger standard deviation. The rate coefficient showed a lower correlation with wave period (r = 0.50) than did that for offshore transport but still a rather high correlation with the initial peak onshore transport rate (r = 0.75). No significant correlation of peak onshore rate with wave or sand parameters was found.

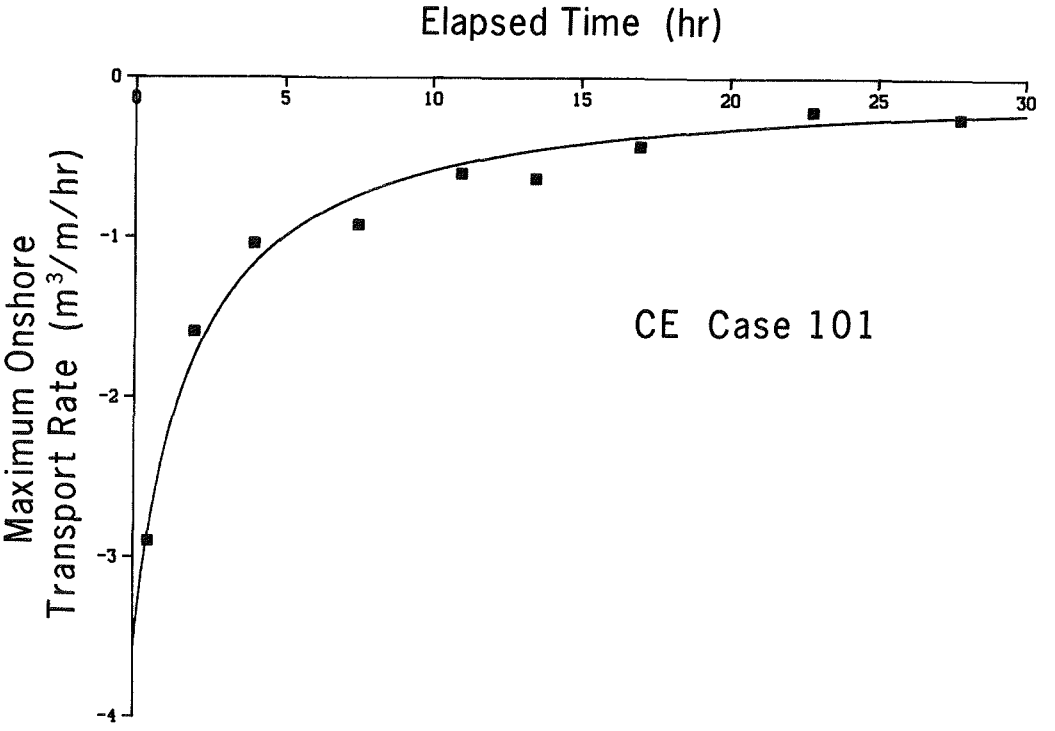

Figure 42. Decay of peak onshore sand transport rate and a best-fit empirical predictive equation

Magnitude of Net Cross-Shore Transport Rate

334. In the LWT experiments, breaking waves caused sand movement that changed the shape of the beach profile. Depending on the wave properties, characteristics of net cross-shore sand transport are expected to vary in various regions along the profile, at least in a morphological sense (Keulegan 1948). In regions of breaking waves, wave energy dissipation is large, maintaining grains in suspension, and more material is transported than in regions of nonbreaking waves. Also, the swash zone is governed by quite different dynamics than the surf zone, even if breaking waves prevail in both zones. Keulegan (1948) identified three regions where "the laws of transportation of sand" were expected to be different: from the point of impending wave break to the point where wave reformation occurs, from the point of impending wave break and seaward, and from the point of wave reformation to the shoreline.

335. A similar division was developed in this study to more closely relate transport rate properties to local wave characteristics. Figure 43 is a definition sketch illustrating division of the profile into four zones. Wave breaking in the surf zone (excluding the swash zone) can be separated into two hydrodynamic regions according to the scale and intensity of the induced vortices, as described by Miller (1976), Svendsen, Madsen, and Buhr Hansen (1979), Basco (1985), Jansen (1986), and others. Svendsen, Madsen, and Buhr Hansen called the region extending shoreward of the wave breaking point for a distance of several breaker depths the "outer or transition region." The more seaward region of the surf zone was called the "inner or quasi-steady state region." The outer region is characterized by large vortices and splash-jet motions, whereas the inner region is characterized by bore-like movement and more gradual change in internal fluid motion. The aforementioned studies showed this classification to be valid for both spilling and plunging breakers, with the intensity of the process being less for spilling breakers. Thus, when waves break, either by spilling or plunging, there is a certain distance between the incipient break point and the location where the waves are fully broken (where the energy dissipation achieves a maximum or near-maximum). Sunamura (in press) similarly hypothesized a plunge point for spilling breakers in analogy to that for plunging breakers. Skjelbreia (1987) conducted a detailed laboratory study of reproducible breaking solitary waves. He reviewed the literature of the wave breaking process and defined four zones of shoaling wave transformation as gradual shoaling, rapid shoaling, rapid decay, and gradual decay. These zones are similar to those developed in the present work based on considerations of cross-shore sand transport, discussed next.

Transport Regions

336. Various regions having distinct sand transport relationships were defined based on generally accepted concepts of nearshore wave dynamics, in accordance with Figure 43. One region, known as prebreaking, extends from the seaward limit of significant profile change to the break point, denoted as Zone I. In the prebreaking region the transport rate is influenced by trans-

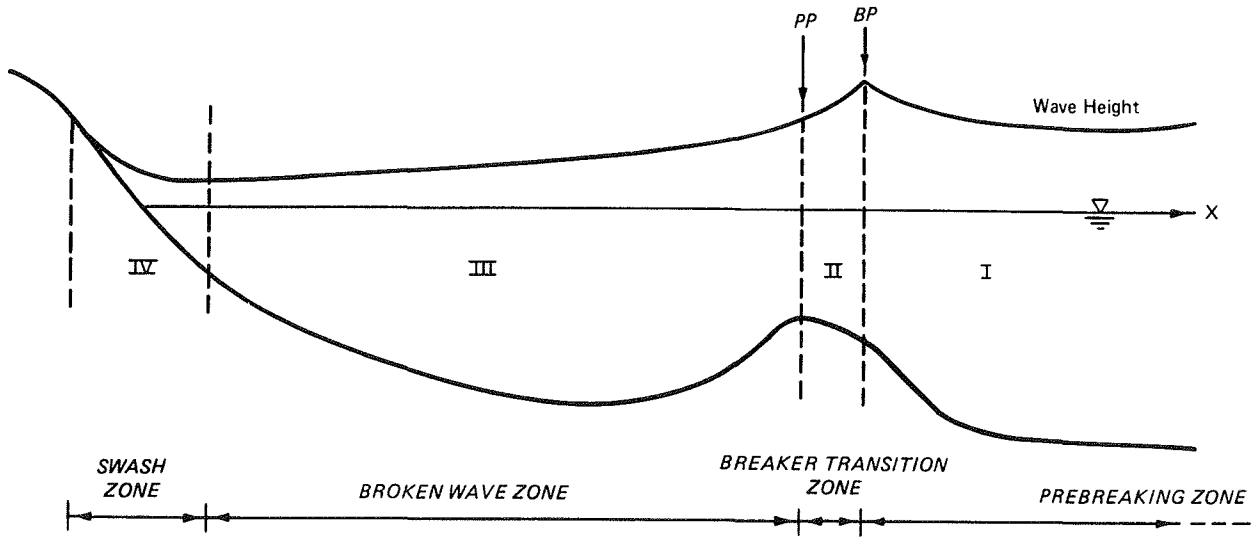

Figure 43. Definition sketch for four principal zones of cross-shore sand transport

port in the zone of wave breaking through the sediment flux at its shoreward boundary, but the governing transport processes on either side of the boundary are quite different. Zone II corresponds to the breaker transition region and is located between the break point and the plunge point. From the location of the plunge point to the point of wave reformation, one specific region, Zone III, is defined where the waves are fully broken and gradually decay (inner region in hydrodynamic terms). In this region the energy dissipation of the waves due to breaking becomes fully developed. If several break points occur with intermediate wave reformation, several zones of type II and III will be present along the profile.

337. Transport conditions in the swash zone differ from those in the surf zone, making it logical to define a fourth transport region, Zone IV. Cross-shore sand transport in the swash zone is expected to depend mainly on properties of the runup bore, local slope, and sediment characteristics. The runup limit approximately constitutes the shoreward boundary for cross-shore transport by waves. In regions between zones of breaking and fully broken waves, where wave reformation occurs, the transport conditions are regarded as similar to what prevails in the region seaward of the main breakpoint.

338. In summary, the four transport zones are located as follows:

a. Zone I: From the seaward depth of effective sand transport to the break point (prebreaking zone).

b. Zone II: From the break point to plunge point (breaker transition zone).

c. Zone III: From the plunge point to the point of wave reformation or to the swash zone (broken wave zone).

d. Zone IV: From the shoreward boundary of the surf zone to the shoreward limit of runup (swash zone).

339. The division of the profile into different transport regions is not immediately recognized viewing the net transport rate distributions (see, for example, Figure 33) since the transport regions interact, and the long-term average represented by the calculated distributions has a smoothing effect. Nevertheless, from a physical point of view it is attractive and productive to divide the beach profile into regions with different governing transport relationships. In the following, net transport rate conditions are investigated in the transport zones and in three zones related to wave and sand characteristics. Empirically-based relationships for the net transport rate are formulated for the different regions based on physical considerations and observations from the data.

Zone I: Net transport rate seaward of the break point

340. The net cross-shore transport rate seaward of the break point has probably been the most intensively studied of all regions on the profile, both in the field and in the laboratory. Transport in the prebreaking zone is in many cases governed by ripple dynamics (e.g., Inman 1957, Dingler and Inman 1977, Nielsen 1979, Sunamura 1981a). Sophisticated transport rate formulas have been developed based on laboratory experiments (e.g., Madsen and Grant 1977, Sato and Horikawa 1987), but these empirically-based formulas must also be supplemented by other information for their application. Such formulas describe sand transport on spatial and temporal microscales which are not compatible with the present approach of quantifying large-scale profile features over intervals of tens of minutes.

341. As a wave approaches the point of breaking, its velocity field becomes more asymmetric with high, narrow peaks of onshore-directed flow and broad troughs of flow directed offshore. This motion could cause material to move either onshore or offshore depending on the elevation in the water column at which a grain is suspended in relation to the duration of the on/offshore

flow. Sorting of material is thus expected along the profile, with coarser material migrating closer to shore (Ippen and Eagleson 1955).

342. Erosional cases. For erosional profiles, in the vicinity of the break point it is expected that diffusion in the seaward direction of sand that was set in suspension by the breaking waves dominates over material moved along the bottom by oscillatory wave forces. As seen from Figure 33, the shape of the net transport rate distribution is well approximated by an exponential decay with distance from a point somewhat seaward of the location of the maximum transport rate. This point is located in the vicinity of the break point, and the transport rate q in Zone I may accordingly be written

$$q = q_b e^{-\lambda(x - x_b)} \tag{21}$$

where

q_b = transport rate at the break point

λ = spatial decay coefficient

x_b = location of breakpoint

343. In analysis of the distribution of the net transport rate seaward of the break point, cases involving mainly onshore transport and offshore transport were studied separately. Equation 21 was least-squares fitted through the data for 12 cases showing mainly erosion and for 13 cases showing mainly accretion. Each case typically comprised 5-10 transport rate distributions for which a spatial decay coefficient was obtained. For a specific transport rate distribution a high coefficient of determination was always obtained (above 90 percent). The estimated decay coefficient λ was quite stable and showed only a slight tendency to decrease with time. Figure 44 illustrates the spatial decay coefficient as a function of time for four of the erosional CE cases.

344. To obtain an overall estimate of the spatial decay coefficient for a specific erosional case, the transport rate for each distribution during a run was normalized with the q_b-parameter as given by the least-squares fit for the individual distribution. Figure 45 illustrates, for CE Case 500, the decay of the normalized transport rate from the break point and seaward for consecutive transport rate distributions (indicated by various symbols)

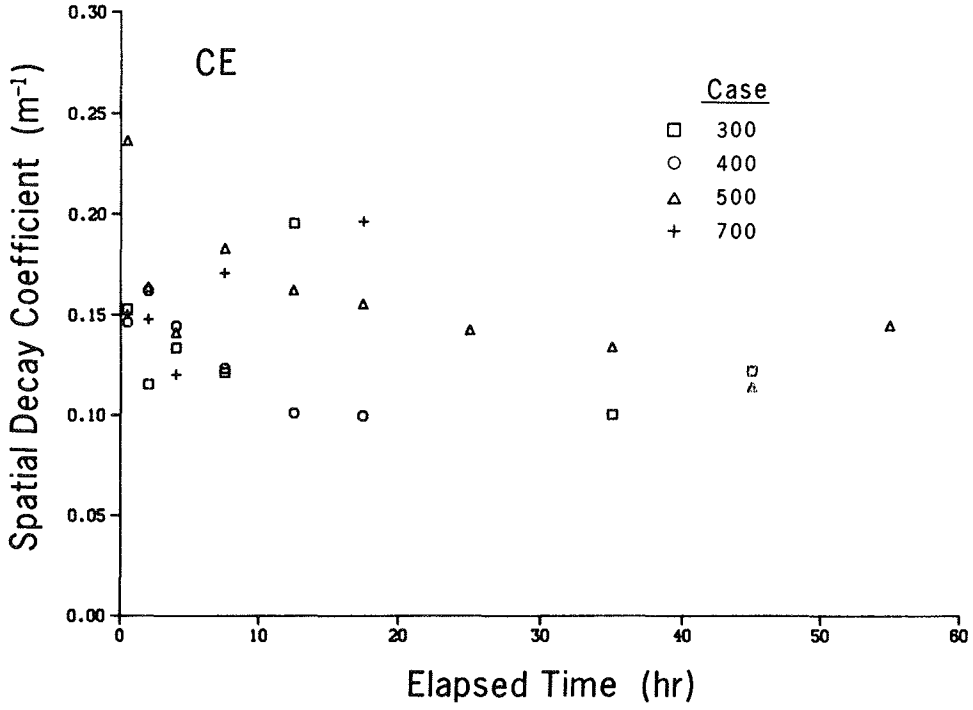

Figure 44. Spatial decay rate coefficient seaward of the break point

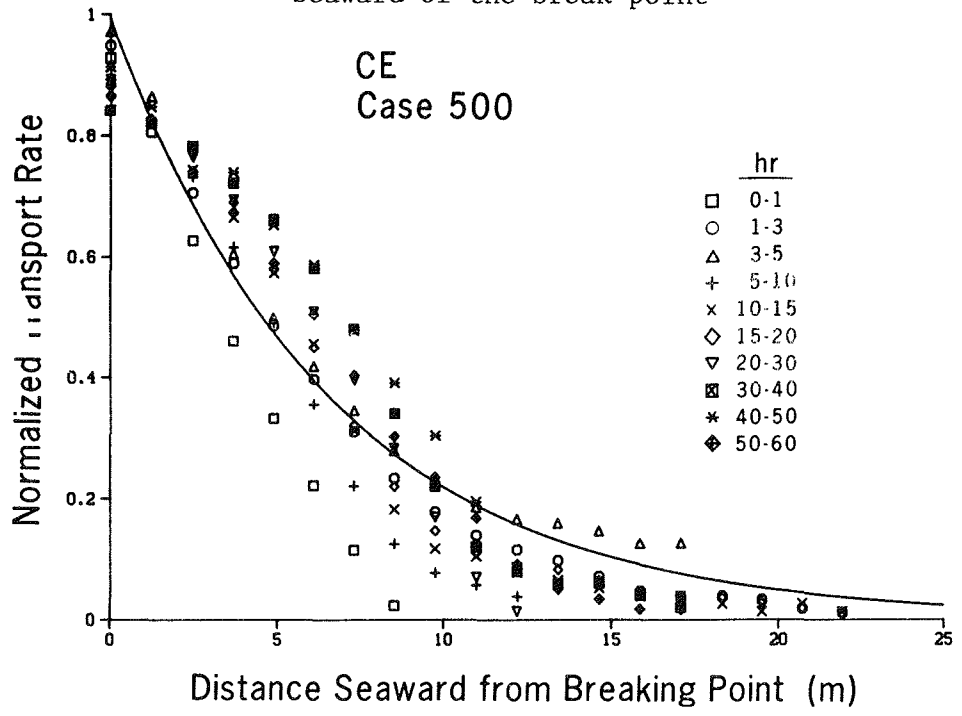

Figure 45. Comparison of net offshore sand transport rates seaward of the break point and an empirical expression

through time, together with a solid line showing the least-squares estimate of the exponential decay. The coefficient of determination in this case was 92 percent. The difference between averaging the individual estimates of the spatial decay coefficient and obtaining an overall estimate by using normalized transport rates was small.

345. The average spatial decay coefficient for erosional cases was calculated for each case and related to wave properties and sand characteristics. The overall average value of the decay coefficient was 0.18 m^{-1} with a standard deviation of 0.06 m^{-1}. Values ranged from a minimum of 0.12 m^{-1} to a maximum of 0.34 m^{-1}.

346. Correlation analysis showed an inverse dependence of the spatial decay coefficient on the breaking wave height and a direct dependence on the grain size (correlation coefficients of -0.70 and 0.75, respectively). In principle, a larger breaking wave height, for a specific grain size, would stir up more sand and thus allow more of the entrained grains to disperse seaward from the break point implying a more gradual decay in the transport rate. For constant breaking wave height, larger sand grains are less likely to be put into suspension and the transport rate distribution decays more rapidly seaward of the break point. This intuitive picture is supported by the correlation analysis.

347. The spatial decay coefficient showed only a weak inverse dependence on the wave period, giving a small correlation coefficient. Regression between the decay coefficient and the breaking wave height and the grain size explained 70 percent of the variation in the data. The regression equation is

$$\lambda = 0.40 \left[\frac{D}{H_b} \right]^{0.47} \tag{22}$$

In Equation 22 the units of D are millimeters and the units of H_b are meters.

348. Figure 46 illustrates decay coefficients calculated from the data compared with values predicted by Equation 22. Note in Figure 46 that one of the points influences the regression and correlation analysis considerably.

The regression relationship given by Equation 22 contains a coefficient (0.40) which is dimensional, since the units of λ are m^{-1}. Effort was made to form a nondimensional quantity involving λ and a relevant wave or sand property, but no significant dependence was achieved.

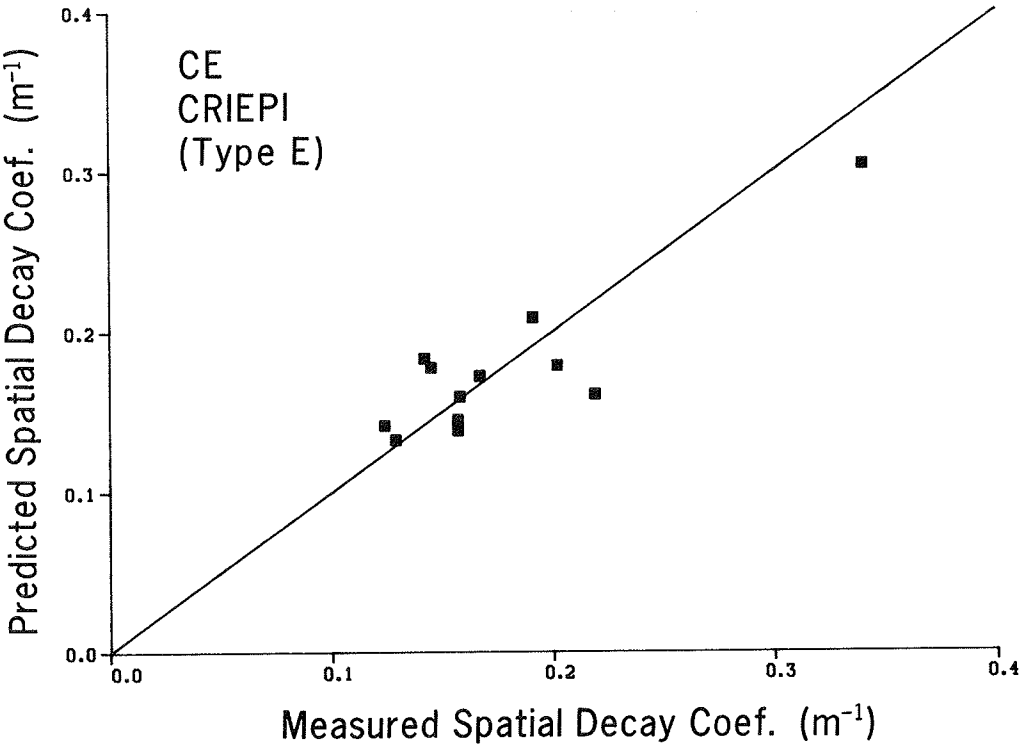

Figure 46. Comparison of spatial decay rate coefficients and an empirical predictive expression

349. Accretionary cases. A similar analysis of the decay of the transport rate for the zone seaward of the break point was carried out for cases which showed mainly onshore transport. Coefficients of determination obtained by least-squares fitting of an exponential decay function were in almost all cases greater than 90 percent for the individual transport rate distributions. Figure 47 illustrates, in analogy with Figure 45, the decay in the transport rate seaward of the break point and the corresponding calculated result from the regression equation (coefficient of determination 95 percent) for a typical case (Case 101). Transport was directed onshore at all times.

350. Spatial decay coefficients for accretionary cases were in general smaller than for erosional cases, indicating that a larger portion of the profile seaward of the break point was affected by the waves for the accre-

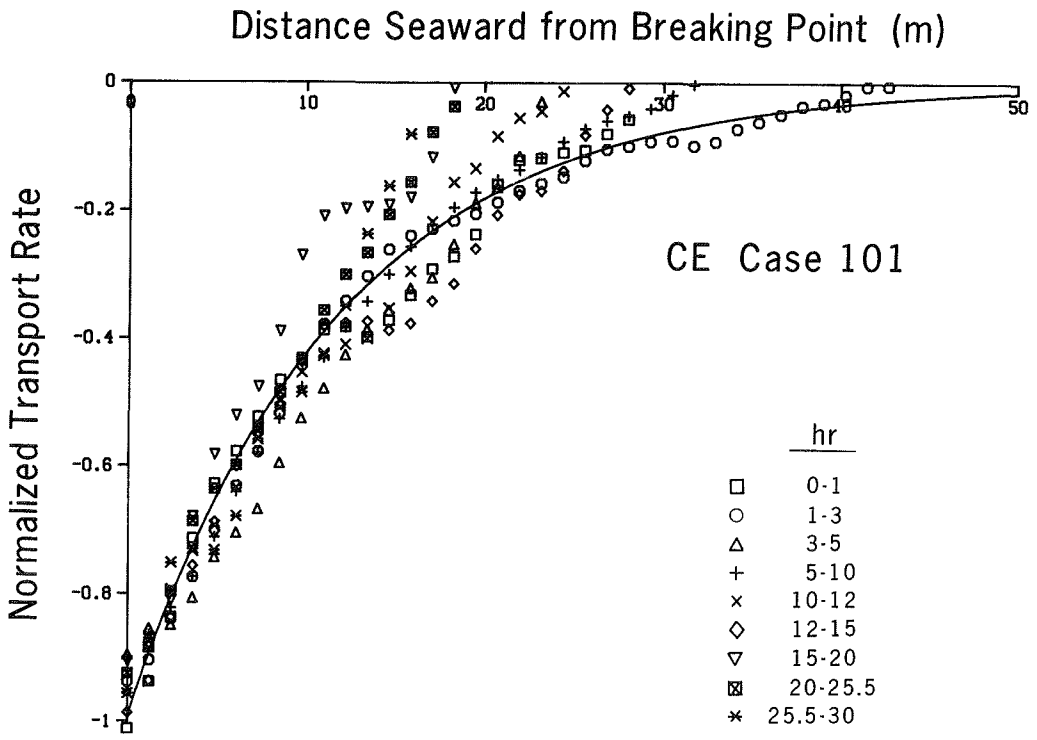

Figure 47. Comparison of net onshore sand transport rates seaward of the break point and an empirical predictive equation

tionary cases. The average value of λ for all accretionary cases studied (13 cases exhibiting mainly onshore transport) was 0.11 m^{-1}, with a standard deviation of 0.02 m^{-1}. There was significantly less spread in the values of λ for accretionary cases, indicated by the smaller standard deviation and the more narrow range between minimum and maximum values (0.08-0.16 m^{-1}). Contrary to the erosional cases, the spatial decay coefficient could not be related with any significance to wave and sand properties.

351. Secondary Zone I transport. The above analysis concerned Zone I, the region from the break point and seaward, in the absence of multiple break points. If wave reformation occurred and waves broke again closer to shore, the region seaward of the second breaker appeared to show transport rate characteristics similar to those in the region immediately seaward of the first breaker line. Only a few of the cases had a second breaker, and often the second breakpoint bar formed during the initial part of the run, rapidly

reaching an equilibrium volume. However, the main breakpoint bar had to develop to a certain size before the trough shoreward of the bar was sufficiently deep to allow the waves to reform. Formation of a second bar was manifested in the transport rate distribution as a local minimum, indicating that material was deposited shoreward of this point, implying a negative derivative of the transport rate. A local minimum in the transport rate was typically found only in the first few transport rate distributions of a run, since the second breakpoint bar soon attained equilibrium.

352. The present data sets do not provide sufficient information to determine reliable quantitative empirical relationships for the net transport rate in areas of wave reformation. Some qualitative observations may be made from the data with regard to the shape of the transport rate. The transport rate decayed in the seaward direction from a point located somewhat shoreward of the second break point, and the spatial decay in the net transport rate appeared to be more gradual than for the region seaward of the main breakpoint bar. It is speculated that even though breaking ceases, more turbulence is generated or convected in areas of reformation than in the area seaward of the main breakpoint, thus making the decay of the transport rate in wave reformation zones more gradual.

Zone II: Net transport rate between break point and plunge point

353. Waves must propagate shoreward a certain distance from the break point before breaking fully develops and energy dissipation reaches a maximum (Miller 1976; Svendsen, Madsen, and Buhr Hansen 1979; Basco 1985; Jansen 1986; Basco and Yamashita 1987; Svendsen 1987). This distance appears to be approximately equal to the plunge distance for plunging breakers and provides the basis for a definition of an equivalent plunge distance for a spilling breaker. The shape of the main breakpoint bar was in many cases well approximated by two linear slopes on the seaward side of the bar (see Part IV). The break in slope was located in the vicinity of the break point, indicating that the properties of the net transport rate were different in regions seaward and shoreward of the break point.

354. It proved too difficult to determine quantitative characteristics of the net transport rate in the region between the break point and the plunge point. This region is of small spatial extent. Furthermore, the breaker

transition zone moves together with the bar during the course of wave action, which makes analysis problematic, as the transport rate calculations are based on average profile changes that occurred over a relatively long time. However, from a conceptual point of view, it is important to recognize this region as being different from neighboring areas.

355. Some distributions provided insight into the nature of the net transport rate in Zone II, particularly during later times of a run, when changes in the beach profile shape were more gradual. Figure 48 illustrates the transport rate distribution in the region between the break point and the location of the maximum transport rate for selected cases and times. The transport rate decreased in the offshore direction at a lower rate than in the region seaward of the break point. Analysis of a small data subset where Zone II transport could be distinguished (as in Figure 48) indicated that an exponential decay was a reasonable approximation, with the spatial decay coefficient approximately 0.20-0.25 of the value of the spatial decay coefficient governing transport seaward of the break point.

Zone III: Net transport rate in broken waves

356. Breaking and broken waves produce turbulent conditions that put grains into suspension and make them available for transport across the profile (Watts 1953, Fairchild 1973, Kana 1977, Kraus and Dean 1987). Thus, it is plausible to assume that the magnitude of the transport rate is closely related to wave energy dissipation (Dean 1977). Different models of wave height decay in the surf zone based on energy dissipation have been developed (e.g., Dally 1980; Mizuguchi 1981; Svendsen 1984; and Dally, Dean, and Dalrymple 1985a, b).

357. The CE data set did not include detailed measurements of the wave height distribution across the profile, whereas the CRIEPI data set provided wave height data for most of the cases with a resolution of 2.5 m. The wave height distribution was usually measured between profile surveys, making the exact beach profile shape unknown for the time of the measurement. To obtain a picture of the relationship between the cross-shore transport rate and local wave parameters in broken wave zones, the CRIEPI data set was used, although the number of cases that contained significant profile change and corresponding measurements of wave height across-shore was limited. Only four cases

allowed thorough analysis of the correlation between local wave properties and transport rate at consecutive times during a run.

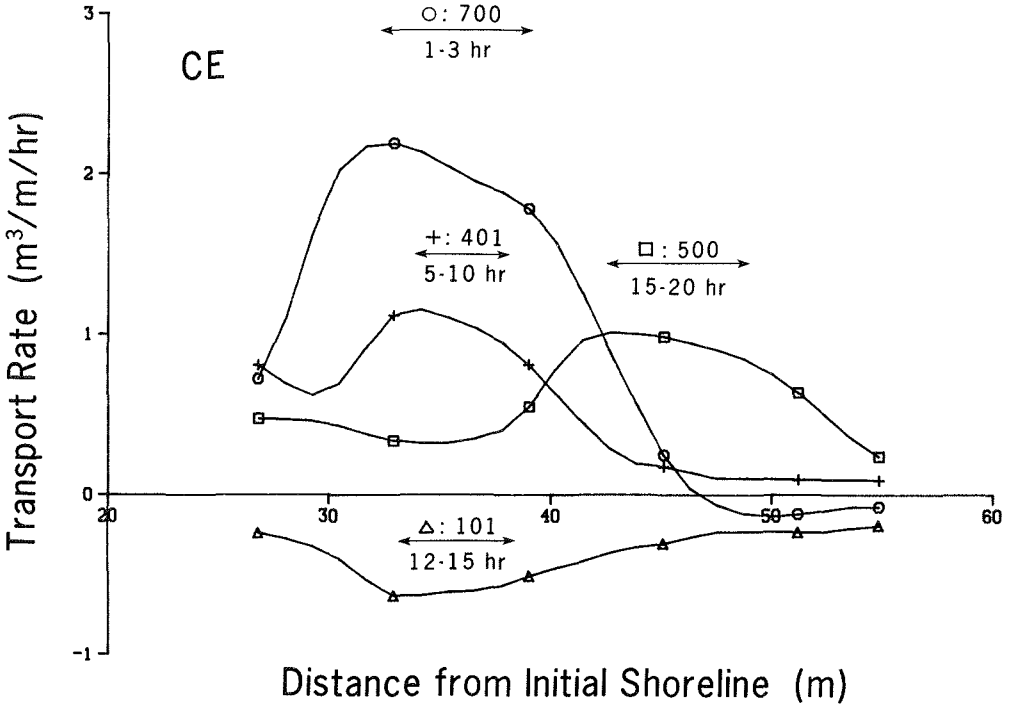

Figure 48. Net cross-shore sand transport rate distributions between break point and plunge point

358. Energy dissipation is related to the change in wave energy flux along the profile. The energy flux F may be written using shallow-water wave theory as

$$F = \frac{1}{8} \rho g H^2 \sqrt{gh} \tag{23}$$

where ρ is the density of water. The energy dissipation is given by dF/dx .

359. Due to the relatively low resolution in the wave height measurement, evaluation of the derivative and transport proved sensitive to individual measurement values. To obtain a better estimate, the wave decay model of Dally (1980) was least-squares fitted through discrete values of each measured wave height distribution from the point of breaking shoreward until wave reformation occurred or the water depth became small (approximately 20 cm).

The wave model is presented in Part VI, where the analytic solution which was used in the least-square fit is given (Equation 29). It is noted that a change in broken wave height is not completely indicative of wave energy dissipation; energy reordering may also occur, as discussed by Svendsen, Madsen, and Buhr Hansen (1979).

360. The empirical coefficient relating stable wave height to water depth employed in the Dally model (still-water depth without setup) was determined from wave height measurements by examining the ratio between wave height and water depth in the proximity of areas of wave reformation. An average stable wave height coefficient was calculated for each case and values ranged from 0.3-0.5, showing a marked dependence on the beach slope (compare with Dally, Dean, and Dalrymple 1985b). Steeper beach slopes yielded larger values of the stable wave height coefficient. The wave decay coefficient was then least-squares estimated, giving values in the range of 0.15-0.3. In most cases, there was a tendency for the wave decay coefficient to decrease with time as the inshore slope became more gentle.

361. At first, both empirical parameters in the wave decay model (stable wave height and wave decay coefficient) were least-squares estimated (cf. Part VI). However, the minima of the sum of squares were located in a very flat region, causing differences between optimum parameter combinations and neighboring values to be small. To achieve a certain increase in the energy dissipation, either the wave decay coefficient could be increased or the stable wave height coefficient decreased (or a combination of these adjustments). Thus, in the optimization process, since the region surrounding the minimum was very flat, almost the same agreement could be obtained with a small value of the stable wave height coefficient and a large value of the wave decay coefficient, or the opposite situation. In some cases the optimum parameter values gave unrealistically low coefficients of stable wave height, such as 0.2. For this reason, the stable wave height was fixed as described in the previous paragraph and only a least-squares estimate of the wave decay coefficient was made, giving a sum of squares deviating only slightly from the mathematically optimum value.

362. Dissipation in wave energy flux was determined from the wave decay model, calculated starting at the location of the maximum transport rate,

somewhat shoreward of the break point, and ending where the wave decay model calculation was arbitrarily stopped. For each case, various quantities connected with the energy flux dissipation were correlated with the cross-shore sand transport rate in Zone III for all distributions obtained during a run. The net cross-shore transport rate showed good correlation with energy flux dissipation per unit water volume for all cases studied (correlation coefficients of 0.7-0.8), which was higher than the correlation resulting from tests using only the energy flux dissipation per unit area of beach. Figure 49 shows the transport rate plotted against the energy flux dissipation per unit volume as evaluated for Case 6-1.

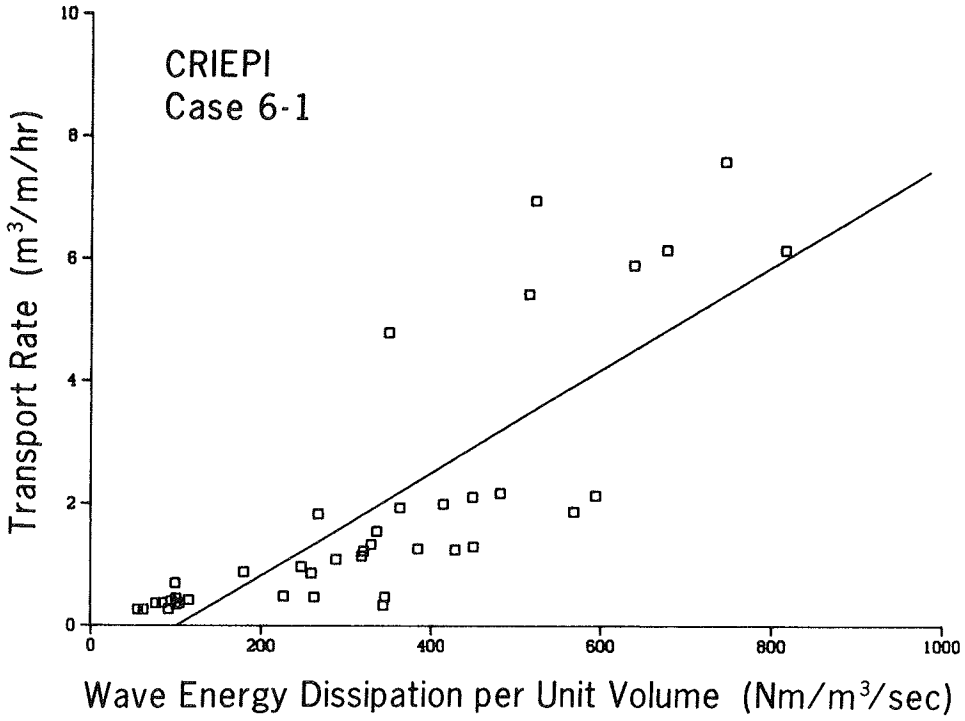

Figure 49. Net cross-shore sand transport rate versus calculated wave energy dissipation per unit volume in broken wave region

363. Correlation was in general higher for individual transport rate distributions than if all values from a specific case were used. Other parameters pertaining to the geometry of the beach profile, such as beach slope and wave characteristics, were also correlated with the transport rate. To determine geometric parameters of the beach profile, the average profile

calculated from surveys taken before and after the measurement of the wave height distribution was used. No significant correlation was found that was consistent for all cases between any other parameter studied and the transport rate. For some cases, there was a positive correlation between transport rate and beach slope.

364. A linear regression equation relating the transport rate to energy dissipation per unit volume and local beach slope was least-squares fitted to the data. The regression relationship explained about 50-70 percent of the total variation in the data for the different cases studied, in which local beach slope accounted at most for 10 percent of the total variation.

365. Kriebel and Dean (1985a) assumed that the cross-shore sand transport rate was proportional to the excess energy dissipation per unit volume over a certain equilibrium value of energy dissipation, which was defined by the amount of energy dissipation per unit volume a beach with a specific grain size could withstand (cf. Part VI). From the regression analysis between wave energy dissipation per unit volume and transport rate, it was possible to obtain an estimate of the transport rate coefficient corresponding to the proportionality constant used by Kriebel and Dean (1985a).

366. For the four cases intensively studied, the average value of the transport rate coefficient was determined from regression analysis to be $1.1\ 10^{-6}\ m^4/N$, which is approximately half the value originally obtained by Moore (1982). Moore developed a numerical model of beach profile change using a transport equation for the cross-shore sand movement in which the transport rate was proportional to wave energy dissipation per unit volume. He arrived at a transport coefficient of $2.2\ 10^{-6}\ m^4/N$ by calibration using profile change measured in one CE case and field measurements from Santa Barbara, California.

367. Two major causes are believed responsible for the difference in values obtained. First, Moore (1982) inferred the transport coefficient by comparison of simulated profile change and measurement, not directly between wave energy dissipation per unit volume and measured transport rate as done here. Second, considerable smoothing of the calculated transport rate was used in Moore's model. By smoothing the energy dissipation along the profile, a larger value of the transport rate coefficient is needed to achieve the same

beach profile response as compared to a simulation with no smoothing. A more thorough discussion of values of the transport rate coefficient is given in Part VII describing application of the numerical model.

368. It was not possible to relate the transport rate coefficient to wave or beach properties. In a numerical model the transport rate coefficient functions largely as a calibration parameter to give the proper time scale of profile change.

369. In the regression analysis between transport rate and energy dissipation per unit volume, other beach and wave parameters were added to quantify their influence. For the cases where the local beach slope showed some influence on the transport rate, the coefficient in the regression equation was typically small, on the order of 0.0006 m^2/sec. The equilibrium energy dissipation was determined from the constant term in the regression equation and varied considerably between the runs evaluated, although the grain size was the same for the studied cases. This variation was probably due to the scatter in the data relating transport rate to energy dissipation, making the least-squares estimate of the constant in the regression equation less reliable. However, two of the cases resulted in equilibrium energy dissipations that were somewhat smaller than the values given by Moore (1982), who used natural beach profiles to determine this parameter (108 and 134 $Nm/(m^3sec)$ from the present data compared to Moore's value of 170 Nm/m^3sec).

370. The purpose of the previous analysis was to emphasize the close relationship between wave energy dissipation per unit volume and magnitude of the transport rate in zones of broken waves. Although the number of satisfactory cases for obtaining quantitative information about wave height and associated sand transport rate distribution was small, the relationship between the two quantities was clearly evident. All of the studied cases encompassed beach profiles which experienced erosion of the foreshore and bar formation in the vicinity of the break point. It is expected that profiles with accretion on the foreshore will also exhibit transport rates that are related to the energy dissipation per unit volume, although it was not possible to directly confirm this assumption by means of the present data.

Zone IV: Net transport rate on the foreshore

371. The net transport rate in the swash zone is expected to be a function of local beach slope, sediment characteristics, and properties of the bore propagating upon the beach. No wave or bore information was available for this study, except for some runup measurements from the CE data. Consequently, it was not possible to derive a relationship connecting the net transport rate on the foreshore to local wave properties and other factors. However, some qualitative observations were made of the shape of the net transport rate distribution on the foreshore. The region discussed in this section extends approximately from the runup limit seaward to some specific depth corresponding to the point of maximum retreat of the waves in the swash. This depth is a function of the incident waves which cause setup at the shoreline roughly proportional to the breaking wave height. Swash oscillates about the mean shoreline elevation with a range dependent mainly on wave height and surf similarity parameter, even in the field (Guza and Thornton 1982, Holman 1986).

372. For some cases, the net transport rate showed a fairly complex spatial dependence on the foreshore, in particular at the early stages of the experiments. However, the net rate had an almost linear decay with distance for a majority of the cases, both for onshore and offshore transport conditions. Figure 50 gives a representative example of the transport rate distribution over the foreshore for CE Case 300, in which different consecutive distributions in time are plotted. The slope of the transport rate decreased with time as the profile approached equilibrium, but the shape of the distribution roughly maintained a linear form. In Case 300, the profile retreated shoreward as the foreshore eroded during the run. (The location of the still-water shoreline is indicated by vertical lines for the various distributions in time.) A linear decay in the transport rate implies that an equal amount of material is eroded at all points along the foreshore up to the runup limit (compare field observations of Seymour 1987).

373. As the foreshore eroded, a step formed extending approximately from the still-water shoreline to the runup limit. The slope of the step may have increased until the angle of initial yield was exceeded (Allen 1970) and avalanching occurred, thereby adjusting the slope to a lower value (residual

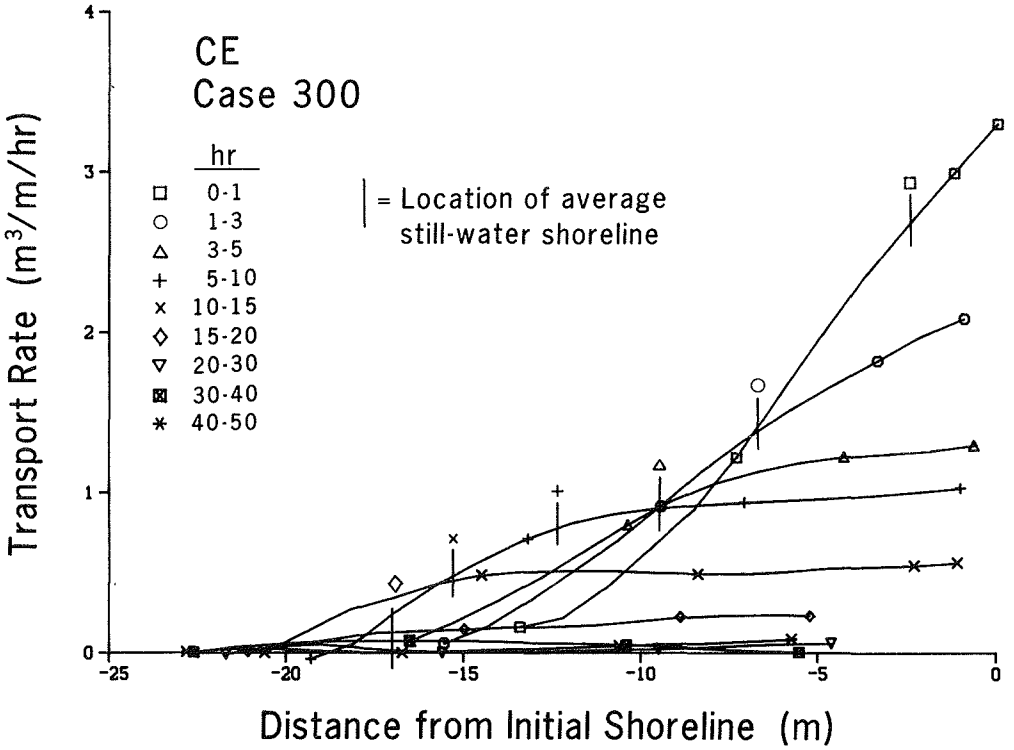

Figure 50. Time behavior of net cross-shore sand transport rate distribution on the foreshore

angle after shearing). Sediment transport produced by slope failure is expected to occur very rapidly and would produce a transport rate distribution of a quadratic shape since the step rotates at a fixed angle around some point along its face. Averaging of the net transport rate smooths over the process of avalanching. Also, the progress of avalanching is probably not ideal with a pure and constant steepening of the step face; rather, transport is probably greater at the base of the step, undermining it.

Summary

374. Calculated distributions of the net cross-shore transport rate from profile change measured over intervals on the order of hours displayed very regular and smooth properties despite the random character of the grain-by-grain movement that actually took place. It therefore appears possible to estimate the net cross-shore sand transport rate with sufficient reliability

to predict the development of main morphologic features of the beach profile. Available equilibrium distributions of the net transport rate could be classified almost exclusively into three main types, two types of which correspond to either onshore or offshore transport along the profile. Transport distributions with one onshore and one offshore peak were not common and occurred mainly for cases which fell close to a derived line delineating bar profiles and berm profiles. As a result, the assumption of a unidirectional transport rate along the profile should give a reasonable first approximation in most cases for describing the overall profile response to incident short-period waves.

375. Division of the profile into four zones with different transport properties, based in part on general observations of nearshore wave dynamics, proved to be a fruitful approach both from the conceptual and predictive points of view. The net transport rate in zones of broken waves, where the most active transport is expected to occur, showed good correlation with the wave energy dissipation per unit water volume. The net transport rate in the prebreaking zone decayed exponentially with distance offshore. On the foreshore, the net transport rate showed an approximately linear behavior decreasing in the shoreward direction from the end of the surf zone. More data on the transport rate in the foreshore are needed to better understand physical processes there.

376. Quantitative information on the net cross-shore transport rate is difficult to obtain in the field due to the limited resolution in time and space of profile surveys, number of instruments that can be deployed, contaminating effects of longshore sand transport, and changing wave conditions. In this respect, data from large wave tanks provided valuable insight into the behavior of the net cross-shore transport rate and enhanced the possibility of modeling beach profile change. Although monochromatic waves were used in the large wave tank experiments, it is expected that the main features of the transport rate are representative of processes associated with random waves in the field. This hypothesis is tested in Part VII where model predictions are compared with field observations.

PART VI: NUMERICAL MODEL OF BEACH PROFILE CHANGE

377. Quantitative prediction of the response of the beach profile to wave action and changes in water level is an important goal of coastal engineering. The capability to quantitatively estimate dune erosion, beach response to large storms, and the initial adjustment and long-term evolution of a beach fill is necessary to design and make economic evaluations of shore erosion and flood protection projects. A numerical model can be an efficient tool to evaluate various design alternatives while easily incorporating detailed process data, such as time series of waves and water level.

378. Many attempts have been made to develop numerical models of beach profile change. The authors are not aware of any existing model, however, which can be applied to an arbitrary beach profile exposed to variable wave and water level conditions to reproduce bar formation and movement in addition to overall change in the profile. It was a major goal of this investigation to model the growth and movement of bars as part of the beach profile response, since these features constitute natural protection for a beach exposed to severe erosional conditions. Furthermore, for long-term simulations, a predictive model must necessarily incorporate events producing onshore transport and berm buildup, which no known engineering model can simulate. Development of such a model would allow simulation of seasonal changes in the profile as produced by cross-shore sediment transport.

379. This chapter describes the numerical model developed in this study for simulating beach profile change. An important feature possessed by the model is the capability to reproduce main morphologic features of the profile, in particular, bars and berms. Many of the assumptions and relationships used in development of the model were founded on observations presented in previous chapters of this report. The numerical model is aimed at reproducing macro-changes of the beach profile in a deterministic fashion, neglecting small-scale features such as ripples and avoiding the extreme complexity associated with detailed specification of the fluid flow and sediment concentration.

380. The model is formally based on the equation of mass conservation, for which mathematical expressions for the cross-shore transport rate are required. Any type of theoretical or empirical transport rate formula can be

used in the model. Therefore, as knowledge of cross-shore fluid flows and sediment transport improves, the model is sufficiently general and flexible to allow inclusion of these advances to supplement the transport rate formulas developed in this study. Under the assumption of linear superposition, contributions from driving forces other than short-period breaking waves can be added if the transport rate relations are known. Examples for future inclusion would be transport by undertow and long-period wave motions.

381. In Part IV, a clear connection was found between macrofeatures of the beach profile and wave and sand characteristics. Reliable prediction of the net cross-shore sand transport rate distribution on the spatial scale of meters and time frame of minutes was demonstrated in Part V. Thus, all preparatory work supports the feasibility of developing a predictive engineering numerical model for simulating macroscale changes in the beach profile.

Methodology

382. At the present state of knowledge, it is clear that any type of numerical model of beach profile change to be used in engineering practice must be based on semi-empirical relationships derived from measurements. The model presented here was developed using data from experiments carried out in LWTs involving waves of prototype size.

383. Dally (1980) and Birkemeier et al. (1987) presented criteria to judge the suitability of a numerical model of beach profile change. In the present work, the following properties were considered to be fundamental. The model should:

a. Accurately simulate time evolution of a profile of arbitrary shape subjected to changes in water level and incident wave parameters.

b. Calculate an equilibrium configuration if all model parameters and input values are held constant.

c. Simulate formation and movement of main morphologic profile features such as bars and berms.

d. Reproduce erosional and accretionary beach change.

e. Be verified for a wide range of realistic conditions.

384. A short description of the capabilities of existing numerical models is contained in the literature review in Part II. Of the various

numerical models proposed prior to the present work, that of Kriebel (1982) (see also Kriebel and Dean 1985a, Kriebel 1986) comes closest to satisfying the five criteria listed above. The Kriebel model was critically evaluated and determined to be the best available tool for estimating erosion on U.S. coasts (Birkemeier et al. 1987). The Kriebel model satisfies criteria a. and b., and, in part e., but not criteria c. and d. The model was originally developed and verified using cases from the CE data set, as well as an erosional event associated with Hurricane Elena, and has since been used in engineering studies (Kriebel and Dean 1985b, Kraus et al. 1988). Development of the present model was stimulated by the success of the Kriebel model.

385. In the following, a short overview of the structure of the numerical model is given as an introduction before its various components are discussed in detail. Changes in the shape of the beach profile are assumed to be produced by breaking waves; therefore, the cross-shore transport rate is determined from local wave, water level, and beach profile properties. The equation expressing conservation of beach material is solved to compute profile change as a function of time.

386. The wave height distribution is calculated across the shore by applying small-amplitude wave theory up to the point of breaking, and then the breaker decay model of Dally (1980) is used to provide the wave height in regions of breaking waves. The profile is divided into specific regions according to the wave characteristics at the given time-step for specification of transport properties. The distribution of the cross-shore transport rate is then calculated from semi-empirical relationships valid in different regions of transport. At the shoreward end of the profile, the runup limit constitutes a boundary across which no material is transported, whereas the seaward boundary is determined by the depth at which no significant sediment motion occurs. Once the distribution of the transport rate is known, profile change is calculated from the mass conservation equation. The described procedure is carried out at every time-step in a finite-difference solution scheme using the current incident wave conditions and water level, and updating the beach profile shape.

387. First, the wave model is described and calculations compared with measurements from the CRIEPI data set. Then the various transport relations

are developed for use in the profile change model. The next section gives a description of the numerical solution scheme and the associated boundary conditions. Finally, calibration and verification of the profile change model with the LWT data set are made. Applications of the model, including sensitivity analyses and tests of predictions with field data, are given in Part VII.

Wave Model

388. As waves approach shore over a gently sloping bottom, they increase in height and decrease in length due to shoaling. It will be assumed that the waves are incident normal to the coast, i.e., that refraction can be neglected. The increase in wave height continues until some critical ratio is reached between wave height and water depth, at which point the waves break. The wave height distribution across the shore is calculated by linear wave theory. In initial model development, the nonlinear shoaling laws proposed by Shuto (1974) were used in an effort to provide an improved description of the increasing nonlinearity of waves as they approach breaking. However, in comparison of predictions of the nonlinear wave model against wave height measurements from the CRIEPI data set, the predicted height increased too steeply before breaking for longer-period waves. In simulations involving development of a prominent breakpoint bar through time, the wave height just prior to breaking was overestimated. It was thus decided to use linear wave theory in all regions of the shoaling calculation and leave the problem of nonlinear wave shoaling to the future.

Breaking criterion and breaker height

389. The ratio of wave height to water depth at breaking (called the breaker index) was evaluated using the CRIEPI data set. Only those cases with an initially plane slope were used and, if no profile survey was taken at the time of the wave height measurement, the depth at breaking was determined by interpolation from the two profiles bracketing the wave measurement in time. In total, 121 pairs of wave height and depth values were obtained from 17 cases having different wave conditions and initial beach slopes. The average breaker index (wave height to water depth at breaking) was 1.00, with a

standard deviation of 0.25. As shown in Figure 51, the distribution of the breaker indices was somewhat positively skewed, and values ranged from 0.58 to 1.79. The steep slope that developed on the seaward side of the growing bar caused the breaker index to increase with time, allowing the wave to break in more shallow water.

390. To evaluate this effect, results were compared with small-scale laboratory data tabulated by Smith and Kraus (1988) for experiments made with fixed plane bottom slopes typically more gentle than the seaward bar faces in the CRIEPI cases. Figure 52 shows the distribution of the breaker index for the small-scale experiment data, in analogy with Figure 51. Because of the more gentle slopes, the average breaker index for the small-scale data was only 0.82 (135 values), with a standard deviation of 0.18. If the beach slope grows steep seaward of the break point, the breaker index should accordingly be increased to account for the bottom slope effect on wave breaking.

391. Correlation analysis showed that the breaker index depended mainly on the slope before breaking and the deepwater wave steepness (see Galvin 1969, Weggel 1972, Singamsetti and Wind 1980, Sunamura 1981b). The slope was evaluated as an average over that part of the beach profile seaward of the break point where waves showed a marked increase in height due to shoaling (typically in the range of 10-20 m). The breaker index increased with an increase in bottom slope and decreased with an increase in wave steepness. For profiles exhibiting bar development during a run, the average seaward slope in general showed an increase with time (Part IV), causing an increase in breaker index. Regression analysis between the aforementioned variables explained 55 percent of the variation and indicated that the beach slope and deepwater wave steepness could be combined to form the surf similarity parameter $\tan\beta/(H_o/L_o)^{1/2}$ (Battjes 1975) without loss of predictability. The regression equation obtained is

$$\frac{H_b}{h_b} = 1.14 \left[\frac{\tan\beta}{\sqrt{H_o/L_o}} \right]^{0.21} \tag{24}$$

where $\tan\beta$ is the local beach slope seaward of the breakpoint.

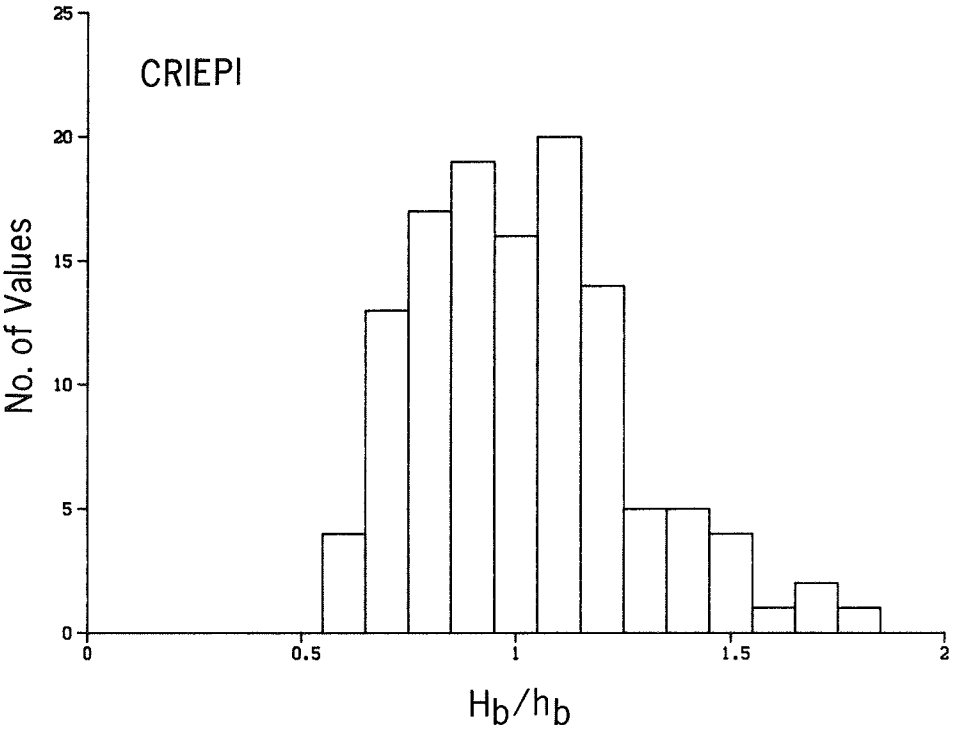

Figure 51. Distribution of breaker ratio for the CRIEPI data

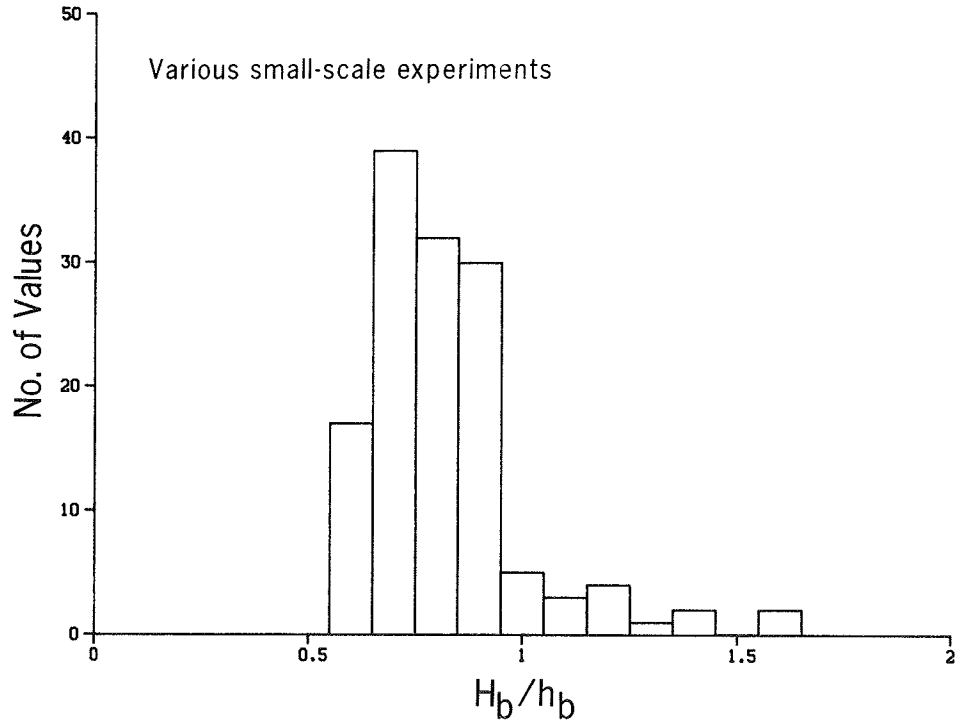

Figure 52. Distribution of breaker ratio for small-scale laboratory data

392. Values of the empirical multiplicative coefficient and exponent in the regression equation are very similar to those obtained by Battjes as reported by Singamsetti and Wind (1980) and Sunamura (1981b) based on small-scale laboratory data. In Figure 53, data from the CRIEPI experiments are plotted together with Equation 24. The wave model uses Equation 24 to predict the breaking condition, for which the bottom slope is evaluated over a distance one third of the local wavelength seaward of the break point.

393. The breaking wave height on the movable bed bottoms of the CE and CRIEPI experiments normalized by the deepwater wave height was related to the deepwater wave steepness. An average breaking wave height was used for each case, making up a total of 32 cases for the analysis. Regression analysis with the deepwater wave steepness explained 80 percent of the variation in the data, leading to the equation

$$\frac{H_b}{H_o} = 0.53 \left[\frac{H_o}{L_o} \right]^{-0.24} \tag{25}$$

394. Inclusion of initial beach slope in the regression equation did not improve predictability, probably due to the significant change in slope that occurred seaward of the break point during the course of wave action. Figure 54 illustrates the prediction from Equation 25 and the data points from the studied cases. Data points associated with different initial slopes have been plotted with different symbols. Note that the value of the empirically determined exponent in Equation 25 is close to that which is obtained with linear wave theory for shoaling of normally incident waves from deep water to breaking (-0.20; see Komar and Gaughan 1973).

Breaker decay model

395. Several numerical models have been developed for describing wave height decay in the surf zone (e.g., Battjes and Janssen 1979, Dally 1980, Mizuguchi 1981, Svendsen 1984). All contain empirical parameters whose values have to be established by calibration against measurements. The wave model proposed by Dally (1980) and further discussed by Dally, Dean, and Dalrymple (1985a, 1985b) was chosen for use here since it has been verified with both laboratory data (Dally 1980) and field data (Ebersole 1987). Furthermore, the

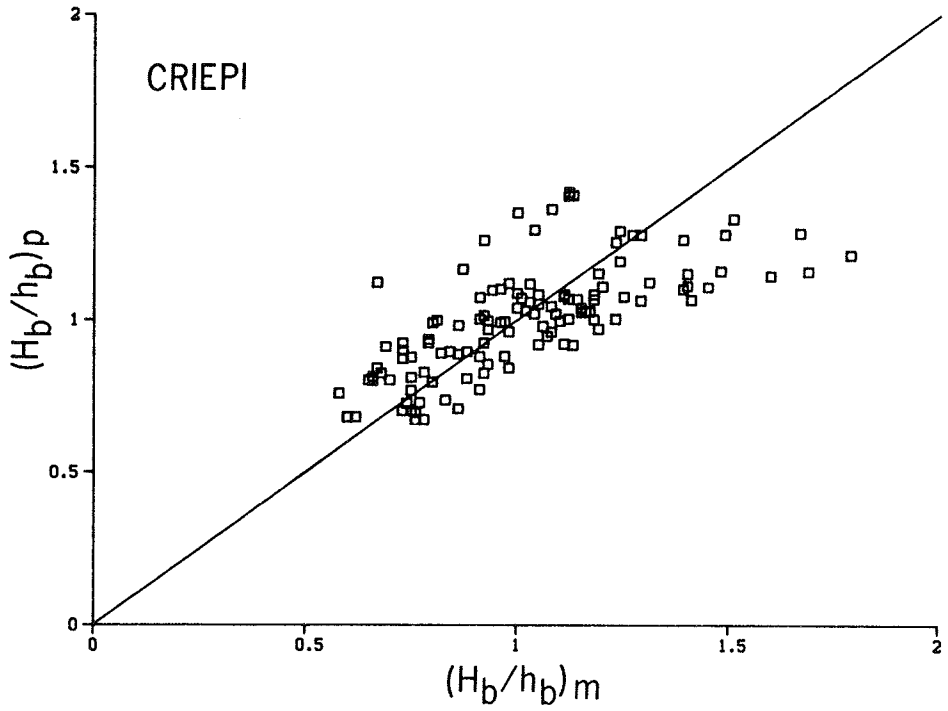

Figure 53. Comparison between measured and predicted breaker ratio

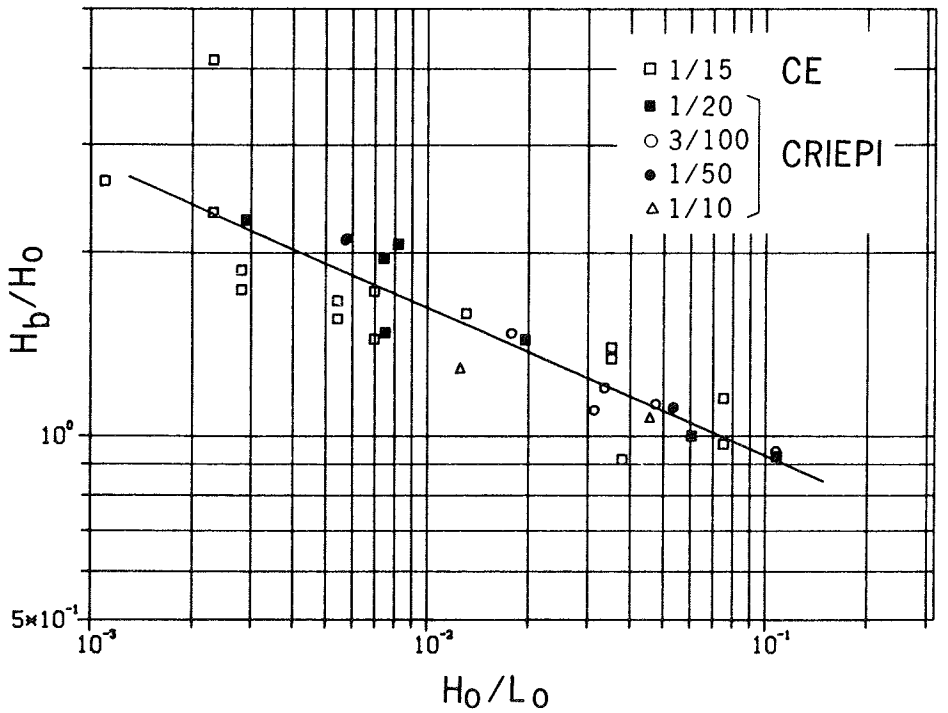

Figure 54. Ratio between breaking and deepwater wave height as a function of deepwater wave steepness

breaker decay model allows for wave reformation to occur, which is an essential feature for modeling profiles with multiple bars. The governing equation for the breaker decay model is written in its general form as

$$\frac{dF}{dx} = - \frac{\kappa}{h} (F - F_s) \tag{26}$$

where

κ = empirical wave decay coefficient

F_s = stable wave energy flux

In this equation, the cross-shore coordinate x has its origin at the break point and is directed positive shoreward.

396. The assumption behind Equation 26 is that the energy dissipation per unit plan beach area is proportional to the difference between the existing energy flux and a stable energy flux below which a wave will not decay. By using linear wave theory, the energy flux in shallow water is

$$F = \frac{1}{8} \rho g H^2 \sqrt{gh} \tag{27}$$

397. The stable energy flux is generally considered to be a function of the water depth (Horikawa and Kuo 1967), and a coefficient Γ is used to express the ratio between the local wave height and water depth at stable conditions according to

$$H_s = \Gamma h \tag{28}$$

398. Measurements of the wave height distribution from the CRIEPI experiments were used to evaluate performance of the breaker decay model and to estimate values of the two empirical parameters (κ and Γ) in the model. As described in Part V, the breaker decay model was least-squares fitted to wave height data from the breakpoint shoreward to the end of the surf zone. The solution of Equation 26 for a beach with an arbitrary shape, applying linear wave theory, is given by

$$H = \left[\frac{1}{\sqrt{h}} \left[H_b^2 \sqrt{h_b}\ e^{-\kappa \int_0^x \frac{dx}{h}} + e^{-\kappa \int_0^x \frac{dx}{h}} \kappa \Gamma^2 \int_0^x h \sqrt{h}\ e^{\kappa \int_0^x \frac{dx}{h}} dx \right] \right]^{1/2} \qquad (29)$$

where, as previously mentioned, the cross-shore coordinate axis originates at the break point. Figure 55 shows a typical fit between results of the breaker decay model and measured wave heights in the surf zone. The symbols connected by straight lines denote the model result for different times, whereas the corresponding single points are the measured wave heights. The breaker decay model was in this case least-squares fitted against all wave height distribution measurements made during one run. To evaluate parameters of the breaker decay model simultaneously for various distributions, wave height was normalized with the incipient breaking wave height, and cross-shore distance and water depth were normalized with depth at incipient breaking.

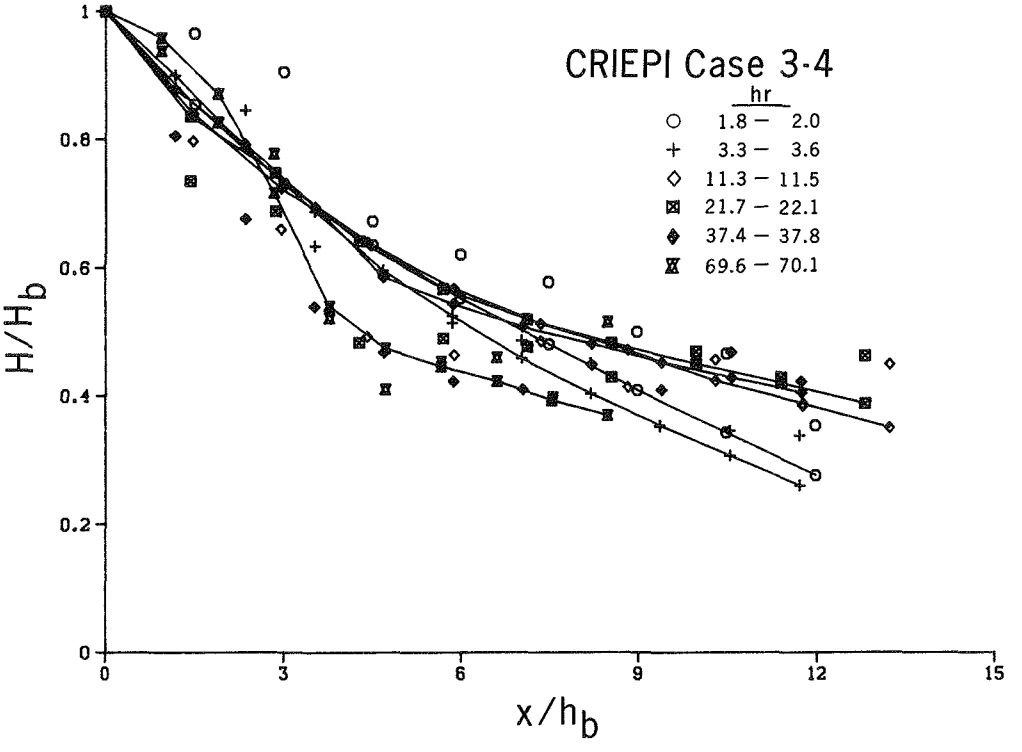

Figure 55. Measured and calculated wave heights

399. Wave setup and setdown are incorporated in calculation of the wave height distribution and determined by solving the following differential equation together with Equation 26 (Longuet-Higgins and Stewart 1963)

$$\frac{dS_{xx}}{dx} = -\rho g(h + \eta) \frac{d\eta}{dx} \tag{30}$$

where

S_{xx} = radiation stress component directed onshore

η = wave setup

400. The radiation stress is, using shallow-water approximations,

$$S_{xx} = \frac{3}{16} \rho g H^2 \tag{31}$$

Setdown in the first calculation cell is determined from the analytical solution to Equation 30 seaward of the break point, assuming no energy losses.

$$\eta = \frac{-\pi H^2}{4L \sinh\left[\frac{4\pi h}{L}\right]} \tag{32}$$

By calculating the wave height distribution across shore at every time-step in the model, a quasi-stationary approach is implied in which it is assumed that the input wave height changes at a time scale significantly longer than the wave period.

401. Energy dissipation by bottom friction is calculated in the model as done by Dally (1980) using linear wave theory to determine the horizontal component of the wave orbital velocity at the bottom and assuming a shear stress proportional to the horizontal velocity component squared. After the waves break, energy dissipation greatly increases due to the generation of turbulence. In the surf zone, energy dissipation produced by breaking is considerably larger than dissipation due to bottom friction.

Transport Rate Equations

402. The distribution of the transport rate was calculated using relationships developed for the four different zones of the profile described in Part V. In the surf zone, i.e., the region of breaking and broken waves, the distribution of the transport rate is mainly a function of the energy dissipation per unit volume. Seaward and shoreward of the surf zone, semi-empirical relationships derived from the LWT experiments are applied to calculate the transport rate distribution. The magnitude of the transport rate in all transport zones is governed by that calculated for the part of the surf zone where broken waves prevail (Figure 43, Zone III).

403. The direction of net cross-shore transport is determined in the model by the criterion described in Part IV, which is based on the deepwater wave steepness and the dimensionless fall velocity (Equation 2). Although the criterion was developed to predict formation of bar and berm profiles, examination of associated cross-shore transport rate distributions showed that this relation was applicable to predict the direction of net transport as well. Onshore transport is predominant if a berm profile is formed, whereas offshore transport is predominant if a bar profile is formed. According to the criterion, material is transported offshore or onshore along the full length of the active profile at a specific instant in time. This is a good approximation if the profile is not too close to the equilibrium shape for the existing incident waves, in which case the transport rate would tend to be mixed, i.e., both onshore and offshore transport might occur along different regions of the profile at the same time. If the model is applied to field conditions, the mean wave height should be used to determine the direction of transport by Equation 2. (As discussed below, significant wave height should be used to calculate the breaking waves and transport rate.)

404. Both Moore (1982) and Kriebel (1982) used transport rate formulas for the surf zone in which the rate was proportional to the excess energy dissipation per unit volume over an equilibrium energy dissipation which the beach profile could withstand without changing shape significantly. Dean (1977) showed that an equilibrium profile derived from the concept of a constant energy dissipation per unit water volume from the break point and

onshore corresponded to a shape governed by a power law with an exponent of 2/3 (Equation 1). The relationship between excess energy dissipation per unit volume and transport rate in zones of broken waves was verified in Part V using wave and profile change data from the CRIEPI experiments.

405. In the profile change model, a transport relationship similar to that used by Moore (1982) and Kriebel (1982) is applied in a region of fully broken waves (Zone III) with a term added to account for the effect of local slope. A steeper slope is expected to increase the transport rate down the slope. The modified relationship for the transport rate q is written

$$q = \begin{cases} K\left(D - D_{eq} + \frac{\epsilon}{K}\frac{dh}{dx}\right) & D > D_{eq} - \frac{\epsilon}{K}\frac{dh}{dx} \\ 0 & D < D_{eq} - \frac{\epsilon}{K}\frac{dh}{dx} \end{cases} \tag{33}$$

where

K = empirical transport rate coefficient

D = wave energy dissipation per unit volume

D_{eq} = equilibrium energy dissipation per unit volume

ϵ = transport rate coefficient for the slope-dependent term

The energy dissipation per unit volume is given from the change in wave energy flux (Equation 27) as

$$D = \frac{1}{h}\frac{dF}{dx} \tag{34}$$

406. Equation 33 indicates that no transport will occur if D becomes less than D_{eq}, corrected with a slope-dependent term. D can become less than D_{eq} due to a variation in water level. For example, if a well-developed bar forms, waves will break seaward of the bar crest, but a water level increase would make the depth inshore sufficiently large to decrease D below D_{eq} without wave reformation occurring. In this case, q becomes zero.

407. As previously described, the transport direction is determined by an empirical criterion (Equation 2) and the magnitude by Equation 33. If D were allowed to become less than D_{eq}, Equation 33 would predict a reversal

in sand transport, which might be in conflict with the imposed criterion specifying transport direction. Furthermore, in such a case, the magnitude of sand transport would increase as D decreased to reach a maximum if no energy dissipation occurred. This is an incorrect description of what is expected to occur, since a cutoff energy dissipation exists under which no sand transport takes place. (See Kraus and Dean (1987) and Kraus, Gingerich, and Rosati (1989) for empirical evidence of an effective cutoff in longshore sand transport in the surf zone.) Consequently, the logical decision is to set q to zero if D falls below D_{eq}. Also, from Figure 48 it can be inferred that the transport rate is small if D approaches D_{eq} (the situation distant from the break point).

408. Physically, the equilibrium energy dissipation represents a state in which the time-averaged net transport across any section of the beach profile is zero. The equilibrium energy dissipation may be expressed in terms of the beach profile shape parameter A in the equilibrium profile equation (Equation 1) according to

$$D_{eq} = \frac{5}{24} \rho g^{3/2} \gamma^2 A^{3/2} \tag{35}$$

where γ is the ratio between wave height and water depth at breaking (breaker index, H_b/h_b). In the derivation of Equation 35, Dean (1977) assumed that the wave height existed in a fixed ratio with the water depth in the surf zone.

409. From Equation 34 it may be deduced that D inherently contains a term proportional to the beach slope. The reason for incorporating an explicit slope dependent term in the transport relationship (Equation 33) is that regression analysis showed a dependence of q on slope for some of the cases analyzed in Part V. Also, numerical stability of the model was improved by inclusion of this term, as will be discussed below. Dean (1984) also modified the equilibrium energy dissipation by reducing it depending on the ratio between the local beach slope and the limiting slope for the sand surface, thus including a further slope dependence (cf. Watanabe 1985).

410. As discussed in Part V, the value of the transport rate coefficient K determined by comparison of calculated energy dissipation per unit

volume from measured wave heights and inferred or "measured" transport rates from the LWT data was about 1.1 10^{-6} m^4/N. In contrast, Moore (1982) and Kriebel (1982) obtained a value of 2.2 10^{-6} m^4/N by making comparisons between calculated and measured profile change. This value was revised by Kriebel (1986) to become 8.7 10^{-6} m^4/N. The coefficient K is not entirely comparable between the models, since the structures of the models are different. The value of ϵ was found to be on the order of 0.0006 m^2/sec (Part V).

411. The equilibrium energy dissipation was determined by Moore (1982) by fitting Equation 1 to 40 field and laboratory profiles. Beach material ranged in size from boulder (30 cm) to fine sand, and D_{eq} was related to the mean sand diameter. Moore's analysis provided the best fit to profiles both with and without bars. These values were used in the numerical model and found to give reasonably accurate estimates of D_{eq} in regions of broken waves. However, in the present study, in order to obtain optimal agreement between model simulations and measured profile change, values of D_{eq} as specified by Moore had to be reduced by 25 percent, as discussed later.

412. By adding the slope term in Equation 33, the shape of the equilibrium profile will be somewhat gentler, since a profile with a specific grain size will be able to withstand a lower energy dissipation per unit volume. The shape of the equilibrium profile, derived from Equation 33 in analogy to Dean (1977), may be written

$$h\sqrt{h} + \frac{\epsilon}{K}\frac{24}{5\rho g^{3/2}\gamma^2} = A^{3/2}\,x \qquad (36)$$

413. In Equation 36 water depth is an implicit function of the cross-shore distance. The effect of incorporating beach slope is only noticeable close to the shoreline for the values of ϵ used in the model. Further seaward the profile agrees with Dean's (1977) equilibrium profile.

414. In the numerical model, regions of fully broken waves are identified at each time-step, and transport rates are determined from Equation 33. Waves are considered to be fully broken from the plunge point to the shoreward end of the surf zone or to the point where wave reformation occurs. The location of the plunge point is defined with respect to the break point to

give the "plunge length." Galvin (1969) estimated the plunge length ℓ_p to be about four times the breaking wave height, showing a dependence upon beach slope $\tan\beta$, where a steeper beach implied a shorter plunge length for the same breaking wave height. The equation given by Galvin (1969) is

$$\frac{\ell_p}{H_b} = 4.0 - 9.25 \tan\beta \tag{37}$$

415. Equation 37 was tested for predicting the plunge length but gave unrealistically short distances for steep bar face slopes. Therefore, in the numerical model an overall value of three times the breaking wave height is used to estimate the plunge distance (see Singamsetti and Wind 1980, Svendsen 1987).

416. For the region seaward of the break point, the transport rate distribution is well approximated by an exponential decay with distance (Equation 21). For offshore transport the spatial decay coefficient is a function of the breaking wave height and grain size (Equation 22), whereas for onshore transport the decay coefficient is effectively constant.

417. For the relatively short region extending from the break point to the plunge point, an exponentially decaying transport rate is also used but with a smaller value of the spatial decay coefficient. Analysis of available data from the LWT experiments indicated the value of the spatial decay coefficient to be approximately 0.20-0.25 that of the spatial decay coefficient applicable seaward of the break point. A multiplicative factor of 0.20 is used in the numerical model to compute the spatial decay coefficient in the zone between the break point and the plunge point. The magnitude of the transport rate at the plunge point is determined from Equation 33, and seaward from this point the transport rate is calculated from the exponential decay functions.

418. The transport rate distribution on the foreshore is approximated by linear decay with distance from the end of the surf zone (Part V). The slope of the transport rate distribution on the foreshore decreases with time as the profile approaches equilibrium shape in the surf zone. Profiles generated in the LWT that either eroded or accreted exhibited this linear

behavior, implying a foreshore which receded or accreted uniformly along its full length. In the model, the transport rate is linearly extended from the end of the surf zone to the runup limit. (The surf zone is arbitrarily ended at a depth of 0.3-0.5 m.) However, as the foreshore erodes, the slope steepens and a pronounced scarp or step develops. Eventually, if erosive waves act for a sufficiently long time, the slope of the step will exceed the angle of initial yield (Allen 1970). In Part IV, time evolution of profile slopes was analyzed and indications of avalanching were found if profile slopes exceeded a value of 28 deg on average. This value is used in the numerical model to limit the growth of slopes along the profile.

419. Since the transport relationships do not explicitly describe avalanching, an algorithm was developed to simulate avalanching if the profile slope steepened excessively. If the angle of initial yield is exceeded, the profile slope decreases to a lower, stable value known as the residual angle after shearing (Allen 1970). Inspection of the LWT profiles indicated that a stable slope appeared to be reached at a value somewhat smaller than 22 deg on average. In the numerical model the residual angle after shearing was therefore set to 18 deg. The reason for this ambiguity was the difficulty of determining the residual angle after shearing from the profile data; instead, Allen's experimental results were used where the dilatation angle (difference between angle of initial yield and residual angle after shearing) was found to be in the range of 10-15 deg for sand. A dilatation angle of 10 deg was chosen, implying a residual angle after shearing of 18 deg.

420. If avalanching occurs in the numerical model, that is, if the angle of initial yield is exceeded, sand is redistributed into neighboring cells so that the slope adjusts to the residual angle after shearing. Once avalanching has started in one cell, it proceeds along the grid until a point is reached where the slope is less than the residual angle after shearing. A definition sketch is shown in Figure 56 illustrating a number of calculation cells and one cell where the angle of initial yield is exceeded (cell 1). Depths after avalanching, denoted with a prime in Figure 56, can be determined once the change in depth in the cell where avalanching is initiated is known. The change in depth in the first cell is given by

$$\Delta h_1 = -\left[\frac{N-1}{N}\right] h_1 + \frac{1}{N} \sum_{i=2}^{N} h_i + \frac{1}{2}(N-1)\Delta h \qquad (38)$$

where

h_1 = depth in the first cell where angle of initial yield is exceeded

N = number of cells where sand is to be redistributed

h_i = depth in cell i

Δh = difference in depth between two neighboring cells as given by the residual angle after shearing

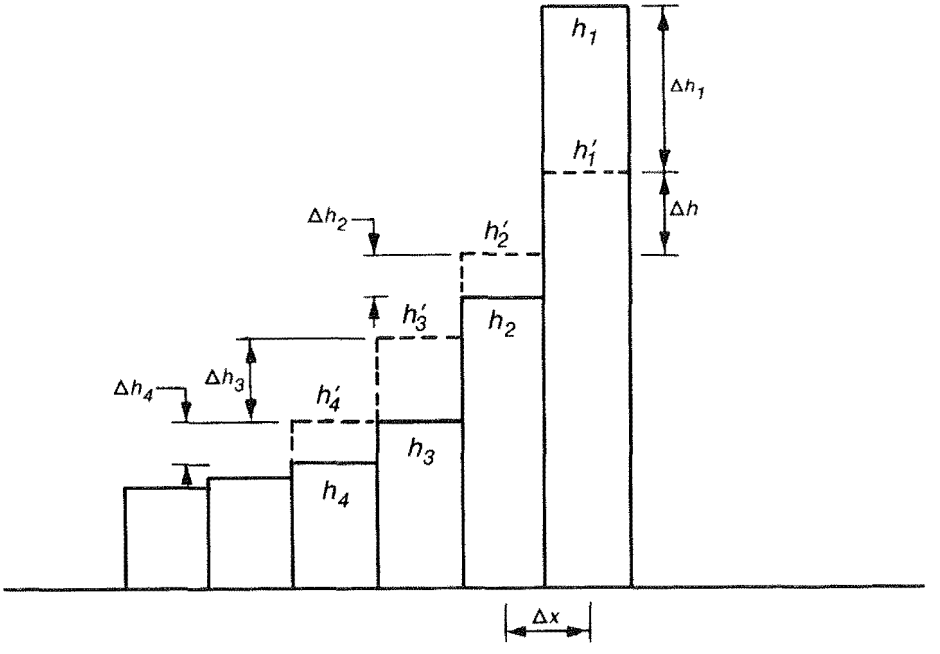

Figure 56. Definition sketch for describing avalanching

421. After the depth change in the first cell has been determined according to Equation 38, depth changes Δh_i in neighboring cells are given by the following expression

$$\Delta h_i = h_1 + \Delta h_1 - h_i - (i-1)\,\Delta h \qquad (39)$$

where the index i refers to the cell number counting consecutively from the starting point of the avalanching in the direction of avalanching. The number of cells N that the avalanching will affect is not known a priori and has to be determined iteratively as more cells are incorporated in the calculation until the slope between cells N and N+1 is less than the residual angle after shearing. The avalanching routine limits the growth of the step and prevents the shoreward slope of a bar from becoming too steep.

Profile Change Model

422. Changes in the beach profile are calculated at each time-step from the distribution of the cross-shore transport rate and the equation of mass conservation of sand. The equation of mass conservation is written as

$$\frac{\partial q}{\partial x} = \frac{\partial h}{\partial t} \tag{40}$$

423. Standard boundary conditions in the model are no sand transport shoreward of the runup limit and seaward of the depth where significant sand movement occurs. The runup height is determined from an empirical expression, Equation 17, derived from the LWT experiment data relating the height of the active profile to the surf similarity parameter and the deepwater wave height. The depth of significant sand movement is determined through the exponential decay of the transport rate with distance seaward from the break point. If the transport rate decreases to a small predetermined value, the calculation stops, and the transport rate is set to zero at the next cell, making that cell the seaward boundary. An expression presented by Hallermeier (1984) for the seaward limit depth was investigated for use in the model. However, this equation failed to predict what were considered to be reasonable closure depths on a wave-by-wave basis, evidently because the formula was developed for extreme annual events. Also, apparently because of the limited range of values from which the equation was derived, the closure depth was found to be too shallow for profiles exposed to the very steep waves that were used in some of the LWT cases.

424. In calculation of the wave height distribution across shore at a specific time-step, the beach profile from the previous time-step is used, and the transport rates are calculated explicitly. The mass conservation is written in difference form as

$$\frac{h_i^{k+1} - h_i^k}{\Delta t} = \frac{1}{2}\left[\frac{q_{i+1}^{k+1} - q_i^{k+1}}{\Delta x} + \frac{q_{i+1}^{k} - q_i^{k}}{\Delta x}\right] \tag{41}$$

where k denotes the time level and i the cell number over which the discretization is carried out.

425. The equation of mass conservation is discretized over two time levels using transport rates evaluated at the present and previous time-step. To obtain a realistic description of the wave height distribution across highly irregular profiles exhibiting bar formations, a moving average is used to obtain representative depth values. Averaging of the profile depth, carried out over a distance of three breaking wave heights as determined from Equation 25, was found to make the model numerically more stable. If the wave calculations are not based on a beach profile which has been filtered to some degree, the wave height will respond in an unrealistic manner to small changes in the profile. The beach profile generated with the moving average scheme is used only for calculation of the wave height distribution, and no changes in the profile itself are made.

426. Since the transport rate distribution is determined using various relationships in various regions of the profile, the derivative of the transport rate may be discontinuous at inter-region boundaries. To obtain a smoother transport rate, a three-point weighted filter is applied to the calculated transport rates. The wave height distribution is calculated explicitly in a manner similar to that of Dally (1980), proceeding from the most seaward cell onshore until the end of the surf zone is detected. The advantage of using an explicit solution scheme is that it easily allows description of initiation of breaking, switching to the breaker decay model, and reformation of broken waves. Use of an implicit solution scheme would considerably complicate the calculation and require an iterative procedure

since the location of the break point and any point where wave reformation occurs are not known a priori.

427. The slope-dependent term in Equation 33 improves numerical stability of the model. Some simulations performed omitting this term experienced numerical oscillation at the shoreward bar face as the slope grew steep and the trough became more pronounced. The slope-term tends to flatten the trough, since the transport rate at the shoreward bar face is reduced.

428. The numerical scheme proved to be very stable under a wide range of conditions in spite of the irregular bathymetry that occurs if bars are formed. Typical length and time-steps used in the model are Δx = 0.5-5.0 m and Δt = 5-20 min. The length step has to be chosen so as to resolve the main morphologic features. A shorter length step requires a correspondingly shorter time-step to maintain numerical stability. An effort was made to derive an explicit stability criterion but was not successful. Therefore, at the present time, trial and error must be used to determine appropriate values of Δx and Δt for the particular application.

429. For a beach profile exposed to constant wave and water level conditions, the profile shape predicted by the model approaches a steady-state, resulting in an equilibrium profile. The approach to equilibrium is controlled by the rate at which energy dissipation in the surf zone attains the equilibrium value D_{eq} . A bar, if formed, causes the break point to translate in the seaward direction as it grows, making the offshore boundary of the surf zone move accordingly. At equilibrium, the break point is stationary and the energy dissipation per unit water volume is constant throughout the surf zone, being approximately equal to D_{eq} , corrected by the slope-dependent term in Equation 33.

Calibration and Verification

430. The numerical model was applied to simulate beach profile evolution for a number of erosional cases from the LWT experiments. As an objective criterion for judging agreement between the simulated and measured beach profile, the sum of squares of the difference of measured and calculated depths was formed according to

$$R = \sum_{i=1}^{N_p} (h_i^m - h_i^c)^2 \tag{42}$$

in which the superscripts m and c refer to measured and calculated profile depths, respectively, and N_p is the number of data points. Values of different model parameters were varied to minimize the sum of the squares. In the calibration process, equal weight was placed on all measurement points along the profile without bias toward bars or eroded areas on the foreshore. Furthermore, the model was restricted to generating one breakpoint bar to limit the effort to reproducing the main breakpoint bar in the calibration. The volume of the main breakpoint bar was always at least ten times greater than that of any secondary inshore bar, thus being significantly more important for determining the wave height distribution across shore.

431. In simulation of beach and dune erosion, it is considered most important to predict the evolution of the main breakpoint bar, since this feature serves as a natural defensive response for reducing incident wave energy that would otherwise arrive at the beach face. Only a small amount of information was available from the LWT data set to quantify the net cross-shore transport rate in zones of wave reformation. As an exercise of the model, simulations to reproduce the inshore bar are presented below. It was necessary to make assumptions on the net transport rate between zones of fully broken waves for these simulations.

432. It is desirable to relate empirical parameters in the model directly to physical quantities or assign them a constant value to minimize the degrees of freedom in the calibration process. For instance, values recommended by Dally (1980) were used in the breaker decay model, i.e., a stable wave height coefficient of $\Gamma = 0.40$ and a wave decay coefficient of $\kappa = 0.17$. (The optimum value of the wave decay coefficient was modified slightly by Dally, Dean, and Dalrymple (1985a) to 0.15.) Although parameters in the breaker decay model showed a qualitative dependence on average beach slope in breaking wave data from the CRIEPI experiments, the above-mentioned constant values were used in the calibration. The number of parameters available for adjustment in the calibration process was thereby reduced with

little loss of accuracy in determining an optimal calibration, since the minimum of the sum of squares in most cases was located in a rather flat region.

433. Based on preliminary calibration runs, the coefficient expressing the slope dependence of the transport rate (ϵ in Equation 33) was set to 0.001 m^2/sec. A smaller value of ϵ will allow the trough to be locally somewhat more pronounced, whereas a higher value will flatten the trough. The angle of initial yield was set to 28 deg according to slope behavior inferred from the LWT experiments, and the residual angle after shearing was set to 18 deg. A larger angle of initial yield will allow the profile slope to become steeper before avalanching occurs. During simulation of an erosional event in the LWT data, avalanching typically takes place on the foreshore step or on the shoreward side of the bar.

434. At the initial stage of model calibration, both K and D_{eq} in the transport equation (Equation 33) were used in the calibration procedure. The transport rate coefficient K was varied together with D_{eq} for 10 erosional cases. Although it was considered desirable to avoid using D_{eq} as a calibration parameter and instead determine its value from the design curve given by Moore (1982), it was found that in order to achieve best agreement between numerical model simulations and tank measurements, the value of D_{eq} had to be reduced. The equilibrium energy dissipation controls the amount of sand that is eroded before the equilibrium profile is attained. Moore's relationship was derived by a least-squares fit of a power curve (Equation 1) to beach profiles in general, making this method not entirely compatible with the concept of regions with different transport rate relationships used in the present numerical model. In most cases, the parameter combination which gave the minimum sum of squares was located in the vicinity of an equilibrium energy dissipation value of about 75 percent of that obtained by Moore's relationship. This fixed reduction (0.75) of the equilibrium energy dissipation was applied in all cases, and the optimal value of the transport rate coefficient K was determined by minimizing the sum of the squares of depths.

435. Values of the transport rate coefficient for the 10 cases simulated which gave the best agreement between measured and simulated profiles varied in the range of 0.3 - 2.2 10^{-6} m^4/N, with an average of 1.4 10^{-6} m^4/N

for 10 separate optimizations. Most of the cases, however, had a value of K in the range of 1.1 - 1.9 10^{-6} m^4/N. The sum of squares was minimized with respect to all profiles measured during the particular case, typically encompassing 5-10 profile surveys per case. Figure 57 shows a representative calibration run with the numerical model and a comparison with the measured beach profile from the last profile survey of the simulated case (Case 6-1). Beach profiles at selected time-steps from the model calculations are shown together with the wave height distribution calculated at the last time step. The optimal K-value for this case was 1.9 10^{-6} m^4/N. As seen in Figure 57, bar formation (size and location) and the amount of erosion on the foreshore were well described by the numerical model. The small inshore bar was purposefully neglected in the calibration simulation. This feature appeared in the LWT experiment after 40 hr of run time, just prior to the last profile survey. Measured wave heights are shown across the profile, indicating that the wave height distribution was satisfactorily reproduced by the breaker decay model.

436. Transport rate distributions calculated at selected times are shown in Figure 58. The magnitude of the transport rate decreased with time as the profile approached an equilibrium shape in accordance with the behavior of transport rate distributions directly inferred from the profile survey data in Part V. Occasionally, the transport rate increased in the vicinity of the break point compared with previous distributions, caused by movement of the break point. As the break point moved offshore, energy dissipation increased because of the decrease in depth occurring at the plunge point, and the transport rate increased accordingly.

437. It was not possible to relate K obtained from individual calibrations to wave or sand characteristics with any significance for the number of cases available for study. Qualitatively, the transport rate coefficient seemed to decrease with increasing grain size and increase with decreasing wave period. A wave period dependence of the profile time response was also shown in the analysis in Part V of peak net cross-shore transport rates calculated from the LWT data.

438. Since it was not possible to relate the transport rate coefficient to any physical property, it was desirable to achieve an optimal estimate of

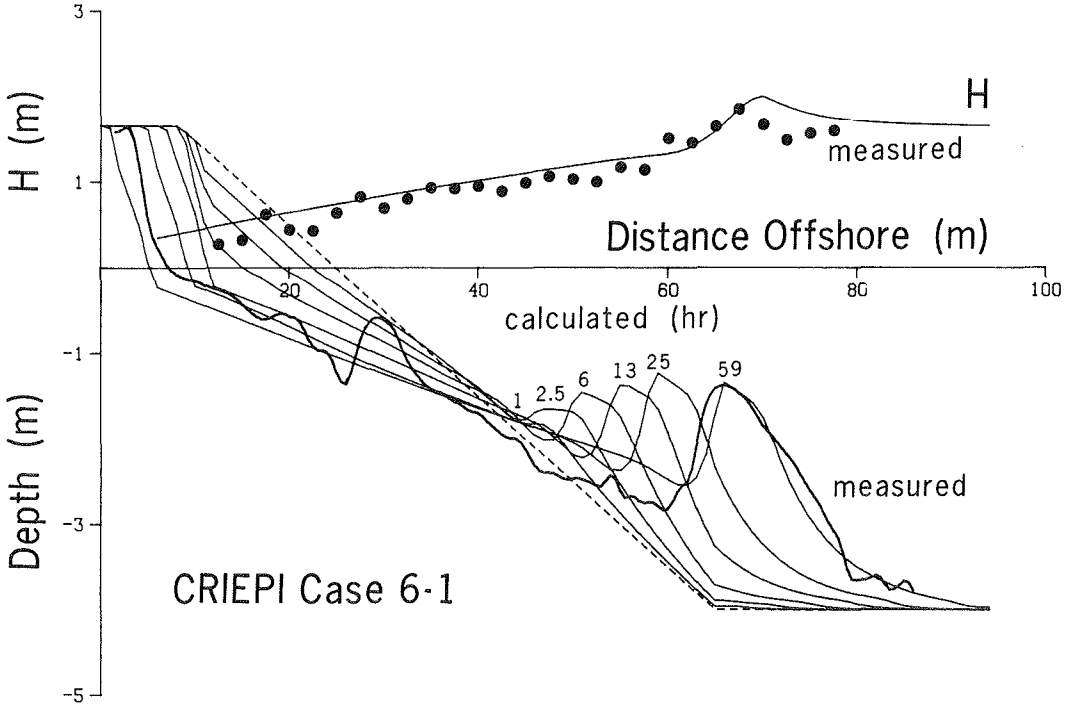

Figure 57. Calibration of numerical model

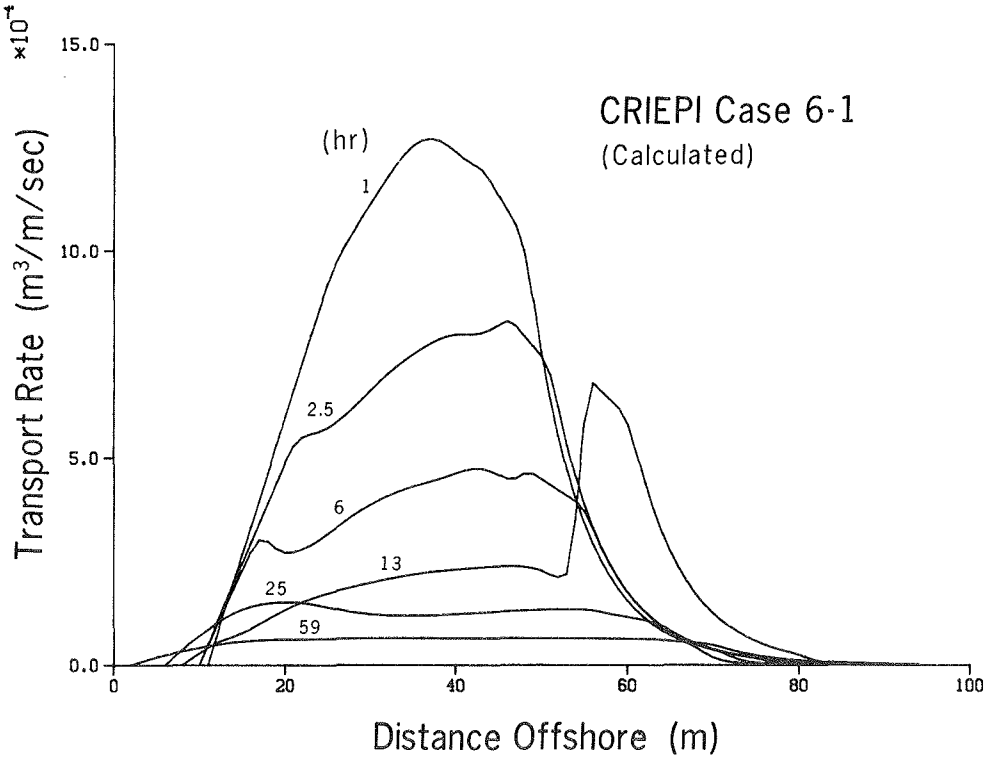

Figure 58. Net cross-shore transport rates at selected times

K for use in simulating all cases. To obtain best overall agreement between simulated and measured profiles with constant K , the model was calibrated for seven of the cases with respect to the total sum of squares. After the optimal value had been determined for K , the model was verified through use of two independent cases. One case (Case 700 with $K = 0.3\ 10^{-6}\ m^4/N$) was eliminated from the overall calibration process since water was released from the tank during the run (probably to reduce wave overtopping), lowering the water level by 0.3 m, thus contaminating the case for the purpose here (see Kraus and Larson 1988a). The sum of squares of the difference in depth between measured and simulated beach profiles was calculated for all profile surveys for all seven cases. Figure 59 illustrates the total sum of squares for all cases as a function of the transport rate coefficient. A minimum occurred around the coefficient value $1.6\ 10^{-6}\ m^4/N$.

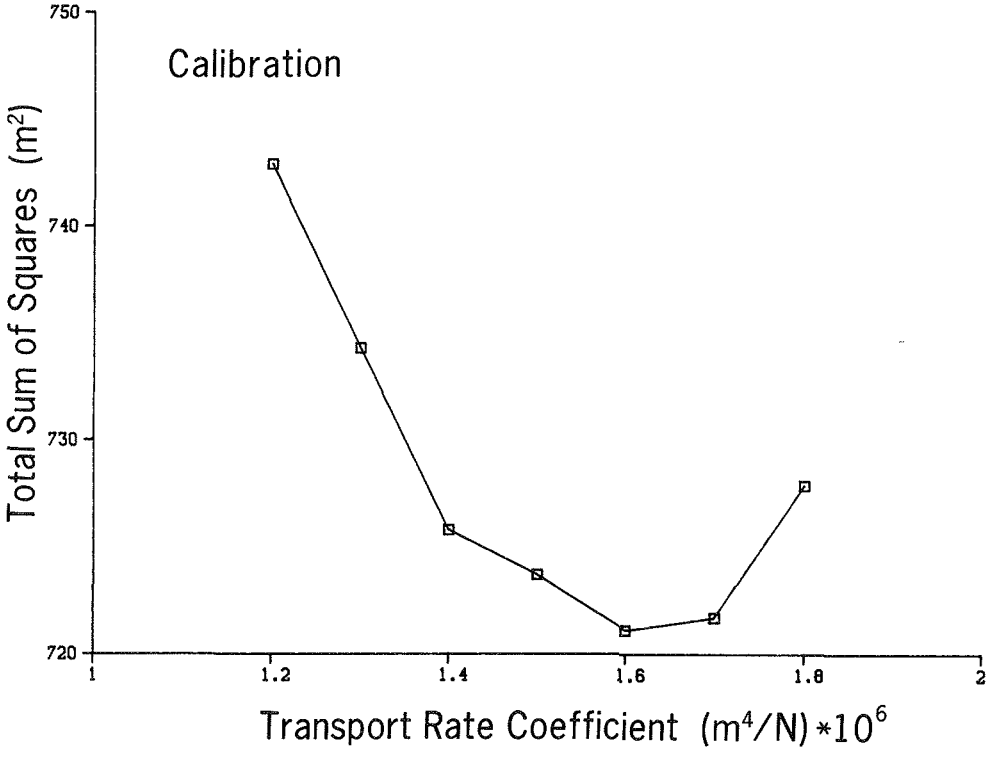

Figure 59. Optimization for model calibration

439. Two cases, one from the CE data set (Case 400) and the other from the CRIEPI data set (Case 6-2), were used to verify the applicability of the numerical model with parameter values obtained from the calibration. Figure 60(a and b) shows the results of the verification runs, illustrating the development in time of the beach profile together with a comparison with the measured profile at the last time-step. The wave height distribution across shore at the last time-step is also shown. The volume of the main breakpoint bar and the amount of erosion on the foreshore are rather well predicted by the numerical model. However, the crests of the bars are located somewhat too far seaward, whereas the trough is not deep enough for Case 400. In general, the trough is not well reproduced in the numerical model, being less pronounced than for the measurements, since the slope term in the transport equation (Equation 33) counteracts the seaward transport of sand on the shoreward side of the bar. Elimination of the slope term, however, seriously affects numerical stability, resulting in a much shorter allowable time-step in relation to the length step.

Summary

440. The developed numerical model was calibrated and verified to simulate erosional (bar-type) profiles with relatively little ambiguity in determining values of the required empirical coefficients. In particular, the time rate of growth, volume, and location of the main breakpoint bar were well reproduced. The location of the shoreline and the steep slope of the foreshore step were also well simulated. Inclusion of avalanching was needed to restrict bottom slopes to within measured angles, and an explicit slope-dependent contribution to the transport rate was found to greatly improve stability of the model.

441. Importantly, in all tests run with constant incident wave conditions and water level, the calculated profile approached an equilibrium form. This property is highly desirable to represent the proper time scale of profile change and to use the model in an arbitrary situation without the problem of numerical stability. Sensitivity analysis of the model is described in the next chapter.

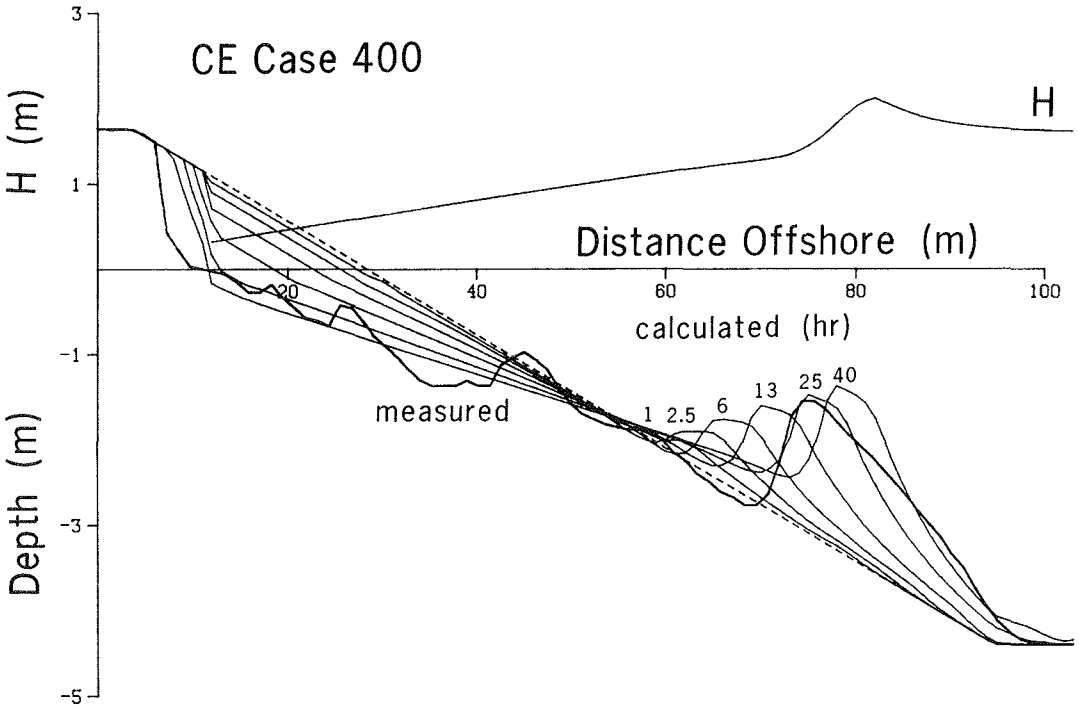

a. Case 400

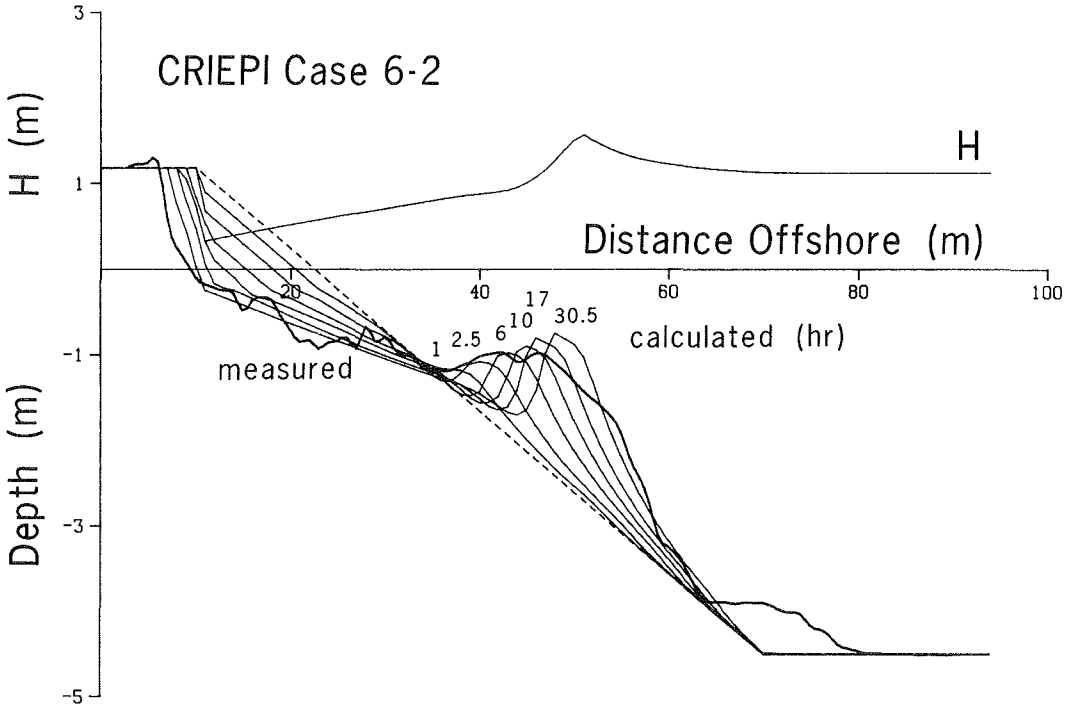

b. Case 6-2

Figure 60. Verification of numerical model

PART VII: APPLICATIONS OF THE NUMERICAL MODEL

442. The numerical model developed in this study and its calibration are described in Part VI. The model was calibrated by comparison to the large data base of LWT experiment results obtained by using constant waves and water level. In this chapter, sensitivity analysis is conducted with respect to a number of model parameters to evaluate their influence on the calculated results. Predictions of the model are examined for a variety of hypothetical cases, including varying wave and water level conditions. Consideration is also given to simulation of multiple bars. The model is then put to the severe test of reproducing beach profile change, in particular, bar movement in the field. Example applications of the model are made to investigate the effect of a vertical seawall on beach profile development, as well as initial adjustment of beach fill. Comparison with an existing model, the Kriebel model (Kriebel 1982), is made for a number of hypothetical conditions to evaluate the importance of bar formation on beach erosion. Finally, model simulations are made to qualitatively reproduce onshore sand transport and berm buildup.

Sensitivity Analysis of Model Parameters

443. A sensitivity analysis was performed to quantify the influence of various model parameters and empirical coefficients on simulation results. Sensitivity analysis gives valuable information about the physical implications of the model parameters and their relative effects on the result. It is important to explore the predictions of the model beyond the range in which it was calibrated to determine if expected and intuitively reasonable trends are obtained. In the following, the influence of principal model parameters on beach evolution is discussed mainly by reference to bar properties. To this end, the change in shape and size of the bar is investigated for a specific case (Case 401) under perturbations of optimal values of model parameters as determined by the calibration.

Influence of K

444. The empirical transport rate coefficient K (Equation 33) primarily governs the time response of the beach profile. A smaller value gives a longer elapsed time before equilibrium is attained, whereas a larger value produces more rapid evolution. However, K also influences equilibrium bar volume, as seen in Equation 36. Although Equation 36 was derived assuming uniform energy dissipation per unit volume everywhere in the surf zone and not just in zones of fully broken waves, it gives important qualitative information about the influence of K and ϵ . A smaller K-value implies a flatter equilibrium beach profile with correspondingly more sand to be moved from the inshore for a fixed initial profile slope before equilibrium is attained.

445. Figure 61 illustrates the growth of bar volume with time for different values of the transport rate coefficient. For K = 2.2 10^{-6} m^4/N, more than 90 percent of the equilibrium bar volume was reached after 20 hr, whereas for K = 0.4 10^{-6} m^4/N only approximately 30 percent of the final bar volume was reached. The dependence of equilibrium bar volume on K is introduced through the slope term in the transport equation. Without this term the shape of the equilibrium beach profile would be independent of K , and this coefficient would only influence the time response of the profile.

446. Calculated maximum bar height (defined with respect to the initial plane beach profile) as a function of time is shown in Figure 62 for various K-values. Maximum equilibrium bar height was insensitive to the value of K . However, as expected, time evolution of the bar height is controlled by K , showing a more rapid change for larger values. The location of the mass center of the bar was only slightly influenced by the value of K , with the mass center somewhat displaced shoreward when the value of K was decreased.

Influence of ϵ

447. The empirical coefficient ϵ in the slope term in Equation 33 mainly influences equilibrium bar volume and thus the amount of sand that is redistributed along the profile to reach equilibrium. Profile response was similar for quite different values of ϵ during the initial phase of the simulation and differed only after longer elapsed times (Figure 63). Equation 36 indicates that a smaller ϵ-value implies a steeper equilibrium beach profile and less sand to be moved before a state of equilibrium occurs. The effect of the slope term on maximum bar height was weak, where a change in

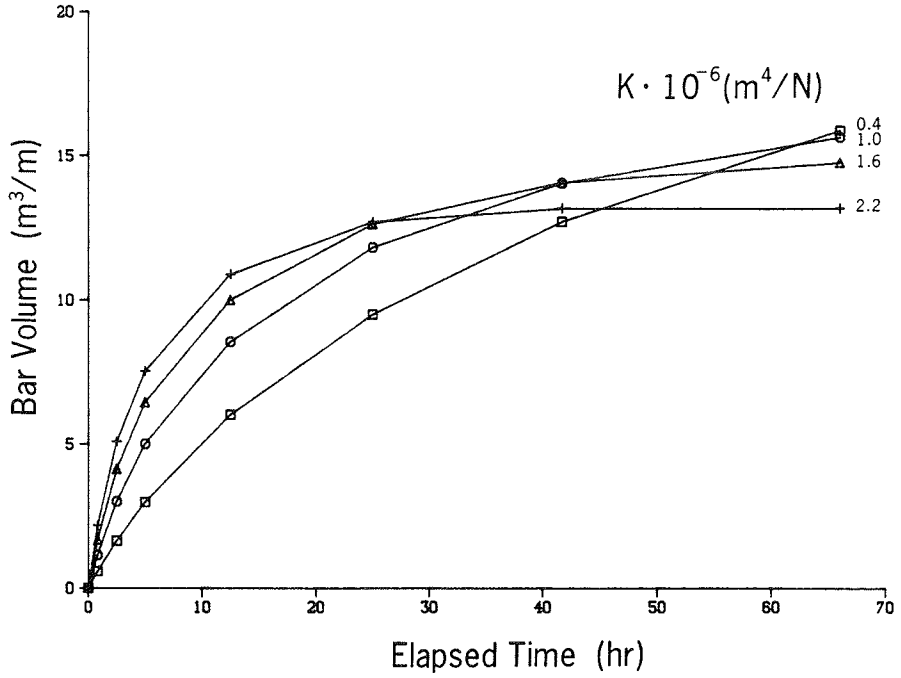

Figure 61. Effect of K on bar volume

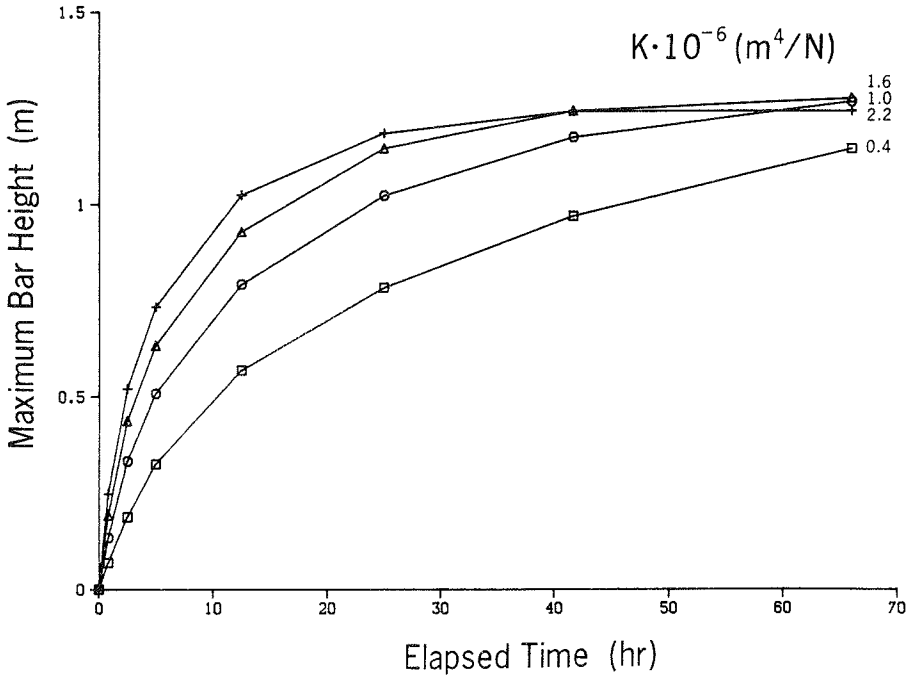

Figure 62. Effect of K on maximum bar height

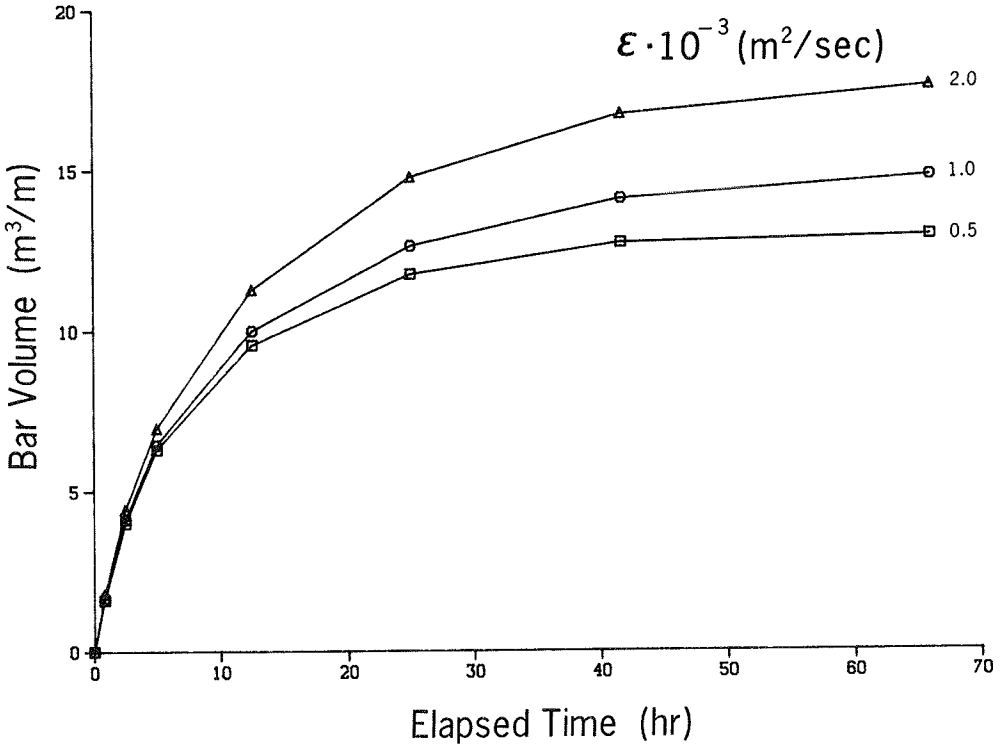

Figure 63. Effect of ϵ on bar volume

ϵ by a factor of four gave a corresponding change in the equilibrium maximum bar height of less than 10 percent. Similarly, the location of the bar mass center was found to have a weak dependence on changes in ϵ .

Influence of wave model parameters

448. Parameter values in the breaker decay model were specified in the calibration procedure as suggested by Dally (1980). To quantify the importance of variations in the wave height calculation, the wave decay coefficient κ in Equation 26 was varied. Figure 64 illustrates the growth of bar volume as a function of time for various values of κ . A smaller value of κ implied a larger equilibrium bar volume, although the time responses were similar at the very beginning of a simulation. As theoretical background it proves valuable to digress and examine the shape of the equilibrium beach profile exposed to a wave height distribution which fulfills the breaker decay model developed by Dally (1980).

449. Dally, Dean, and Dalrymple (1985a, b) presented analytical solutions for the cross-shore distribution of wave height for simple beach profile

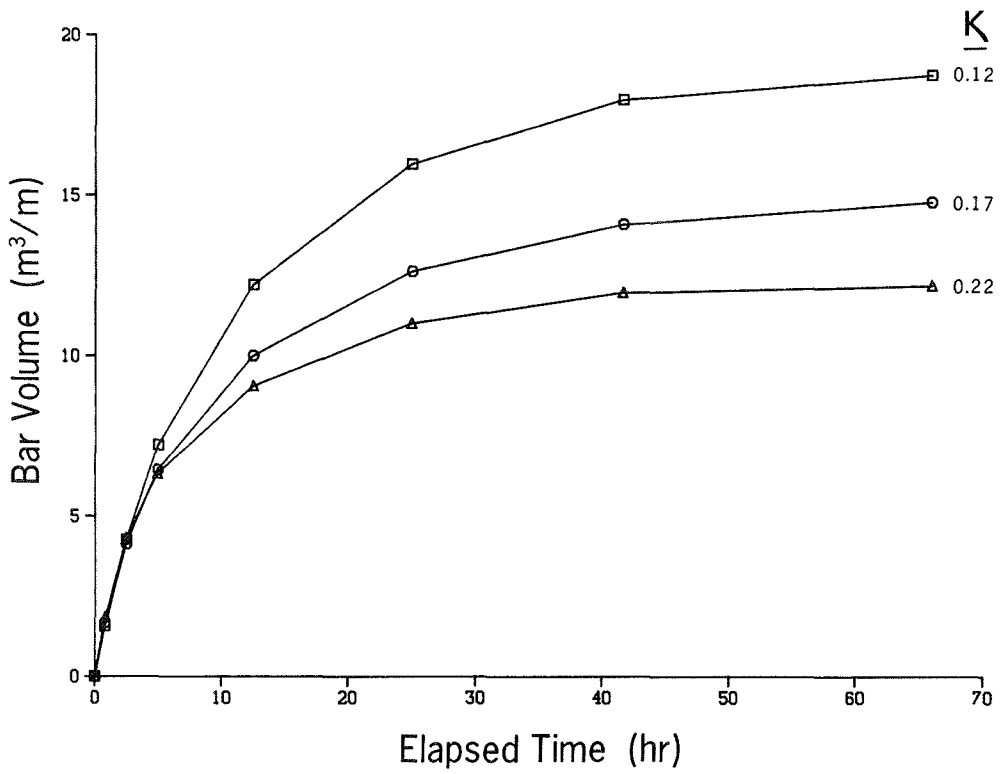

Figure 64. Effect of κ on bar volume

shapes. However, these solutions did not fulfill the Dean criterion of equal energy dissipation per unit volume for equilibrium conditions to prevail on a beach. If the slope-dependent term in the transport equation (Equation 33) is dropped, it is possible to solve the coupled problem of requiring constant energy dissipation per unit volume subject to the Dally breaker decay model. The coupled system of equations consists of Equations 26 and 33, for which the slope term is neglected and D is set equal to D_{eq} according to

$$\frac{1}{h}\frac{dF}{dx} = D_{eq} \tag{43}$$

$$\frac{dF}{dx} = \frac{\kappa}{h}(F - F_s) \tag{44}$$

Note that here the x-axis originates from the shoreline, making Equation 44 differ in sign from Equation 26.

450. The depth of the beach profile is obtained as an implicit function of the location across shore according to

$$\left[\frac{2}{\kappa} + \frac{5}{3} \frac{\Gamma^2 \rho g^{3/2}}{8 D_{eq}} \sqrt{h} \right] h = x \tag{45}$$

The corresponding wave height distribution is given by

$$H = \left[\frac{8 D_{eq}}{\kappa \rho g^{3/2}} h^{3/2} + \Gamma^2 h^2 \right]^{1/2} \tag{46}$$

451. As seen from Equation 45, a smaller value of the wave decay coefficient κ gives a flatter shape of the equilibrium beach profile and thus requires redistribution of a greater amount of sand before equilibrium is attained. On the other hand, a smaller value of the stable wave height coefficient Γ gives a steeper equilibrium beach profile, resulting in a smaller equilibrium bar volume, since less material has to be moved from the inshore to attain equilibrium.

452. Figure 65 shows the effect on bar volume of varying the stable wave height coefficient, supporting the qualitative result as predicted by Equation 45. The influence of changes in parameter values in the breaker decay model on maximum bar height was less pronounced compared with the effect on bar volume. The stable wave height coefficient affected the equilibrium maximum bar height only slightly, and the development in time was very similar during the initial phase of a simulation. The wave decay coefficient had a somewhat greater influence on the equilibrium maximum bar height, in which a smaller value implied a larger bar height.

Influence of equilibrium energy dissipation

453. Equation 45 also reveals the importance of the magnitude of the equilibrium energy dissipation, which was shown to be a function of grain size by Moore (1982). A change in grain size causes a marked change in the shape

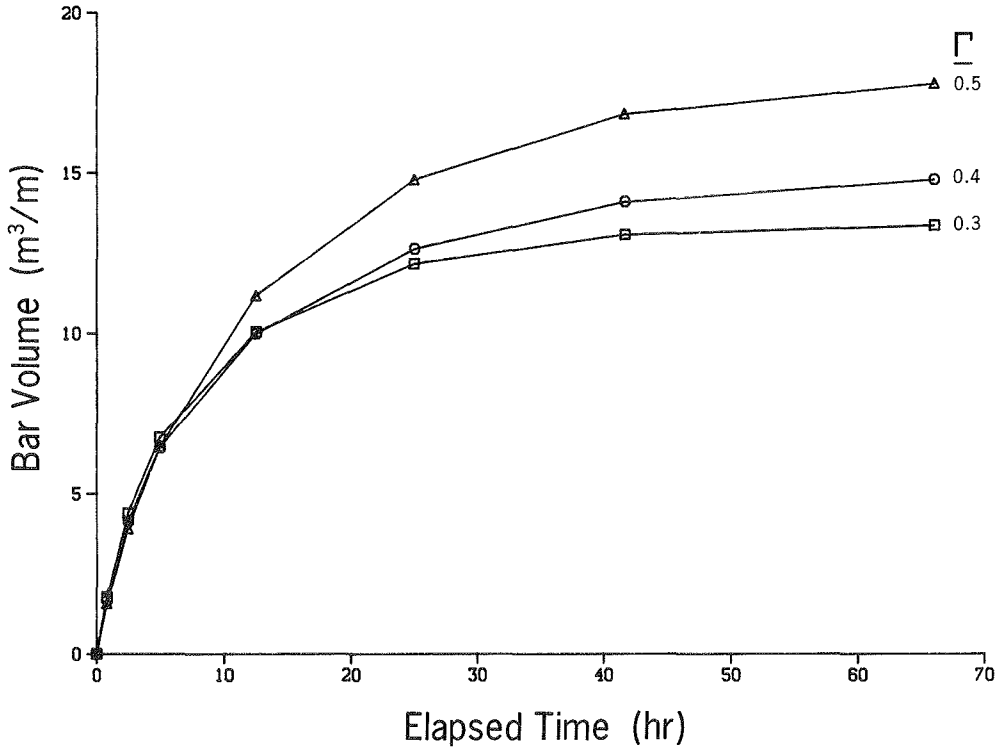

Figure 65. Effect of Γ on bar volume

and size of the bar, which is more pronounced for finer material. A smaller value of D_{eq}, occurring for finer grain sizes, corresponds to a flatter equilibrium beach profile, thus requiring more sand to be moved before equilibrium is attained.

454. Sensitivity of model predictions on grain size was investigated. Since equilibrium energy dissipation decreases rapidly with grain size (Moore 1982), bar volume correspondingly increases, as illustrated in Figure 66. (Values of D_{eq} used to obtain the curves in Figure 66 are 0.75 the value of those obtained by Moore (1982), according to the results of the model calibration in Part VI.)

455. Changing the median grain size from 0.50 to 0.40 mm increased the equilibrium bar volume by about 20 percent, whereas a decrease in median grain size from 0.40 to 0.30 mm gave an increase of about 90 percent. Corresponding changes in values of D_{eq} were 10 percent and 70 percent, respectively. Changes in maximum bar height were also significant as the grain size was decreased, although not as great as for bar volume.

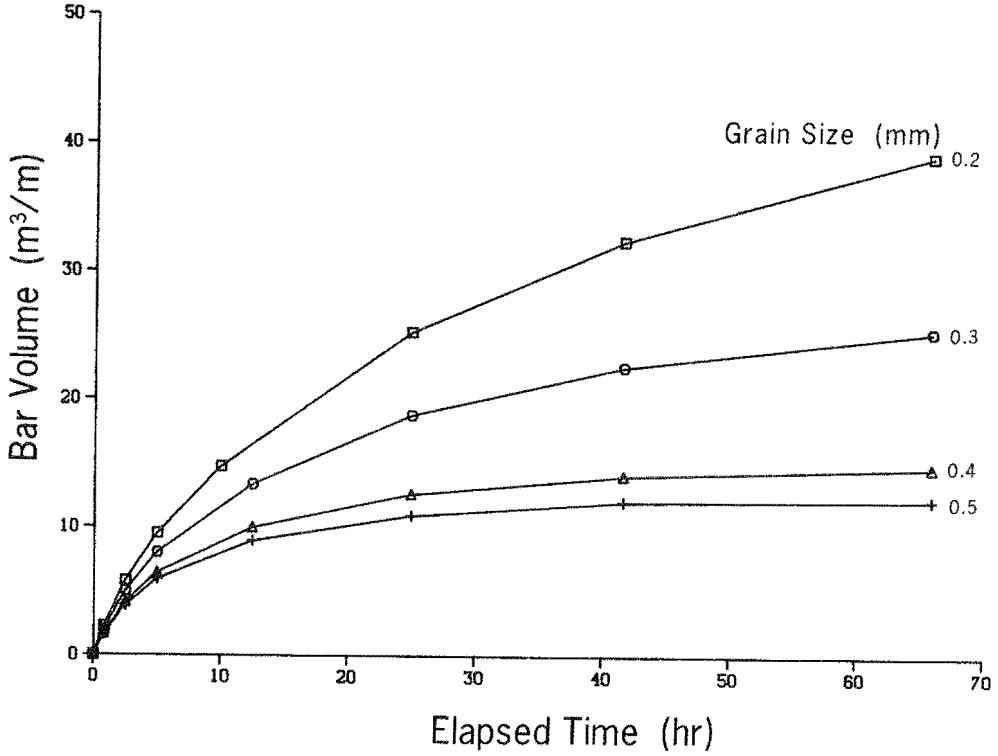

Figure 66. Effect of D on bar volume

456. Equilibrium maximum bar height increased by percentage values about half those of bar volume for the same changes in grain size. Movement of the bar center of mass was only slightly affected by changes in most model parameters. However, change in grain size did have a significant influence on the location of the center of mass, as seen in Figure 67. Initiation of bar formation occurred roughly at the same place, independent of grain size; however, after initiation, bar movement was considerably greater for the finer grain sizes.

457. Grain size also influences the spatial decay coefficient for the transport rate seaward of the break point (see Equation 22). The decay coefficient increases with grain size, implying that the transport rate decreases more rapidly, moving sand less seaward.

Influence of wave period and height

458. So far in the sensitivity analysis, only parameters which are expected to be effectively constant for a specific beach have been investigated. Since the driving force in the numerical model is wave breaking, it

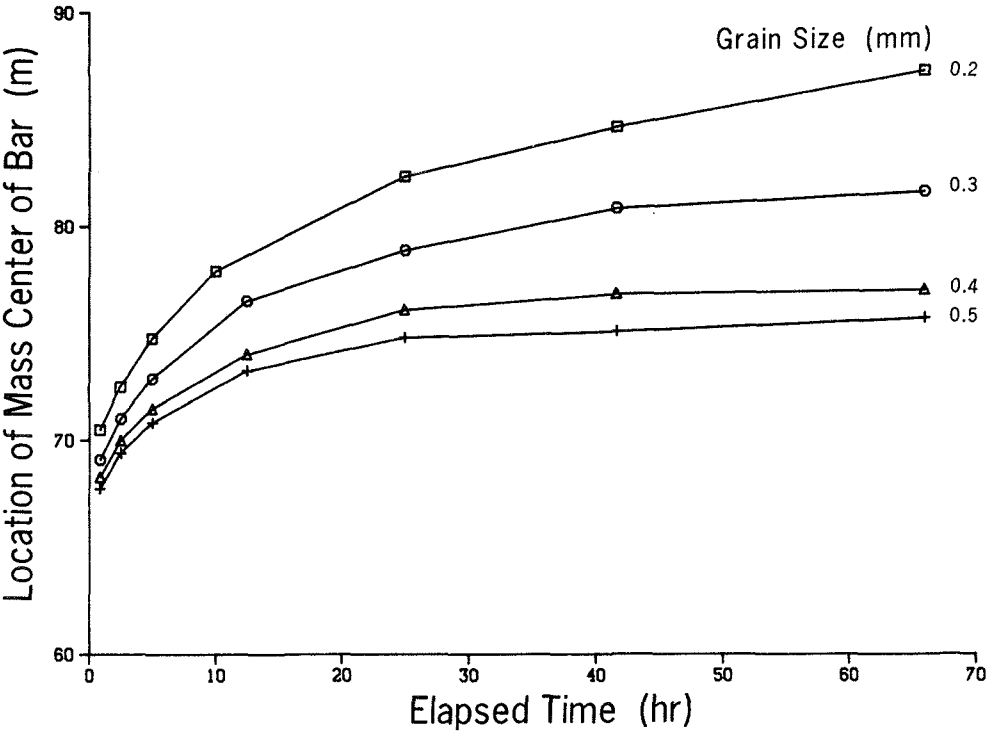

Figure 67. Effect of D on bar center of mass

is of considerable interest to analyze the response of the beach profile to changes in wave input parameters. Therefore, wave height and period were varied to investigate the sensitivity of the numerical model to changes in wave input.

459. An increase in wave period resulted in an increase in bar volume. Figure 68 shows the evolution in time of bar volume for various wave periods. Since small-amplitude wave theory for shallow-water conditions is applied in the numerical model, wave period does not enter explicitly in the shoaling calculation within the grid, but through shoaling from deep water to the seaward boundary of the grid and through the breaking wave criterion (Equation 24) (and, of course, in the criterion determining direction of transport, Equation 2). A longer wave period will allow a specific wave to shoal further inshore before it breaks, producing greater energy dissipation and moving more sand before equilibrium is attained. Maximum bar height was influenced by wave period in the same manner as bar volume; an increase in period gave a larger maximum bar height.

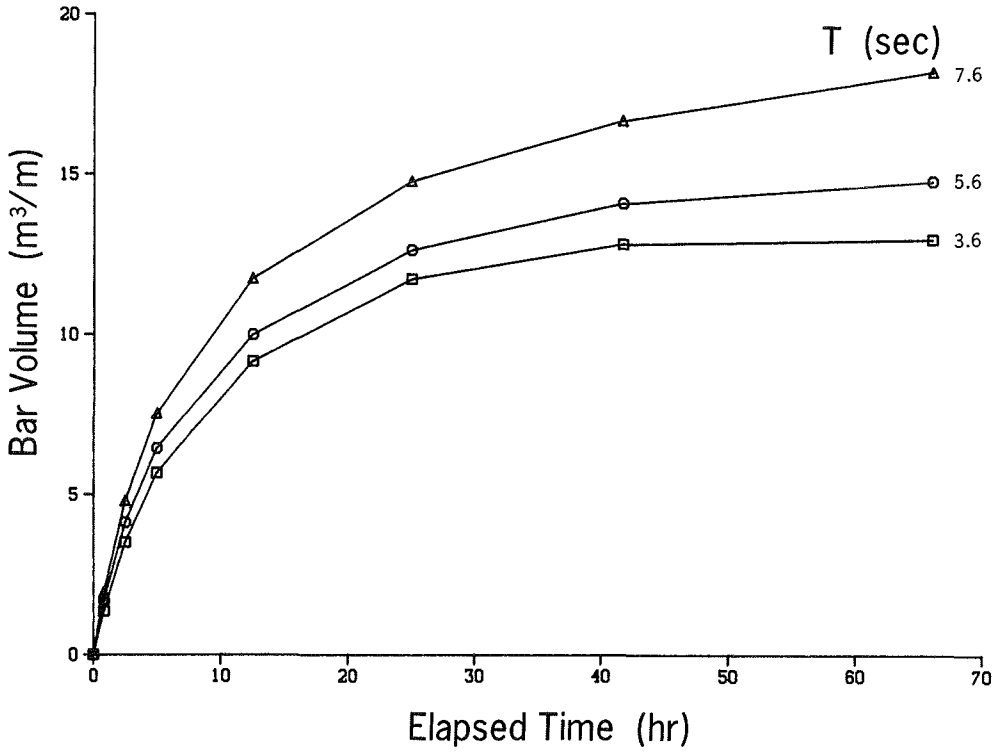

Figure 68. Effect of T on bar volume

460. The effect of an increase in wave height on bar properties is readily understood, since a larger wave height involves a larger amount of wave energy for the beach profile to dissipate in a state of equilibrium. Both equilibrium bar volume and equilibrium maximum bar height increased significantly as wave height increased.

Influence of runup height

461. The location of the shoreward boundary in the model is closely related to the runup height and can be predicted by an empirical relationship (Equation 17). Since Equation 17 contains the slope of the beach, a difficult parameter to quantify in a field application, it is of significance to estimate the influence of runup height on the simulation result. Figure 69 illustrates growth of bar volume with time for various runup heights calculated through Equation 17. Evolution of bar volume was only slightly affected by the considerable variation in runup height. Consequently, even a significant error in estimation of the runup height will not notably degrade the

representation of the time evolution of the bar. However, model prediction of the amount of erosion occurring on the foreshore may be substantially in error.

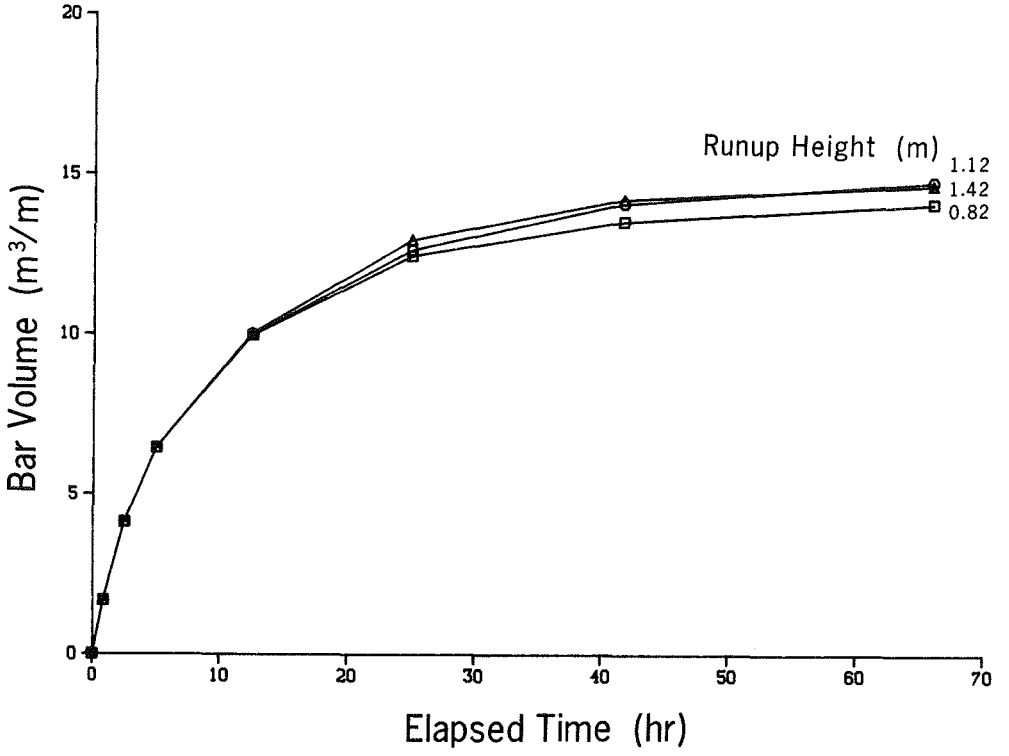

Figure 69. Effect of runup height on bar volume

Effect of Time-Varying Water Level and Waves

462. In the preceding calibration, verification, and sensitivity analysis, all simulations were conducted with a fixed water level and constant wave conditions. However, in one of the LWT experiments (Case 911), water level was varied in a sinusoidal manner to simulate the influence of a tidal variation on beach profile evolution. This case provided an opportunity to evaluate model predictions of profile change induced by constant incident waves with a realistic variation in water level. The water level variation had an amplitude of 0.45 m and a period of 12 hr. Optimal model parameters obtained in the overall calibration were used in the simulation of Case 911.

463. Figure 70 illustrates the result of the model run and a comparison with the measured beach profile at the end of the tank experiment. Develop-

ment of the beach profile as predicted by the numerical model was as follows. The first increase in water level resulted in the formation of an almost stationary emergent bar, as observed in the first few profiles. As water level dropped, the break point rapidly moved seaward, and the bar correspondingly moved in the seaward direction. When the water level increased at later cycles and a well-developed bar existed at the seaward end of the profile, waves passed over the bar and broke inshore creating a small second feature just shoreward of the main breakpoint bar.

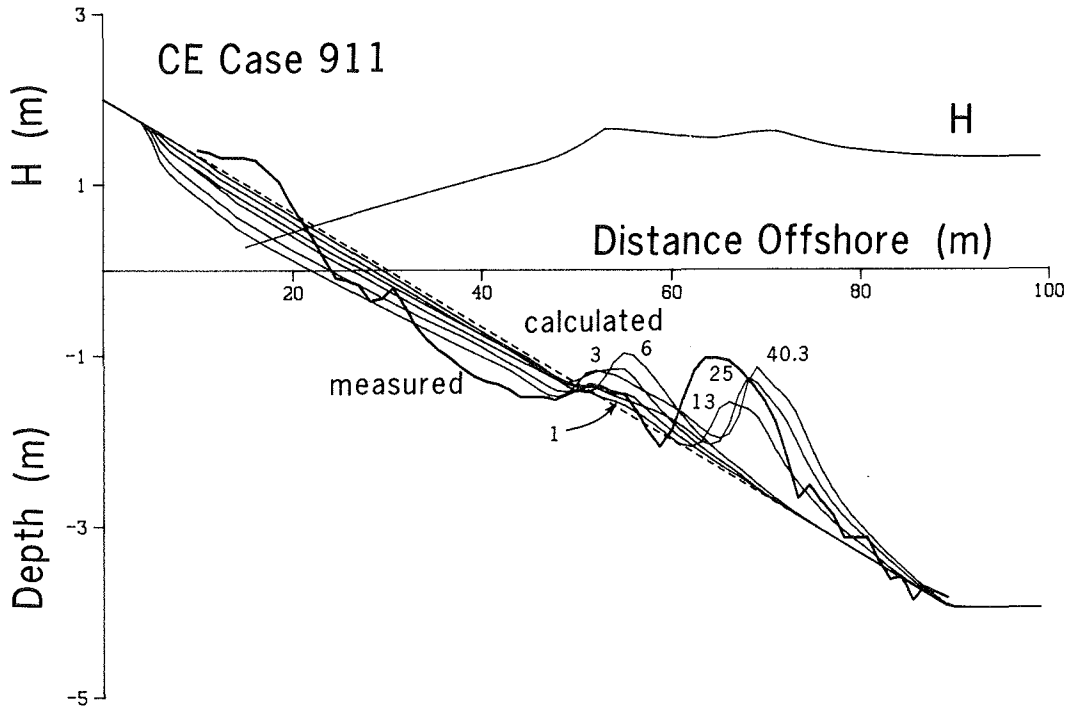

Figure 70. Verification for case of varying water level

464. As observed on the measured profile, a small berm formed on the foreshore during the latter part of the run which was not described by the model. Otherwise, the model reproduced the main shape of the beach profile, that is, a main breakpoint bar with a smaller bar-like feature inshore, separated by a distinct trough. Locations of calculated bars were somewhat farther seaward compared with those of the measured profile, but bar volume was reasonably well predicted.

465. It was possible to obtain better agreement between simulated and measured bar locations by changing model calibration parameters. However, it was not possible to simulate berm buildup on the foreshore because the empirical criterion for the transport direction (Equation 2) predicted seaward-directed transport during the entire run. Wave and sand parameters for Case 911 are such that the intersection of quantities involved in the criterion determining transport direction is very close to the line separating bar and berm profiles. This may explain the somewhat mixed response of the profile.

Water level, wave height, and wave period

466. To qualitatively evaluate model performance for varying water level, wave height, and wave period, a number of hypothetical cases were simulated. In all cases, the initial beach profile consisted of a dune with a steep face having a plane slope (1:5) joined to a more gentle plane slope (1:15) at the still-water shoreline. The cycle of the variation for wave period, wave height, and/or water level was set at 200 time-steps (Δt = 5 min), and the simulation was carried out for 1,000 time-steps.

467. The effect of a varying wave period was investigated first, where the deepwater wave height was chosen as 2.0 m and the water level was fixed. The wave period was varied sinusoidally between 6 and 10 sec with the previously-mentioned time cycle. Figure 71 shows the simulated beach profile at selected time-steps and the wave height distribution at the last time-step. The shape of the bar is somewhat more gentle than for a fixed wave period (see Watts 1954) and changes in the profile decrease with time, approaching a near-equilibrium state, even though the wave period continues to change. The direction of bar movement was seaward during the entire simulation period.

468. Beach profile change produced by a sinusoidally varying water level showed features similar to those in the Case 911 simulation. The simulated example had a water-level amplitude of 1 m, a wave height of 2 m, and a wave period of 6 sec. Figure 72 shows the calculated beach profile at selected time-steps and the wave height distribution across-shore at the last time-step. As the water level increased, the bar was stationary or even moved some what shoreward, whereas during the decline in water level the bar moved rapidly seaward. Once the bar formed, a rise in water level allowed waves to

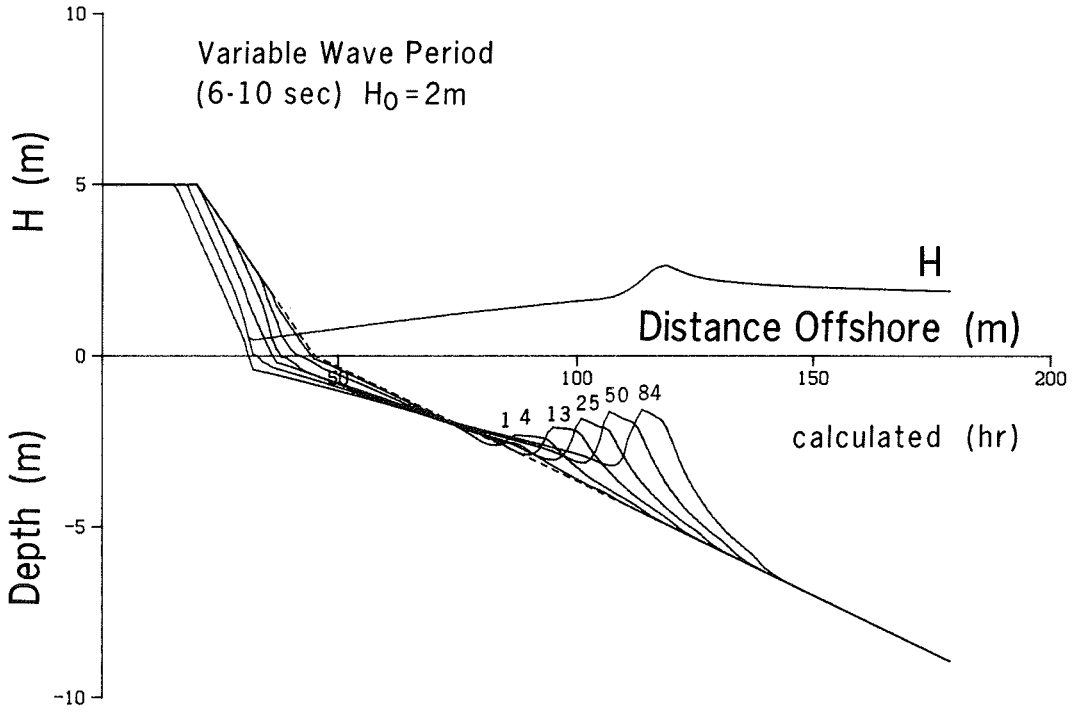

Figure 71. Simulation with varying wave period

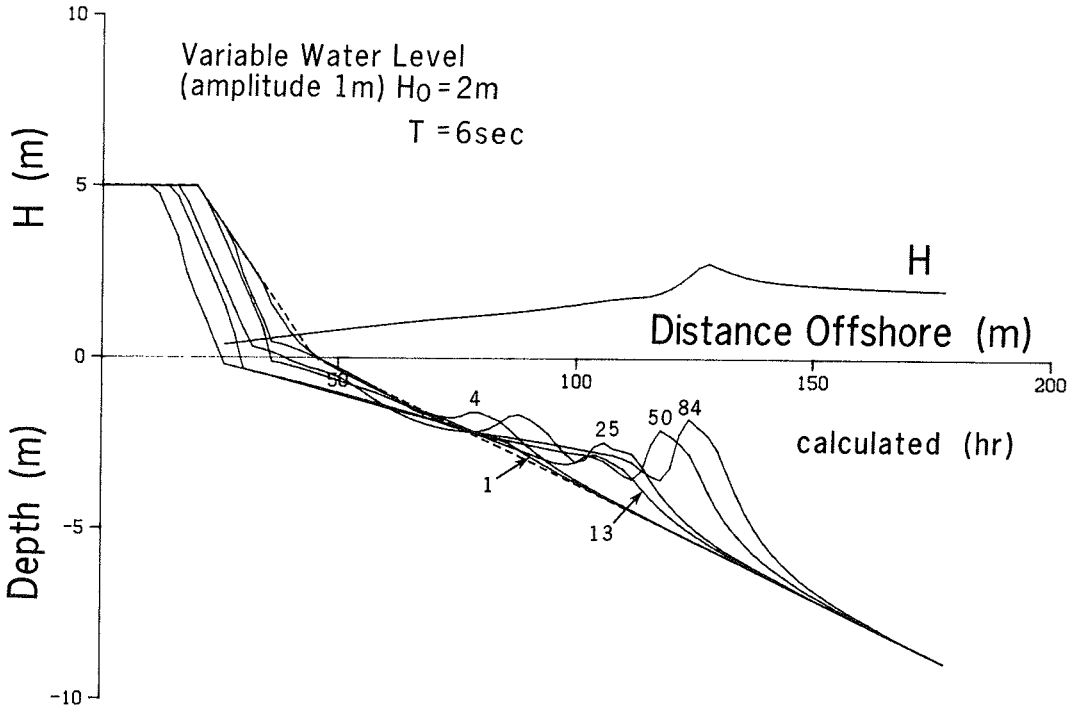

Figure 72. Simulation with varying water level

pass over the main bar and break inshore, causing deposition of sand shoreward of the bar. The flat portion of the bar was a result of waves breaking shoreward of the bar crest. The seaward peak of the bar was created from waves breaking at the bar crest when water level was at a minimum.

469. Somewhat similar profile development occurred when wave height was varied sinusoidally. As an example, deepwater wave height was varied between 1 and 3 m, with the wave period fixed at 10.0 sec and the water level constant. In Figure 73, selected profiles predicted by the model are displayed at consecutive times, together with the calculated wave height distribution at the last time-step. The bar had a flat shape initially, but a pronounced peak formed after a number of wave height cycles had been completed.

470. The constant supply of sand from the dune as the wave height changed, together with the movement of the break point, prevented the inshore from developing a characteristic monotonic shape. However, if the wave height is held constant, the beach profile would approach an equilibrium shape with a concave inshore profile.

471. As an example of the shape of the net cross-shore transport rate, distributions associated with Figure 73 are plotted in Figure 74. The peak of the transport rate distribution moved across-shore with movement of the break point as wave height varied. At some time-steps, a small peak appeared at the foreshore (not shown in Figure 74, but seen in Figure 58), particularly if avalanching took place on the dune slope. In this case, sand accumulated in the foreshore cells as the slope adjusted to the residual angle after shearing. The corresponding decrease in depth produced a larger energy dissipation per unit volume in those cells, resulting in a greater transport rate. Figure 74 also shows that the transport rate distribution exhibited a more complex shape at later times, when the depth was not monotonically decreasing.

472. A hypothetical case was also numerically simulated for concurrent sinusoidal variations of water level (±1 m) and wave height (2 m ±1 m). Variation of the two parameters was in phase with a period of 200 time-steps (Δt = 5 min). The total simulation time was 1,000 time-steps, and the wave period was 8 sec. As seen from Figure 75, the bar is higher and wider than in previous examples. Also, the dune face retreated more than for the example with only wave height variation, since the waves could attack higher on the dune because of the water level variation

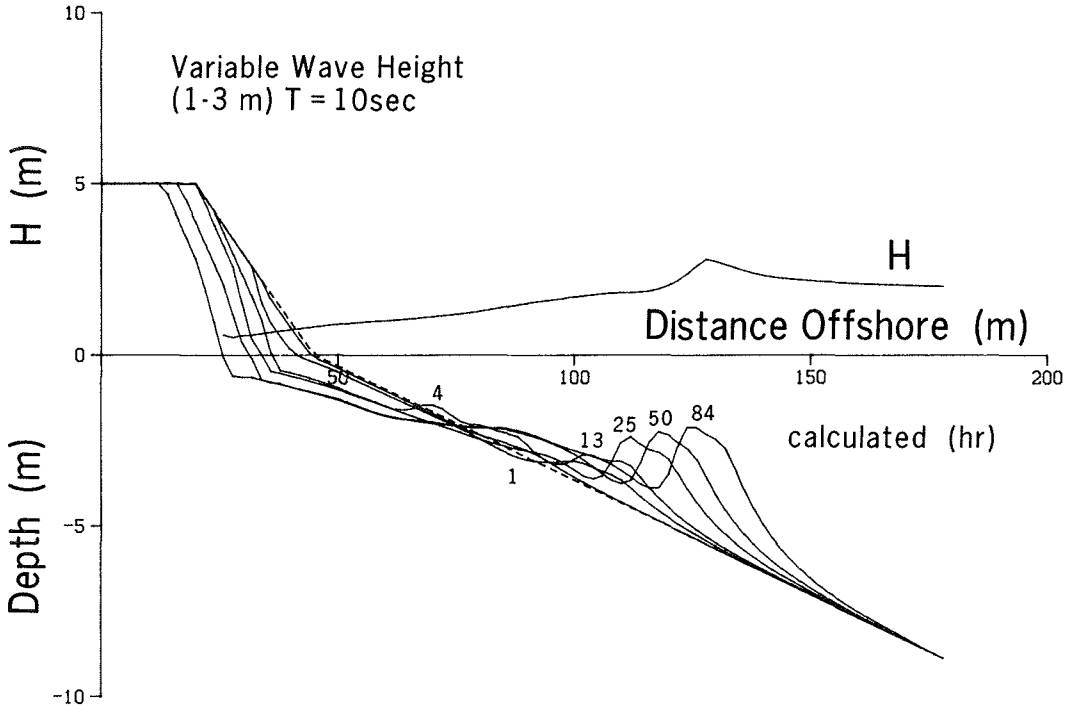

Figure 73. Effect of varying wave height

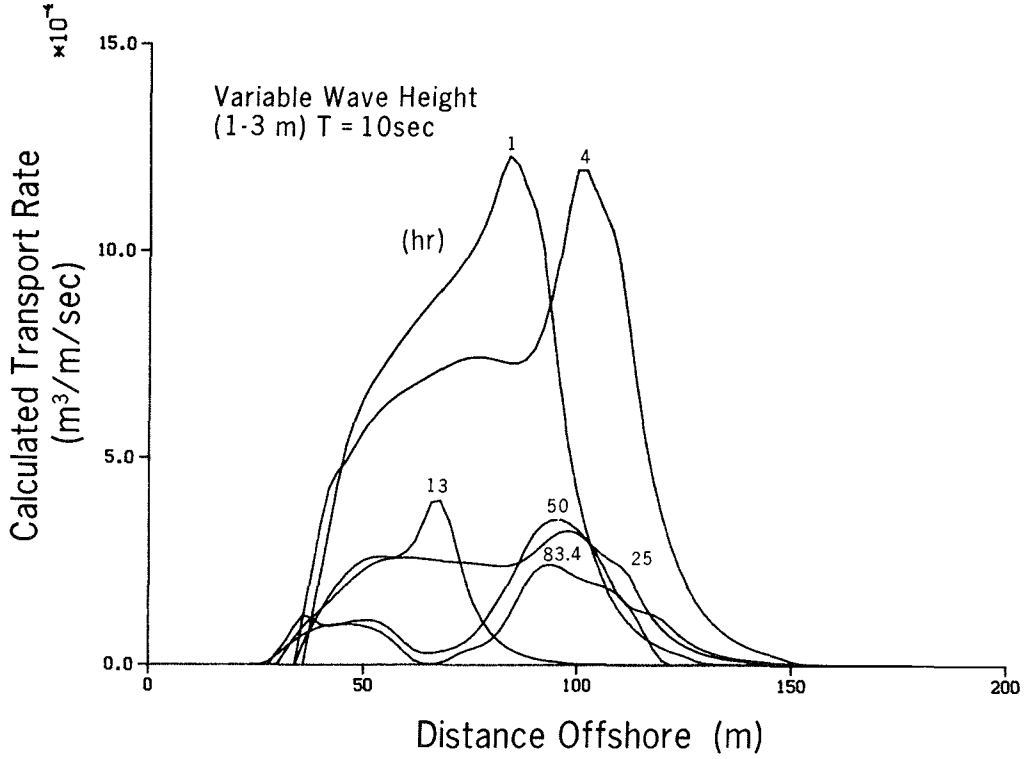

Figure 74. Transport rate distributions for varying wave height

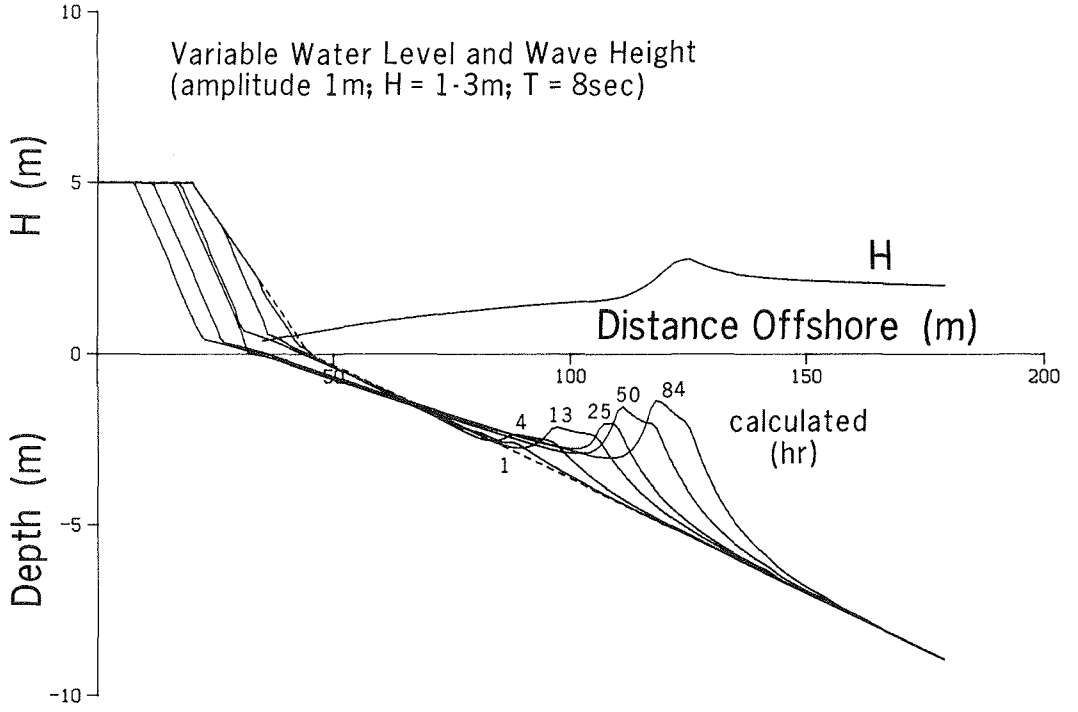

Figure 75. Simulation with varying water level and wave height

Multiple Barred Profiles

473. If the water level varies simultaneously with the wave height, waves may reform as they pass over the trough. The reformed waves will break further inshore and create another bar, thus producing a multiple barred profile. The shape and properties of the net transport rate in zones of broken waves, seaward of the break point, and on the foreshore were investigated in Part V, whereas in zones of wave reformation less empirical information was available for analysis and deduction. However, some conclusions of a qualitative nature can be made from observations of transport rate distributions obtained from the LWT studies.

474. Formation of a second bar inshore is recognized in the transport rate distribution as a local minimum, with monotonically decreasing transport rates seaward and shoreward of this point. Since calculated net transport

rate is obtained from profile surveys separated by several hours, the inshore peak of the distribution was sometimes not clear. Also, the number of cases studied in which wave reformation occurred was limited. This made information scarce about the net transport rate in zones of wave reformation, and choice of the shape of the transport rate distribution became somewhat arbitrary.

475. It is reasonable to assume that the transport rate in zones of wave reformation is a function of the transport characteristics in the bordering zone of broken waves, since mobilization and transport are expected to be most intense in the broken wave zone. It is therefore assumed that the magnitude of the transport rate at the boundary of the broken wave zone determines the magnitude of the transport rate in the wave reformation zone. Then, only information about the functional form of the decay of the transport rate to the point of minimum transport and the location of this minimum are required to completely specify the transport rate distribution in the wave reformation zone. The magnitude of the minimum transport rate in the wave reformation zone is given by a decay function once the location of the minimum is specified.

476. Various trial functions were investigated to find a suitable description of the transport rate distribution in the wave reformation zone, focusing on exponential and power functions. A qualitatively acceptable representation of beach profile evolution was obtained by an exponential decay from the point of wave reformation shoreward to the point of minimum transport. From the second break point seaward to the point of minimum transport, a power law was applied to describe the transport rate. By introduction of these empirical functions, additional parameters are introduced in the model, and their magnitudes must be determined through calibration against measurement. The two empirical transport relationships used to describe the transport rate q in zones of wave reformation are

$$q = q_r \, e^{-\nu(x_r - x)} \qquad x_m \leq x < x_r \tag{47}$$

and

$$q = q_b + (q_m - q_b) \left[\frac{x - x_b}{x_m - x_b} \right]^n \qquad x_b < x < x_m \tag{48}$$

where

q_r = transport rate at wave reformation point

ν = spatial decay coefficient

x_r = location of wave reformation point

x_m = location of minimum transport rate

q_b = transport rate at second break point

q_m = minimum transport rate in wave reformation zone (determined from Equation 47)

x_b = location of break point

n = exponent determining spatial decay in transport rate

477. To investigate the possibility of modeling wave reformation and multiple bar formation, one of the CE cases was used for which measurements of a second break point were made (Case 500). Since the wave height in the surf zone approaches the stable wave height Γ asymptotically as the waves progress onshore (Horikawa and Kuo 1967, Dally 1980), wave reformation will not occur in the model for a beach with monotonically decreasing depth in a surf zone that is exposed to constant wave conditions and water level. As a bar grows in size, the trough becomes more pronounced, but the slope-dependent term in the transport equation (Equation 33) will not allow the trough to become sufficiently deep to initiate wave reformation.

478. One method of forcing waves to reform in the model is by turning off breaking at a predetermined level somewhat higher than the value of the stable wave height coefficient (see Dolan 1983, Dolan and Dean 1984). A physical argument for a higher value is that an asymptotic decay toward the stable wave height is unrealistic in nature, and wave reformation is initiated through a delicate balance between competing processes close to stable conditions. Consequently, by forcing wave reformation to occur, the phenomenon is included in the model, although the details of the process are simplified.

479. In this particular simulation, a stable wave height coefficient of $\Gamma = 0.4$ was used in all simulations, whereas breaking was turned off at a value of $\Gamma = 0.5$ to initiate wave reformation. A typical simulation result is displayed in Figure 76. Simulated beach profiles at consecutive times are

given together with the measured beach profile at the last time-step. The wave height distribution across-shore for the last time-step is also shown.

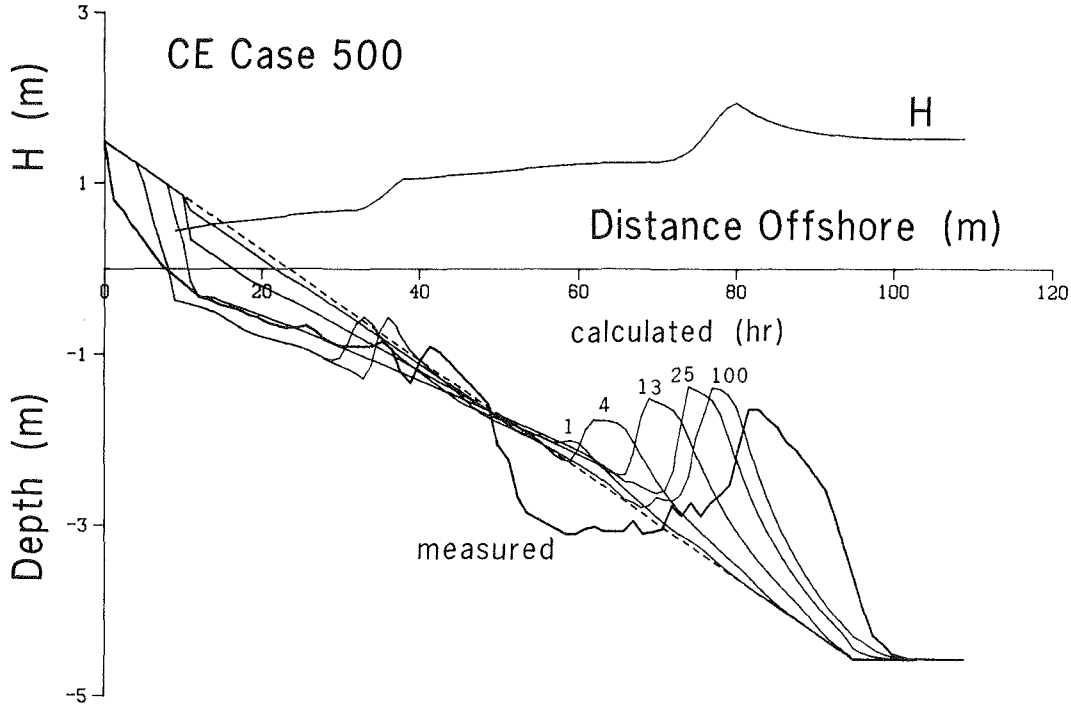

Figure 76. Reproduction of the second breakpoint bar

480. Locations of the two bars and the amount of erosion on the foreshore were well described by the model, whereas the distinct trough shoreward of the main break point was not reproduced. When the second bar appeared, sand transport to the main breakpoint bar was hindered in the model and growth of the main bar slowed.

481. As previously mentioned, between the shoreward break point x_b and the point where the transport rate attains a minimum in the reformed wave zone x_m , a power function was used to describe the decrease in transport rate. An exponent of 0.5 proved adequate, although the calculation was not sensitive to changes in this value. Changes in the exponent did not affect the shape or size of the outer bar but did influence somewhat the location of the inner bar. A larger value of the exponent caused the inner bar to move farther seaward, whereas a smaller value hindered seaward bar movement. From the point of wave reformation x_r shoreward, an exponential decay was used, thus introducing another spatial decay coefficient ν . Typical coefficient

values were around 0.10 m^{-1} between those found for the main breakpoint bar from the plunge point to the break point and from the break point seaward (Part V).

482. The location of the minimum transport rate x_m must be specified to completely determine the transport rate distribution in the wave reformation zone. Once this point is known, the transport rate is calculated from the exponential decay starting from the wave reformation point. The power curve then connects the minimum transport rate thus determined with the transport rate at the second break point. As waves reform, turbulence is advected onshore with the waves, keeping grains in suspension and making them available for transport. However, because the generation of turbulent motion through wave energy dissipation decreases considerably, the transport rate decreases correspondingly. Closer to the second break point on the seaward side, the transport rate is expected to increase again, caused by the large energy dissipation shoreward of the break point. Since the sand transport capacity of a reformed wave is probably larger than for waves in the zone immediately seaward of a break point, the point of minimum transport should probably be located closer to the second break point than the point of wave reformation. In the model, the location of the minimum transport rate in zones of wave reformation was arbitrarily placed seaward of the second break point one third the distance to the wave reformation point.

483. In initial simulations of multiple bar formation, the inshore bar typically formed too close to the main breakpoint bar, compared with measured beach profiles from the LWT experiments. This was caused by rapid shoaling in the model after wave reformation, making the break point form too far seaward, since wave energy dissipation drastically changed as waves reformed and shoaling became dominant. Because wave reformation is a gradual phenomenon, it was believed that successive turn-off of energy dissipation would provide a more adequate representation of what actually happens in this zone. The turn-off is implemented in the numerical model by decreasing the wave decay coefficient κ exponentially with distance from the wave reformation point. A decay coefficient of 0.025 m^{-1} in the exponential damping function proved sufficient to accurately describe the location of the second bar.

Simulation of Field Profile Change

484. The numerical model was used to simulate beach profile change measured at the FRF in Duck, North Carolina. The FRF is operated by CERC at the US Army Engineer Waterways Experiment Station. Beach profile surveys along four shore-normal lines and associated wave and water level measurements have been obtained regularly for more than 4 years at the FRF. Measurement procedures and a listing of the data are given by Howd and Birkemeier (1987). Surveys are carried out at approximately 2-week intervals, statistical wave parameters are calculated from gage data every 6 hr, and water level is recorded every 6 min.

485. Five time periods were chosen for model simulation, each distinguished by two profile surveys between which erosional conditions prevailed (storm events). Erosional conditions were characterized by offshore movement of one or two bars, whereas shoreline position in most cases was very stable and no retreat was noted. Anomalous stability of shoreline position is characteristic of the FRF beach and may be caused in part by the presence of coarser sediment that produces an armoring effect on the foreshore, thus requiring a larger amount of wave energy to move the material.

486. Figure 77 shows the sediment size distribution across the profile on 17 March 1981 as given by Howd and Birkemeier (1987). The median grain size was more than an order of magnitude greater on the foreshore compared to the seaward region. Because of the large grain size, the slope of the foreshore at the FRF is usually very steep, allowing waves to break directly on the beach face.

487. Although profile data from the FRF are unsuitable for evaluating shoreline change and the prediction of eroded subaerial volume, movement of the bar may still be simulated with reasonable confidence. Furthermore, beach changes may be highly three-dimensional in the field, making it essential to identify profile change in the record for use here that was likely minimally affected by longshore transport and rip currents. Howd and Birkemeier (1987) documented a wave event 821013 - 821015 (notation: year-month-day) during which time closely spaced profiles showed very different responses, with a bar moving onshore on one survey line and offshore on the other line, illustrating

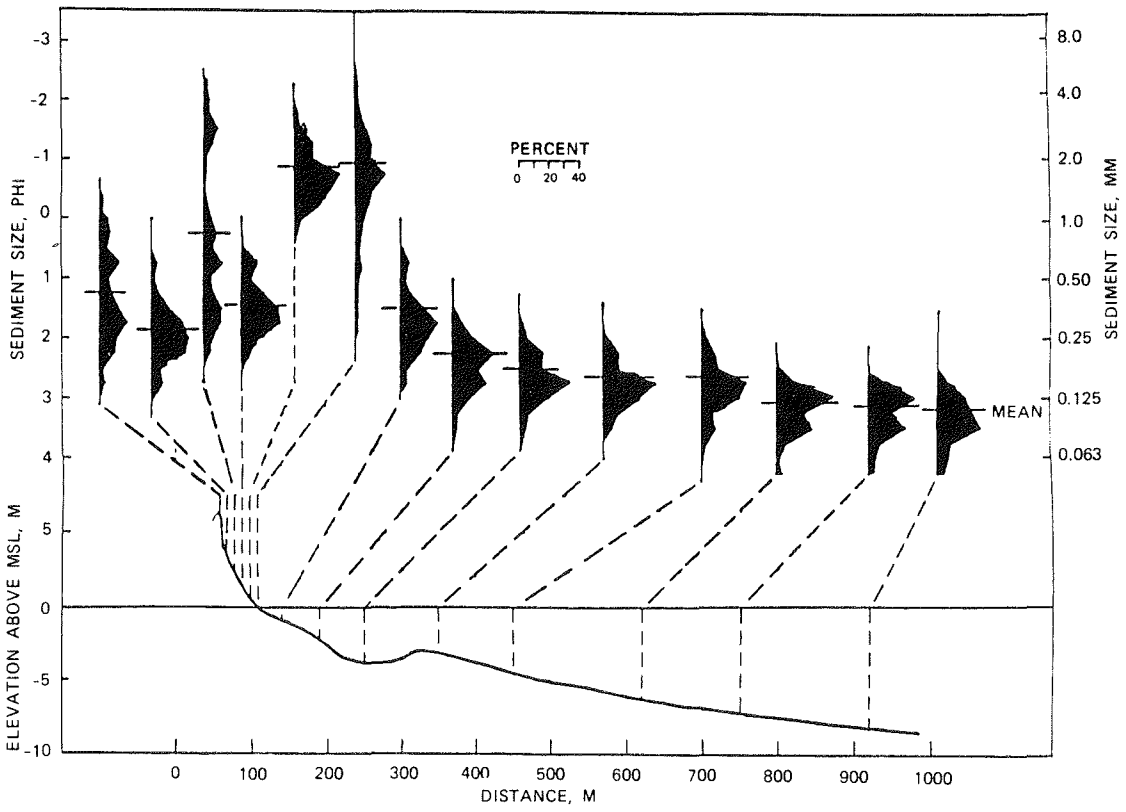

Figure 77. Distribution of grain size across profile line 188 (from Howd and Birkemeier 1987)

the importance of choosing events which show similar profile response alongshore. Therefore, in the present study time intervals were selected during which adjacent profile lines displayed similar development.

Data set

488. Survey line 188 (Howd and Birkemeier 1987) located southeast of the FRF pier was selected for profile simulation. The survey line is beyond the influence of the pier and located in an area of characterized by nearly straight and parallel bottom contours. To minimize the effect of longshore variability in profile change in selecting storm events for simulation, the response of line 188 was compared with line 190, located less than 100 m away. Five events were selected for which profile evolution was similar for the two survey lines, making it reasonable to believe that beach changes were predominantly two-dimensional during the storm events. However, for most events used, mass was not rigorously conserved in comparison of consecutive surveys, indicating that longshore effects influenced profile response to some degree.

489. Measured wave height and period were available every 6 hr and water level every hour. Since a shorter time-step (typically, Δt = 20 min; Δx = 5.0 m) was used in the numerical model, cubic spline interpolation was used to provide input values for time-steps between measurements. The energy-based wave height H_{mo} was determined from the wave spectrum as four times the standard deviation, which corresponds to the significant wave height if a Rayleigh distribution of the wave height is assumed. Wave period was given as the peak period of the spectrum. Wave input data were obtained from gage 620, located in 18 m of water directly seaward of the pier. The height was then transformed using linear wave theory to the beginning of the model calculation grid, located at a depth of about 8 m below mean sea level.

490. The tide gage is located at the end of the pier and measures the total water level variation with respect to mean water level. Thus, water level measurements include both storm surge and tidal variation, the latter being semidiurnal (two high and two low waters in a tidal day).

491. Profile surveys were made at an average interval of 2 weeks, with more frequent surveys when greater profile change took place. Although profile data from the FRF represent one of the most detailed and accurate data sets on profile change, horizontal spacing between measurement points along a profile line is typically tens of meters. Small features along the profile are not resolved, and the general shape has a more smoothed character than actually exists. However, the data set is highly suited to the present application.

Calibration of numerical model with field data

492. Parameter values given by calibration with the LWT data sets were initially used in simulation of the field profile change data. However, it became apparent that values of some empirical coefficients would have to be modified to achieve agreement between measured and calculated profiles. Four storm events (811022 - 811103; 811110 - 811116; 840210 - 840216; and 840403 - 840406) were chosen for calibration of the numerical model, and one event (821207 - 821215) was used for verification. Calibration was performed by minimizing the total sum of squares of the difference between calculated and measured depths. The optimum transport rate coefficient K obtained for the four events was smaller than the value obtained for the LWT data. As

previously described (Part VI), the optimum K-value for the LWT calibration was determined to be 1.6 10^{-6} m^4/N. For the field data, a value of 0.7 10^{-6} m^4/N proved to give the best agreement. Three cases had a best fit for 0.9 10^{-6} m^4/N, whereas the remaining case gave 0.4 10^{-6} m^4/N.

493. A smaller value of the transport coefficient is not unexpected since the coefficient showed an inverse dependence on wave period for the LWT experiments, and wave periods in the field data were somewhat longer than in the LWT data set. Calibration of K using the LWT data set is somewhat biased toward shorter period waves. Use of the K-value determined from the LWT data caused the beach profile to respond too quickly and the bar to become too pronounced, not having the smooth character of the field measurements. Transport induced by irregular waves that exist in the field, i.e., wave heights and periods varying above and below the representative monochromatic (but time-varying) waves used in the model, is also expected to alter the value of the transport coefficient, as both transport thresholds and mean rates will be different (Mimura, Otsuka, and Watanabe 1987). From these considerations, the amount of change in K between LWT and field calibrations is surprisingly small.

494. Values of other empirical coefficients appearing in the various transport rate relationships were kept at the values given by the LWT calibrations. In the breaker decay model, the stable wave height coefficient was set to $\Gamma = 0.4$ as for the LWT calibration, whereas a wave decay coefficient of $\kappa = 0.13$ gave better agreement between measured and simulated profile evolution. A smaller wave decay coefficient is expected for the FRF data compared to the LWT data since this coefficient depends slightly on beach slope (Part V), and the field profiles had more gentle slopes than the LWT profiles. The stable wave height coefficient was also varied, but the simulation was insensitive to changes in this parameter.

495. The breaking criterion developed from the LWT data caused waves to break too far offshore, creating a bar farther seaward than found in the measurements. Instead, a constant value of the breaker ratio of 1.0 was applied, which gave a better description of the bar location. In the breaker criterion derived from the CRIEPI data set, the slope seaward of the break point was used. At the seaward side of the bar the slope was normally

relatively steep, making the breaker ratio correspondingly high. Beach profiles from the FRF data set showed more gentle slopes than the CRIEPI experiment, causing the predicted breaker ratio to become lower, and the waves to break farther offshore. As a result, the relationship derived from the LWT data produced a slope dependence which appears not to apply to the more gently sloping bars found in the field.

496. The energy-based significant wave height was used in the numerical model to determine the wave height distribution across shore. On a field beach, the break point constantly moves back and forth due to random variation in wave parameters. A problem is to find a measure of the wave height that will on the average reproduce properties of the random breaking waves. As an alternative to the significant wave height, the mean wave height $\bar{H}$, determined by assuming a Rayleigh distribution, was used in some simulations. Since $\bar{H}$ is smaller than H_{mo}, the waves broke farther inshore but moved less sand. However, better agreement was not achieved using $\bar{H}$, in contrast to what was reported by Mimura, Otsuka, and Watanabe (1987) based on their small tank experiments.

497. The nonlinear shoaling law derived by Shuto (1974) was also tested in some field data simulations. It seemed to overestimate shoaling just before breaking, as was the case for the LWT experiments. Longer period waves calculated by the nonlinear theory markedly increased in height in shallow water, creating a bar too far offshore. Consequently, linear wave theory was judged to be more satisfactory and was used throughout.

498. Median grain size probably varied across the beach profile (see Figure 77) with a notably larger grain size on the foreshore. To represent this variation in the model, two different grain sizes were used along the profile. A larger grain size (2.0 mm) was specified on the foreshore to a distance approximately 130 m from the baseline, and a finer grain size (0.15 mm) was employed from this point and seaward. The larger grain size requires larger equilibrium energy dissipation with correspondingly more wave energy needed to move material. As for the LWT simulations, the equilibrium energy dissipation design curve of Moore (1982) was reduced by a factor of 0.75. Additional variation in median grain size across shore somewhat improved the fit of the model in trial simulations but was considered to be

unrealistic because of the added complexity and because the movement and mixing of individual grains are not simulated in the model.

Results

499. Calibration. Figure 78(a and b) illustrates the result of a typical calibration for one event (840403-840406) together with the wave and water level data. The initial measured profile is displayed together with the measured and calculated final profiles. Movement of the bar was rather well predicted by the model regarding location, but the amount of material moved was underestimated, and the trough was not sufficiently pronounced. Also, even though a larger equilibrium energy dissipation was used on the foreshore corresponding to the measured 2-mm grain size, the simulated shoreline still receded somewhat, whereas this did not occur in the field. One reason for this retreat was transport produced by small waves that passed over the bar and broke immediately on the beach face. Indeed, wave breaking at the step is commonly observed at the FRF; nevertheless, little shoreline movement takes place. Application of the concept of cross-shore transport being proportional to energy dissipation may be questionable if a surf zone is absent and waves break directly on the beach face. Lack of shoreline movement at the FRF is anomalous, and model results cannot be interpreted in this region based on the data.

500. Verification. Optimum parameter values determined from the calibration were used to simulate an independent storm event (821207-821215), and thus evaluate the applicability of these values for an independent erosional case. The result of the model verification is shown in Figure 79(a and b), together with the input wave height, wave period, and water level. The initial beach profile exhibited two bars, with the outer bar having a very smooth shape. The model simulation reproduced the main changes of the beach profile in that both bars moved offshore. However, the amount of material moved was underpredicted as in the calibration, and the calculated shoreline receded farther than the measured. Movement of the inner bar was overestimated by the model, whereas the outer bar was located correctly but with less volume than measured. Also, the long, smooth trough located shoreward of the outer bar was not produced in the model simulation, and only a small amount of material was eroded from this region.

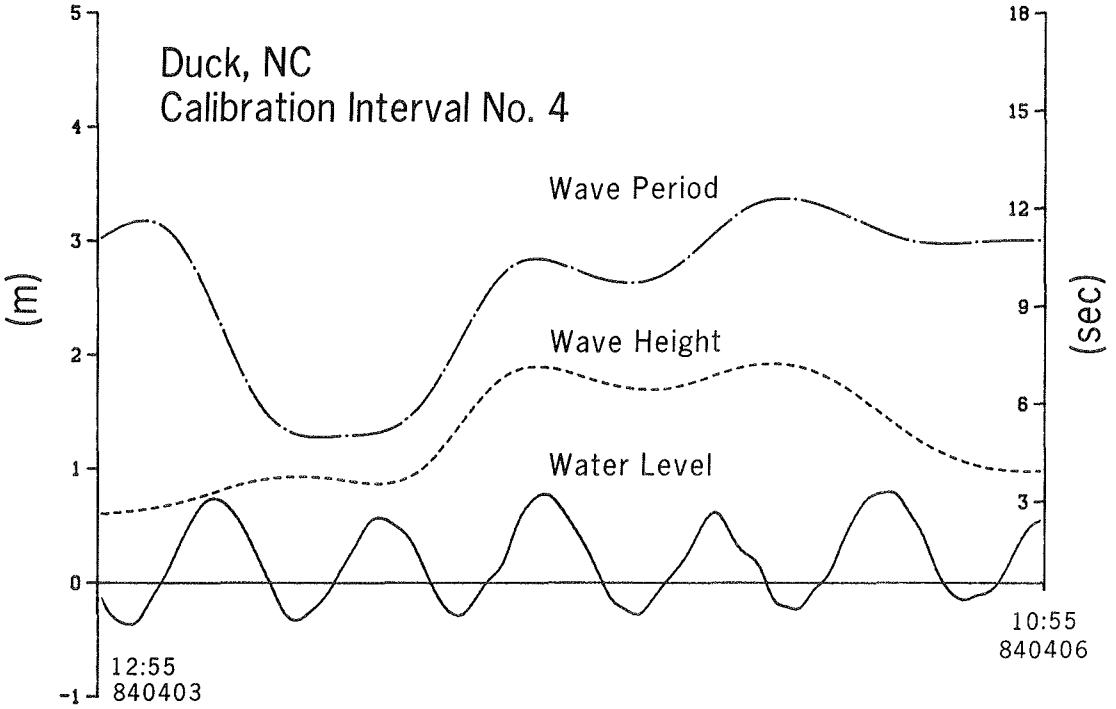

a. Input measured wave height, wave period, and water level

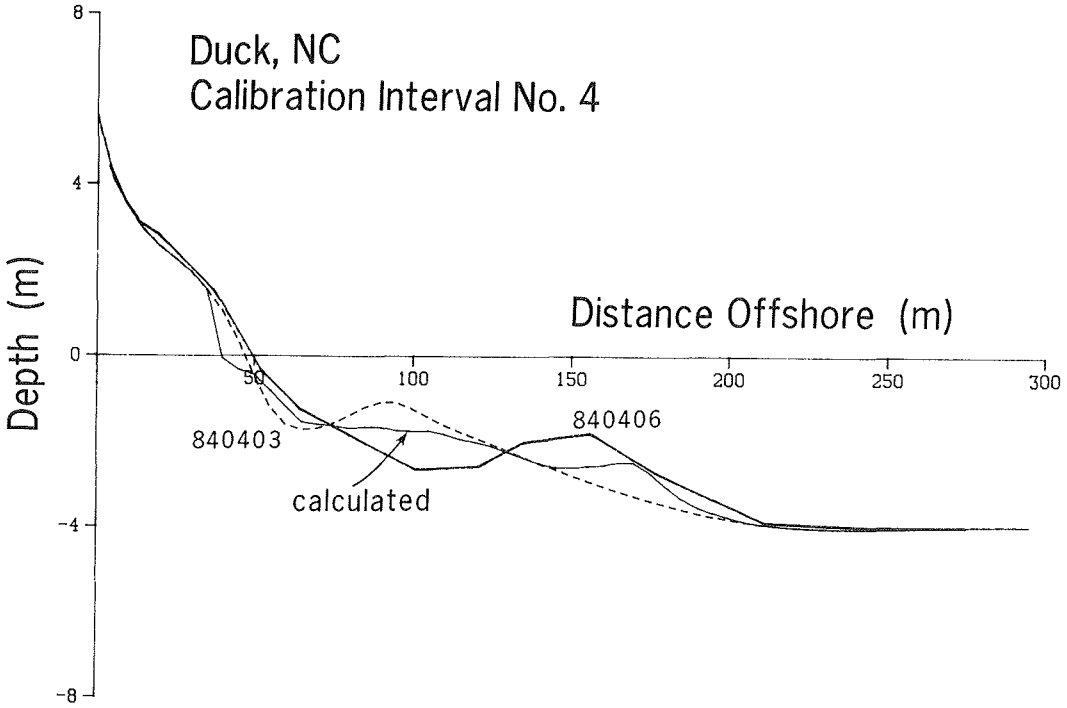

b. Result of simulation

Figure 78. Field calibration, event 840403-840406

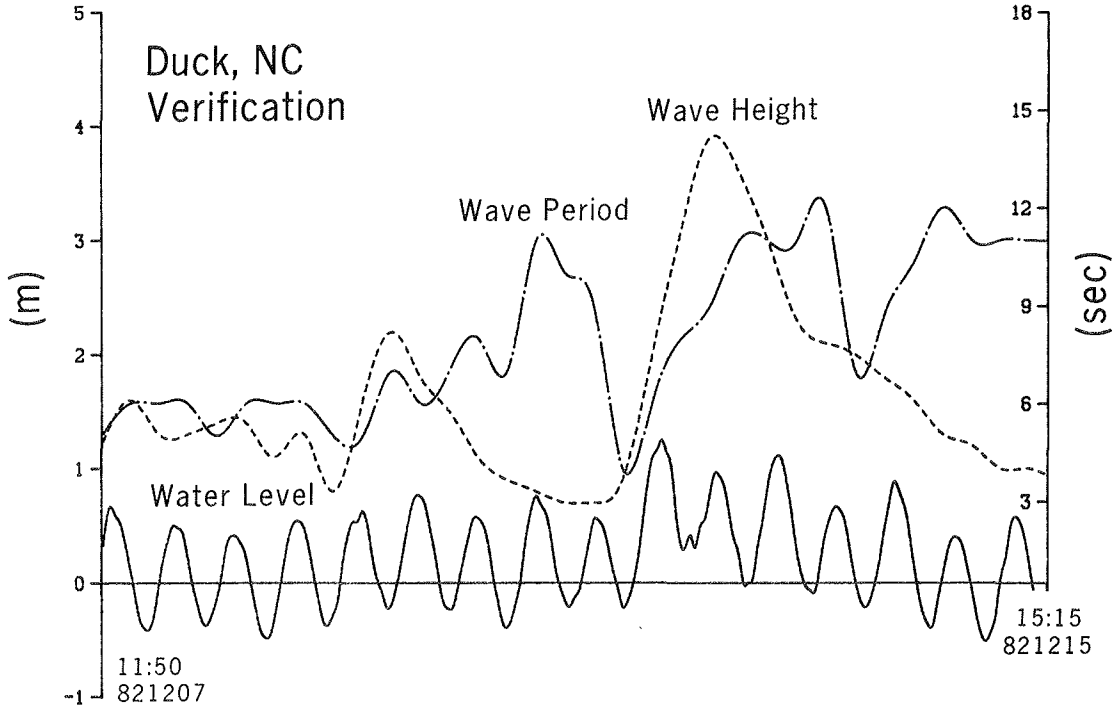

a. Variation of wave height, wave period, and water level

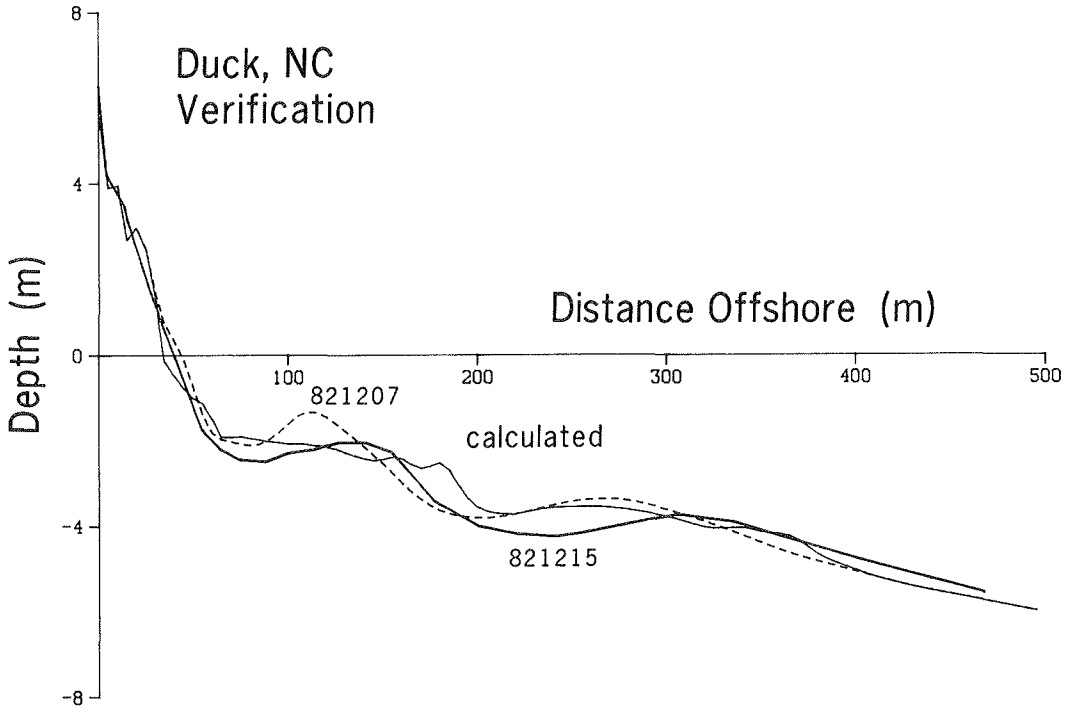

b. Result of simulation

Figure 79. Field verification, event 821207-821215

Sensitivity tests

501. To determine the influence of input wave and water level conditions and to put the results in perspective, variant simulations using the verification case 821207-821215 were performed. Since calibration was not carried out for this case, changes in wave parameters and water level better reflect model sensitivity to these input data. Parameter values given from calibration were used in these simulations. First, the extent to which changing water level improves or degrades model results was investigated.

502. In one simulation, water level variation was neglected completely, and neither the storm surge nor the tidal variation were represented. Figure 80 compares the measured 821215 profile and the simulated profile obtained by omitting water level changes. A constant water level implied that only wave height and period would determine the location of the surf zone and the amount of energy dissipation. Comparison with Figure 79b shows that the bar closest to shore developed a double-peaked shape. The most seaward bar was smaller and not as smooth as the corresponding bar formed under a varying water level. The sum of squares of the difference between measured and calculated profiles was smaller for the case including the water level variation, thus giving a better objective measure of agreement with the actual profile change. However, the constant water level simulation showed less shoreline retreat, which is artificial since the waves did not attack the beach as high as in the variable water level case as would take place in the field.

503. In another simulation, both wave height and period were kept constant at their average values for the verification period, and the water level was fixed at its mean position. The calculated result is shown in Figure 81, together with the measured initial and final profiles. The shoreward bar grew very steep and pronounced due to the constant wave and water level conditions. Also, the seaward bar did not move, since, without higher waves, all waves broke further inshore. This oversimplification of the input wave parameters and water level variation did not adequately represent the main features of the driving forces. When wave height and period were held constant, but water level was allowed to vary, a pronounced bar developed. The main difference compared with the constant water level case was a smoother bar and greater retreat of the shoreline.

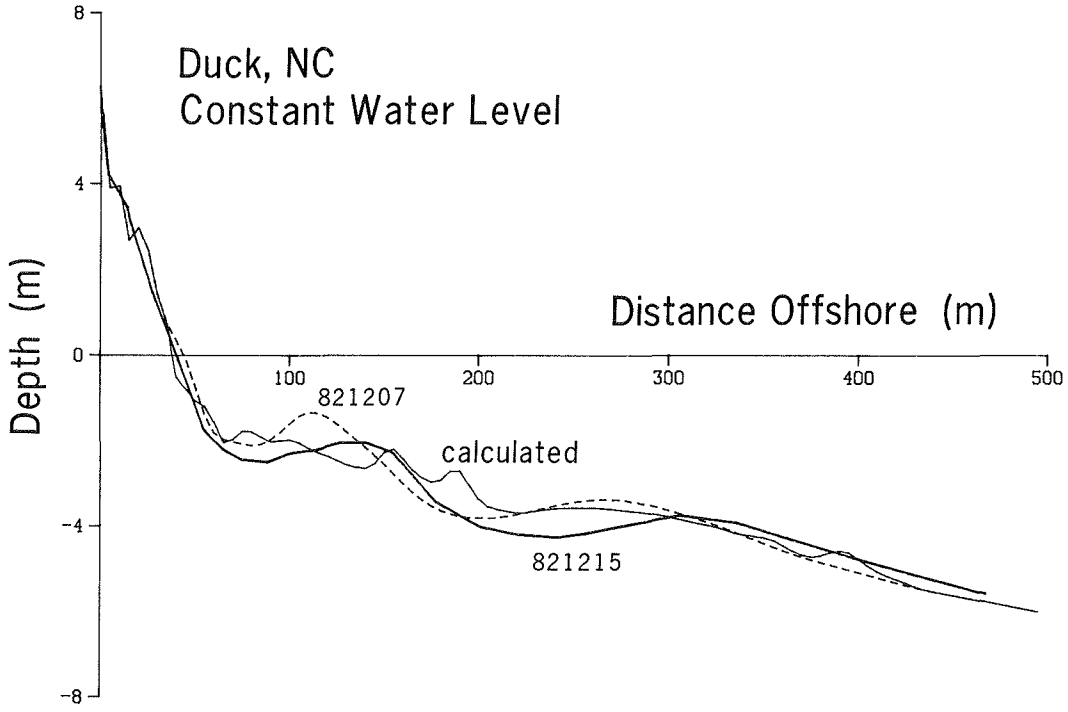

Figure 80. Field verification omitting water level variation

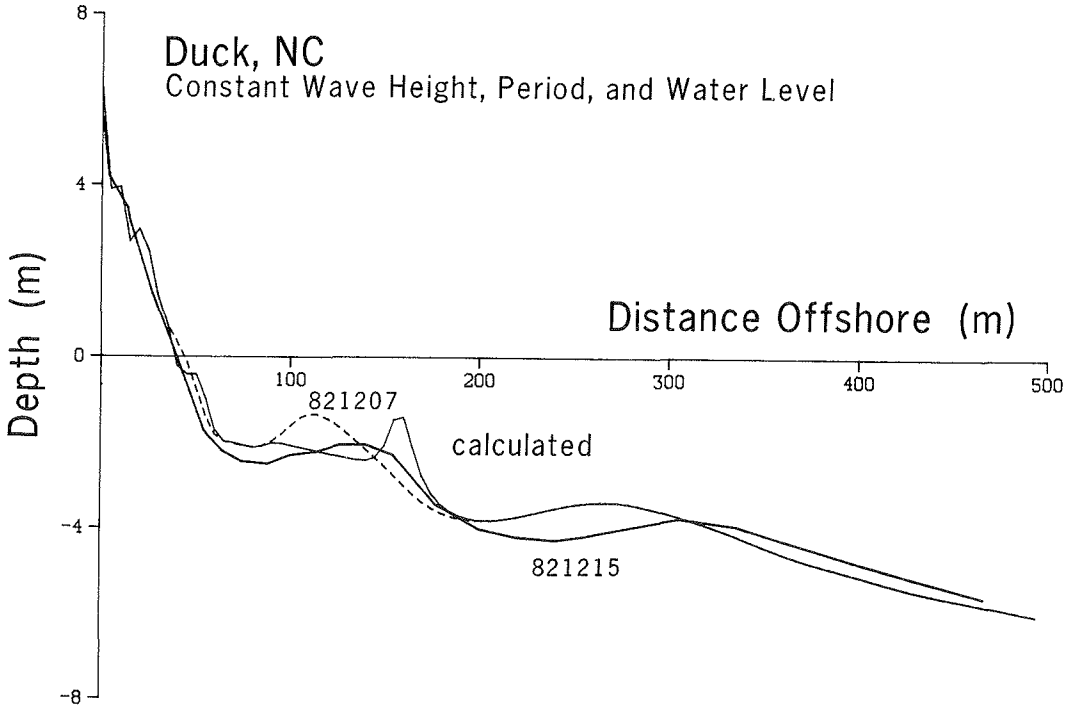

Figure 81. Field verification with fixed wave height, wave period, and water level

Discussion of field simulation

504. The numerical model best reproduced the measured response of the beach profile with the most detailed, realistic input of wave height, wave period, and water level variation. To correctly simulate the behavior of the profile under changing forcing conditions, the variation in the input data should have a time scale compatible with the profile response. Changes between individual waves is not necessary or meaningful for use of the present model, but differences occurring at a time scale of about an hour should be represented for best results. Constant wave and water level conditions will produce bars that are too steep and do not exhibit the smooth character usually encountered in the field.

505. The concept of breaking waves as a major cause of bar movement was verified by the model simulation of the field profile change. Locations of the bars were surprisingly well predicted considering the great variability in water level during the modeled storm events. A mass conservation check between measured initial and final profiles showed that none of the cases simulated were free from three-dimensional effects. In Figure 79b the difference in beach volume between initial and final volume was 45 m^3/m (a loss in beach volume constituting 25 percent of the total absolute volume moved across the profile). This difference is attributed mainly to differentials in longshore sand transport, and, possibly, to limitations in the surveys (spacing and accuracy). It is speculated that incorporation of longshore sand transport in the numerical model might produce a more pronounced trough because a maximum in the longshore sand transport rate is believed to occur somewhat shoreward of the break point.

506. Although the model was developed using laboratory data from situations with constant wave parameters, the capability to generalize and simulate profile change on natural beaches with variable wave and water level conditions was demonstrated. The steep foreshore and bar slopes produced in the large wave tanks and well simulated by the numerical model were a product of regular waves and constant water level. However, the important effects on the profile of variable wave and water level could be represented fairly well by superimposing regular waves with time changing height and period and stepwise changes in water level. Thus, a single regular wave and fixed water level

serve as elemental conditions that can be combined in a time series of varying conditions to approximately replicate natural conditions.

Comparison with the Kriebel Model

Overview

507. Presently, there is only one other known numerical model available to the engineering community that allows simulation of time-dependent changes in beach profile produced by breaking waves, the model developed by Kriebel (1982, 1986) and Kriebel and Dean (1985a). Simulations were performed with the present model and the Kriebel model for hypothetical cases to evaluate differences in calculated profile response. The Kriebel model does not simulate bar formation and, a priori, is expected to produce more erosion than the present model. Furthermore, the Kriebel model was developed to simulate profile behavior during erosional conditions, particularly dune erosion, with no capability for simulating berm buildup in its original formulation.

508. Since the two models differ in structure and purpose and contain different parameters, direct comparison using identical parameter values is not possible. For example, in the present model wave height is calculated at grid points across the shore, requiring specification of two empirical parameters. In the Kriebel model, wave height is assumed to be related to water depth in a fixed ratio. To facilitate comparison, parameter values were used as given by calibration against the LWT data for the respective models. Parameter values for the Kriebel model were taken from Case 300 which was used for calibration (Kriebel 1986).

Calibration

509. Parameter values in the present model were identical to those obtained from calibration against seven of the LWT cases. Even though the transport relationships are similar in the two models, values of the transport rate coefficient K resulting from the calibration were quite different (in the present model, $K=1.6\ 10^{-6}\ m^4/N$; in the Kriebel model, $K=8.7\ 10^{-6}\ m^4/N$). The transport rate coefficient is basically a calibration parameter determining the time scale of profile change, and its value is affected by the amount of smoothing applied in the model. Also, incorporation of a bottom

slope-dependent term in the transport rate equation in the present model increases the transport rate on positive slopes. By calculating the wave height distribution in the surf zone with a wave decay model, a more realistic description of surf zone wave properties is obtained. Such calculation also produces a difference in values of the optimum transport rate coefficient.

Comparisons of model simulations

510. A hypothetical beach profile with a dune having a slope of 1:4, no distinct berm, and a foreshore slope of 1:15 to 0.6-m depth was used in the model comparison. Seaward of 0.6 m, an equilibrium profile shape according to Bruun (1954) and Dean (1977) (Equation 1) was used, where the shape parameter A was determined from the design curve of Moore (1982) corresponding to a median grain size of 0.25 mm. Water level was varied sinusoidally to go through a maximum in a manner similar to a storm hydrograph and with a half-period of 24 hr, and wave conditions were held constant with a wave height of 3 m and period of 10 sec. (see Figure 86 for an example surge hydrograph.) Figure 82a shows that both numerical models produced similar amounts of erosion. Figure 82b gives a detailed view of the dune and foreshore.

511. The main difference between model results for this particular case is the area over which material was deposited. The Kriebel model distributed eroded material approximately evenly over the beach profile, whereas the present model tended to deposit sand closer to the toe of the dune. Experiments performed by Vellinga (1982) with a large wave tank showed time evolution of the profile qualitatively in agreement with the present model, but for a shorter surge hydrograph.

512. The dune face of the eroded profile was steeper for the present model, whereas the Kriebel model produced direct translation of the initial profile. Only a low-relief bar feature developed at the seaward end of the profile in the present model because of the varying water level, which caused the break point to move first shoreward and then seaward as the surge rose then receded. Since the break point was not stationary, movement of the transport rate maximum did not give the bar sufficient time to evolve.

513. Wave period does not directly enter in the Kriebel model, but it is of importance for the shoaling, breaking, and runup of waves in the present model. Therefore, wave period was changed in the test case to 14 sec to

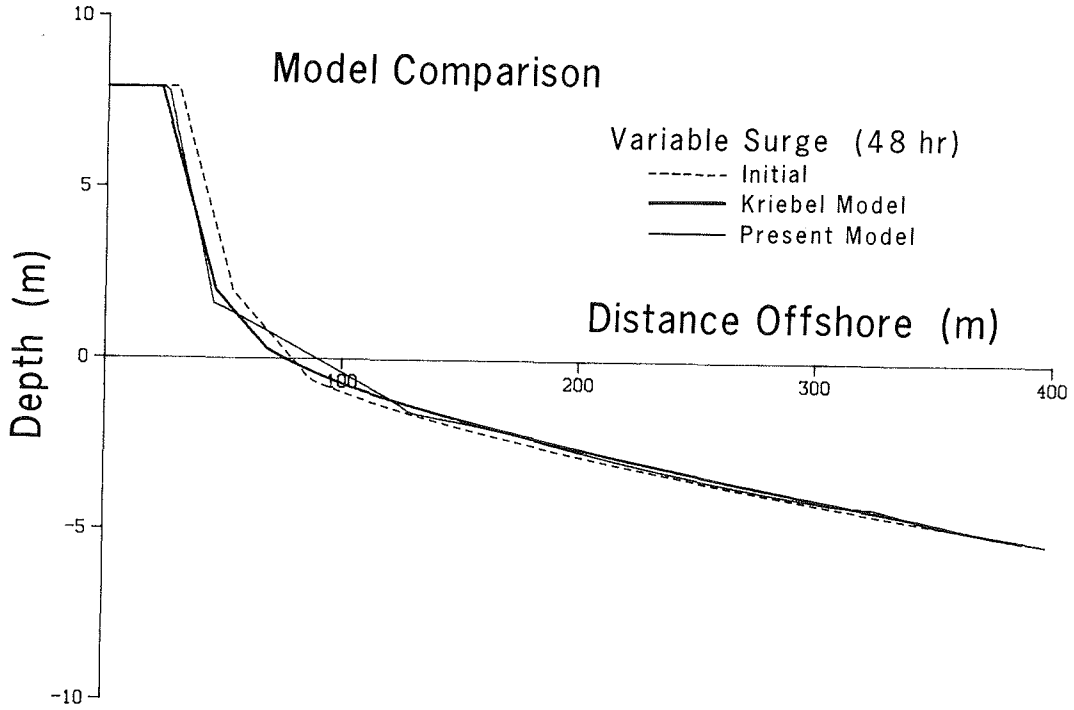

a. Full simulated profile

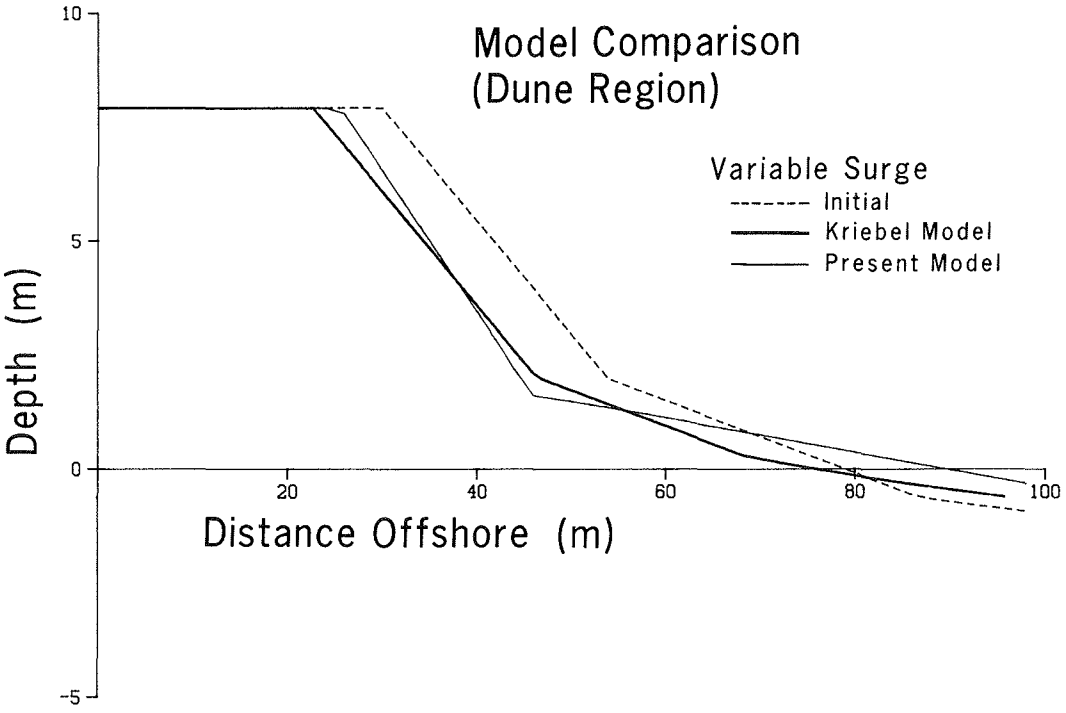

b. Details of dune region

Figure 82. Comparison of present model and Kriebel model for a surge case

evaluate its effect on the simulation. The result with the present model was formation of a gently sloping, wide bar of low height; the amount of dune erosion was approximately the same for both models.

514. To illustrate the difference between model predictions, another example was simulated in which the water level variation was contrived to promote bar formation. The same initial beach profile and wave conditions were used as in the previous case, but the water level variation consisted of an instantaneous rise of 2 m (surge) at the start of the simulation. The simulation period was 48 hr, and the result is displayed in Figure 83(a and b). A distinct bar was developed by the present model, reducing the incident wave energy at the dune and thus reducing the amount of dune erosion compared with the Kriebel model. The shoreward slope of the bar is quite steep due to constancy of the incident wave conditions.

515. Summary. In general, the two models produce similar dune erosion if wave and water level conditions are such that bar development is limited. However, if conditions allow a bar to form, the present model will predict a smaller amount of nearshore erosion than the Kriebel model. The beach profile shape seaward of the dune toe is probably more realistically described in the present model where the area of material deposition is more concentrated, implying a narrower surf zone as the water level increases.

Simulation of Beach Profile Accretion

Background and review

516. Most development work with the numerical model was focused on simulating beach profile response to erosional waves and water levels, since prediction of erosion is of immediate engineering importance. Although berm construction was discussed in the data analysis and geometric properties of the berm quantified, initial model development was not primarily directed toward simulating accretionary stages of a beach. Transport rates from the LWT experiments that resulted in berm buildup were determined from profile surveys, together with some associated characteristics of the transport rate distribution. However, due to lack of suitable test cases having sufficient information of the wave height distribution across the shore, it was not

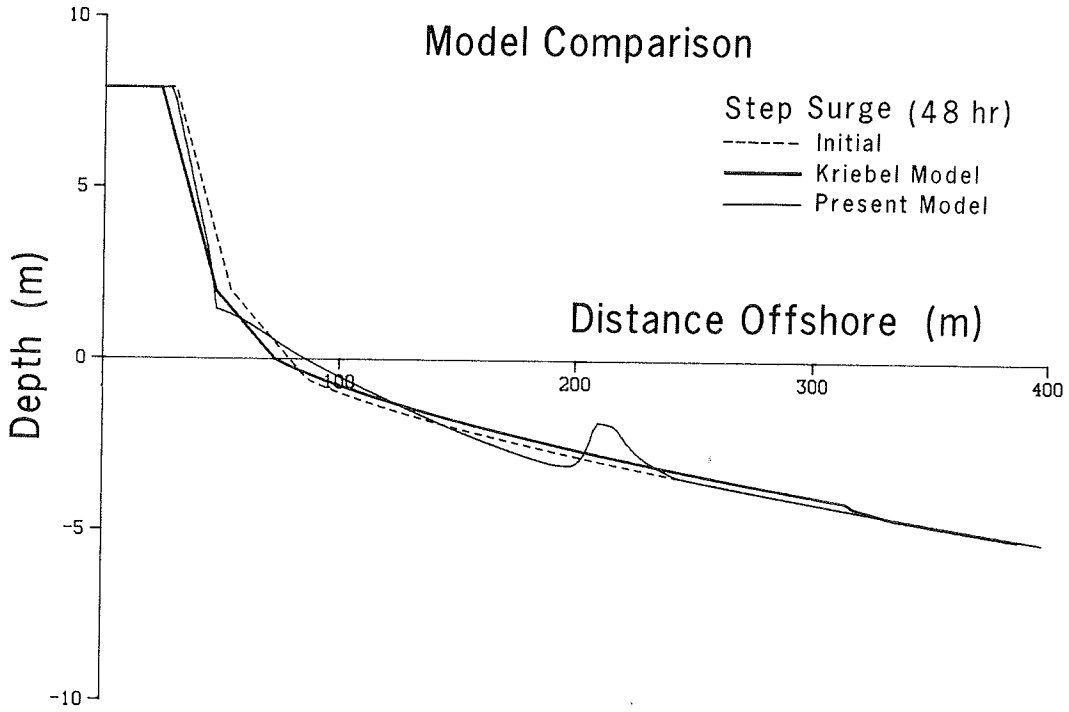

a. Full simulated profile

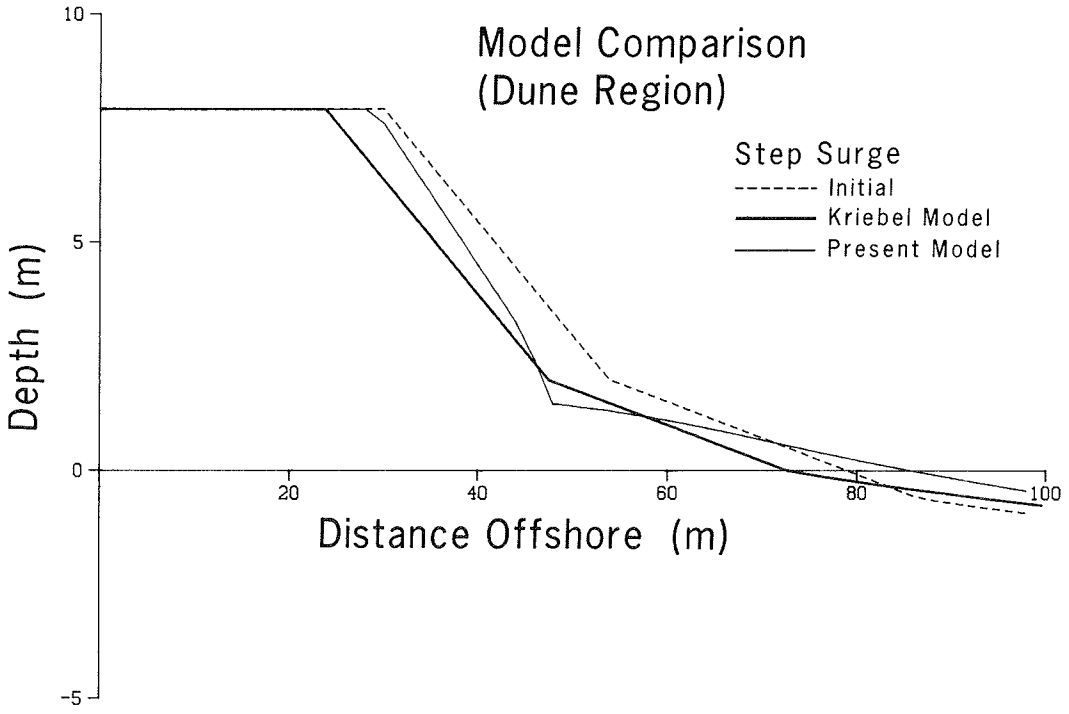

b. Details of dune region

Figure 83. Comparison of present model and Kriebel model for a step increase in water level

possible to derive an empirical transport relationship for the surf zone specifically applicable to onshore-directed transport.

517. The net direction of cross-shore transport may be predicted using Equation 2 in terms of the deepwater wave steepness and dimensionless fall speed. As the grain size increases for given waves, the tendency for onshore-directed transport also increases. By consideration of the dimensionless fall speed, Dean (1973) explained the tendency for onshore transport to occur in terms of the relation between the elevation to which a particle is suspended and the distance it falls during wave passage. A hydraulically heavy particle falls to the bottom during the onshore portion of the wave motion because of the greater settling speed, resulting in net movement onshore.

518. The criterion for distinguishing bar and berm formation is closely related to the transport direction and used in the model to determine transport direction, as discussed previously. The same basic transport relationship (Equation 33) is used whether onshore or offshore transport occurs. A beach that is not in equilibrium with the waves and unable to dissipate incident wave energy uniformly over its length will experience transport until equilibrium is attained if exposed to the same wave climate for a sufficiently long time. For onshore transport, the net transport rate in the model is assumed to be proportional to the energy dissipation per unit volume, similar to the situation for offshore transport. Also, the term which modifies the net transport rate due to the local bottom slope is incorporated. Seaward of the break point, exponential decay (Equation 21) of the transport rate is imposed with a spatial decay coefficient as given from the LWT experiments. The same value of the spatial decay coefficient, 0.11 m^{-1}, is applied independently of wave and sand parameters.

519. Both the location of the plunge point and the value of the spatial decay coefficient between the break point and plunge point are determined in the same manner for both accretionary and erosional profiles. Since the magnitude and direction of the transport rate seaward of the plunge point depend on the transport rate in the surf zone, the transport will be onshore if the transport is directed onshore in the surf zone. On the foreshore, a linearly decreasing transport rate is applied to the runup limit with the decay starting from the shoreward end of the surf zone. This shape is

identical to that chosen for the transport rate distribution on the foreshore for erosional transport. The linear shape of the transport rate on the foreshore was supported by the data analysis for both onshore and offshore transport.

520. Parameter values used in the breaker decay model are identical to the ones applied for erosional conditions, and these values are considered to be representative averages for various slopes. Also, the same criterion for incipient breaking is applied for both erosional and accretionary transport conditions, although this was primarily derived from cases showing erosion and having a distinct breakpoint bar.

Berm simulation

521. Case 101 from the LWT experiments was used to qualitatively evaluate the capability of the model to simulate beach profile accretion. As shown in Figure 84, a berm rapidly formed on the foreshore by onshore transport from breaking waves, and material was deposited up to the limit of runup. As sand was transported onshore, the surf zone and offshore eroded, increasing the depth along this portion of the profile. The increase in depth caused the break point to move onshore and, at about the same time, the berm retreated somewhat at the shoreline while its seaward slope became steeper. Continuous onshore movement of the break point made the surf zone become narrower through time, restricting the onshore transport to a smaller area of the profile. The seaward berm slope steepened because of the continuing transport, limited only by the angle of initial yield. The angle of initial yield had to be reduced somewhat on the foreshore to achieve a less steep slope, considered realistic because of the strong turbulent conditions. A large region of erosion appeared immediately seaward of the foreshore, where a deep trough developed, allowing waves to break at the beach face.

522. The profile approached equilibrium, exhibiting a well-formed berm together with a deep seaward trough. The measured and simulated berm volume and location are in good agreement. However, the seaward slope of the berm grew too steep in the numerical simulation, and the profile shape in the surf zone was not well reproduced. The small bar that developed slightly shoreward of the breakpoint in the wave tank was not obtained with the model. The main

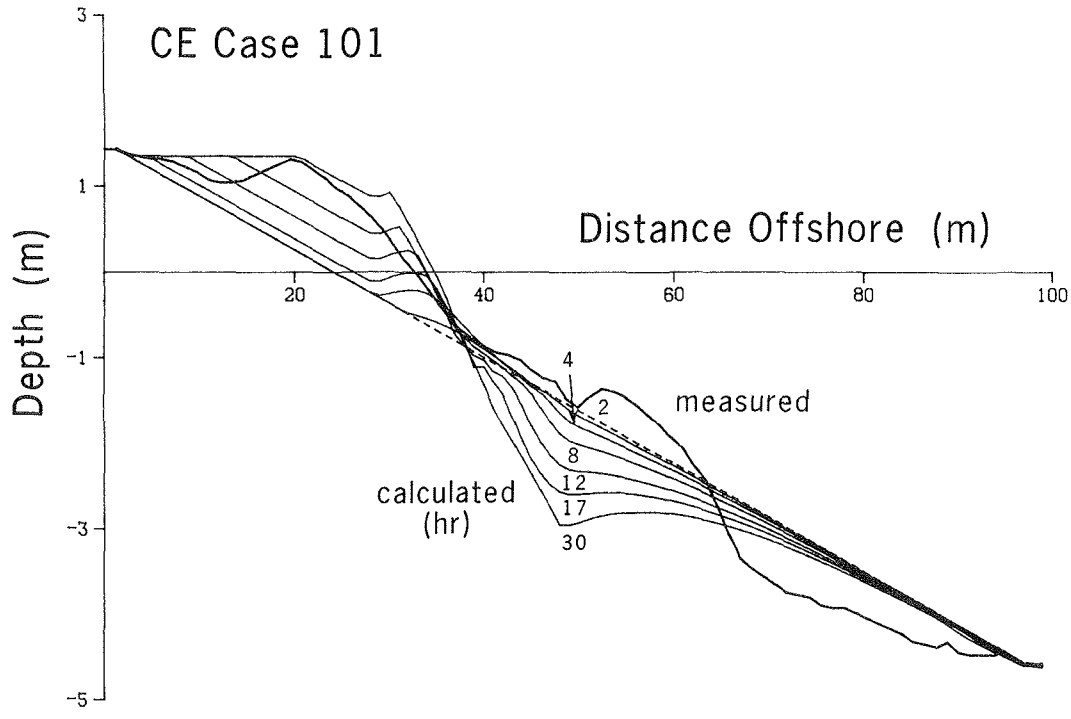

Figure 84. Simulation of berm formation and growth

zone of erosion in the tank occurred more seaward than the location predicted by the numerical model.

523. In other model simulations of accretion, the zone of fully broken waves became very narrow as the break point moved onshore and the waves directly struck the berm or foreshore. The length of the broken wave zone eventually decreased to only one calculation cell, and a transport rate equation based on energy dissipation per unit volume was no longer realistic. In these cases, the transport rate calculated from the energy dissipation was reduced. If no reduction was employed, very local erosion and accretion occurred in the vicinity of the shoreline, giving rise to numerical instability. The value of the reduction factor was typically around 0.2 in these cases. This problem might have been circumvented by using extremely small spatial and temporal steps.

Influence of a Seawall and Beach Fill

524. The numerical model has the capability of simulating the influence of a seawall on beach profile evolution. The shoreward boundary of the calculation grid is located at the seawall preventing transport of material across this cell. The seawall only affects changes in the beach profile if it is exposed to incident waves. Overtopping is not simulated by the model, and it is assumed that the height of the seawall exceeds the runup height (or local wave height).

Profile with seawall

525. A hypothetical example was modeled to evaluate the effect of a seawall on beach profile evolution during storm conditions. The initial profile and wave data from CE Case 400 (Figure 60a) were used, and a seawall was placed on the foreshore, approximately at the still-water shoreline, protecting the subaerial part of the profile from wave attack. The simulation result is displayed in Figure 85, which shows the calculated beach profile at selected time-steps with a seawall on the foreshore and the beach profile at the last time-step without a seawall. The wave height distribution across shore is shown at the last time-step for the seawall calculation.

526. The evolution and size of the bar were similar in the simulation with and without the seawall, the bar being somewhat larger and located more seaward for the case without the wall. The main difference was the amount of material eroded in front of the seawall and shoreward of the bar. With the seawall present, the width of the surf zone was much shorter, requiring more material to be moved before an equilibrium beach shape developed. The subaerial eroded volume for the case without the seawall approximately agreed with the extra volume eroded in front of the seawall.

527. The approach to equilibrium was more rapid for the seawall case, indicated by the slightly more gentle inshore profile slope. The longer time elapsed before equilibrium was obtained for the case without the seawall was caused by the larger extent of the profile involved in redistribution of sand. Since the depth in front of the seawall was greater than for the case without the wall at the corresponding location, the height of the broken waves was larger (compare with wave height distribution in Figure 60a).

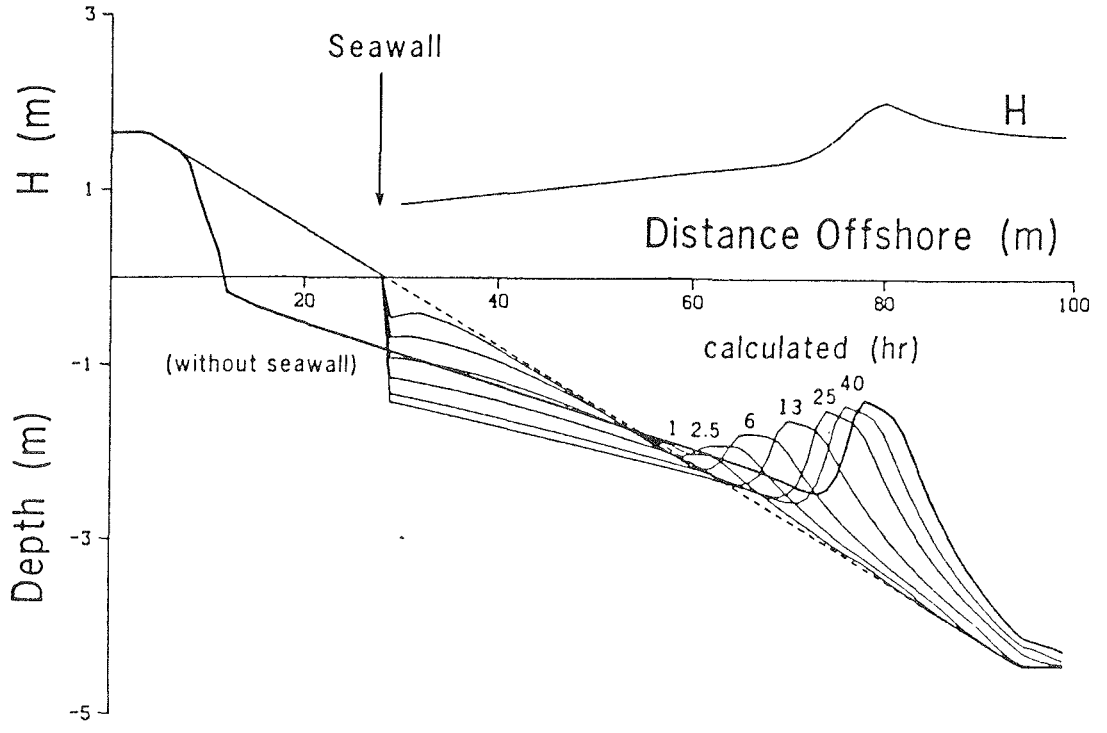

Figure 85. Simulation with and without seawall

Profile with seawall and beach fill

528. To evaluate the performance of the model for more complex conditions, a simulation was carried out for a time period involving both mildly erosive or accretionary waves, a storm event, and a recovery period. Furthermore, a seawall was located in the subaerial part of the profile, and beach profile response was calculated both with and without beach fill. Two different beach fill schemes and grain sizes were evaluated, one case where material was added as an artificial berm above the still-water level and another case where the material was spread out mainly below the still-water level according to the equilibrium shape associated with the natural sand. The wave height and water level of the simulated event are illustrated in Figure 86 (note that the time scale is distorted).

529. During the first 21 days of the simulation, the wave height was 0.5 m and the wave period 8 sec, producing mildly erosional or accretionary conditions depending on the grain size. The beach profile was thus allowed to attain its equilibrium shape for the prevailing wave conditions. At day 21, a

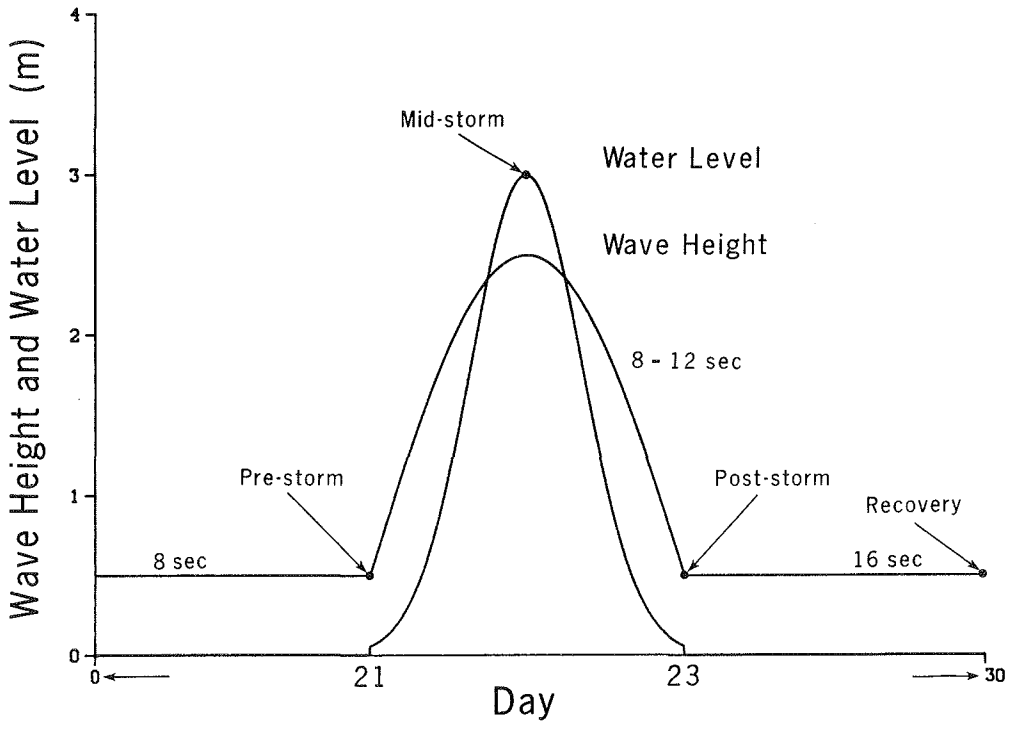

Figure 86. Wave height and water level for beach fill simulations

storm was imposed which lasted 3 days, during which the wave height increased sinusoidally up to a maximum of 2.5 m. Simultaneously, a storm surge occurred with a Gaussian shape, raising the water level to a maximum of 3 m above the still-water level. The wave period varied sinusoidally between 8 and 12 sec during the storm with the maximum period occurring at the same time as the maximum wave height. After the storm, accretionary conditions were imposed with long-period swell of height 0.5 m and period 16 sec, producing beach recovery.

530. Original profile. At first, model simulations were performed without adding fill for the two grain sizes 0.25 and 0.40 mm. The initial profile consisted of two linear slopes to a depth of 0.5 m, joining to an equilibrium profile shape (Equation 1). Figure 87(a and b) shows the beach profiles at selected times during the simulated time period; just before the storm (Day 21, prestorm), during the storm (middle of Day 22, midstorm), after the storm (Day 23, poststorm), and at the end of the simulation period (Day 30, recovery).

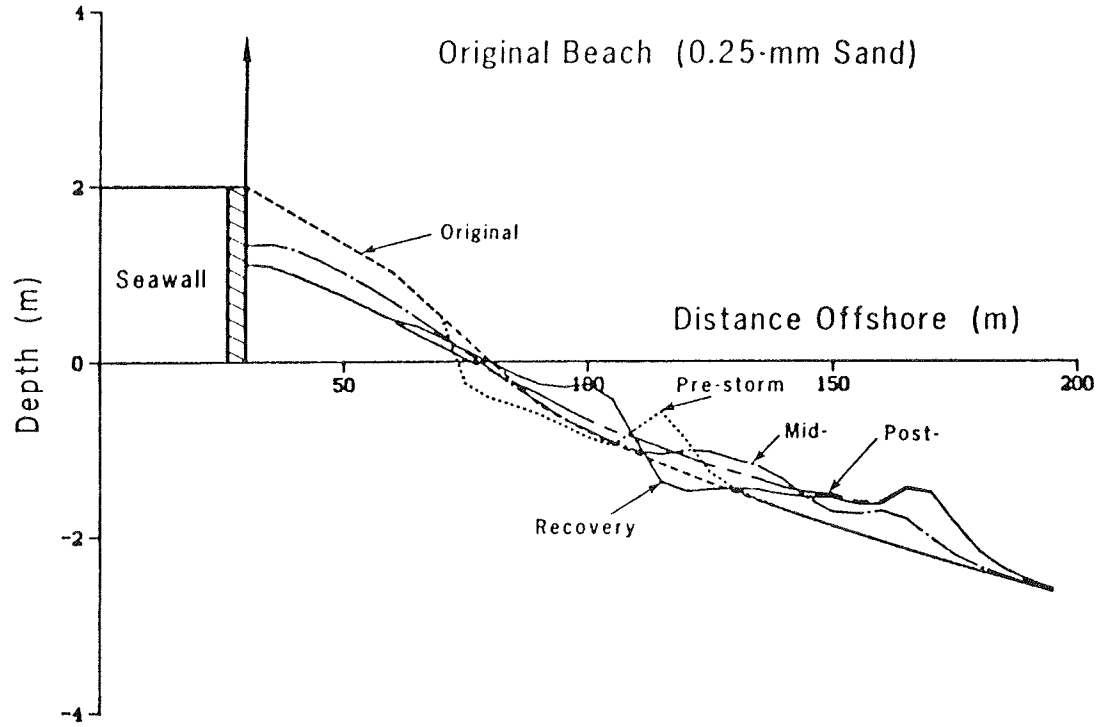

a. 0.25-mm beach

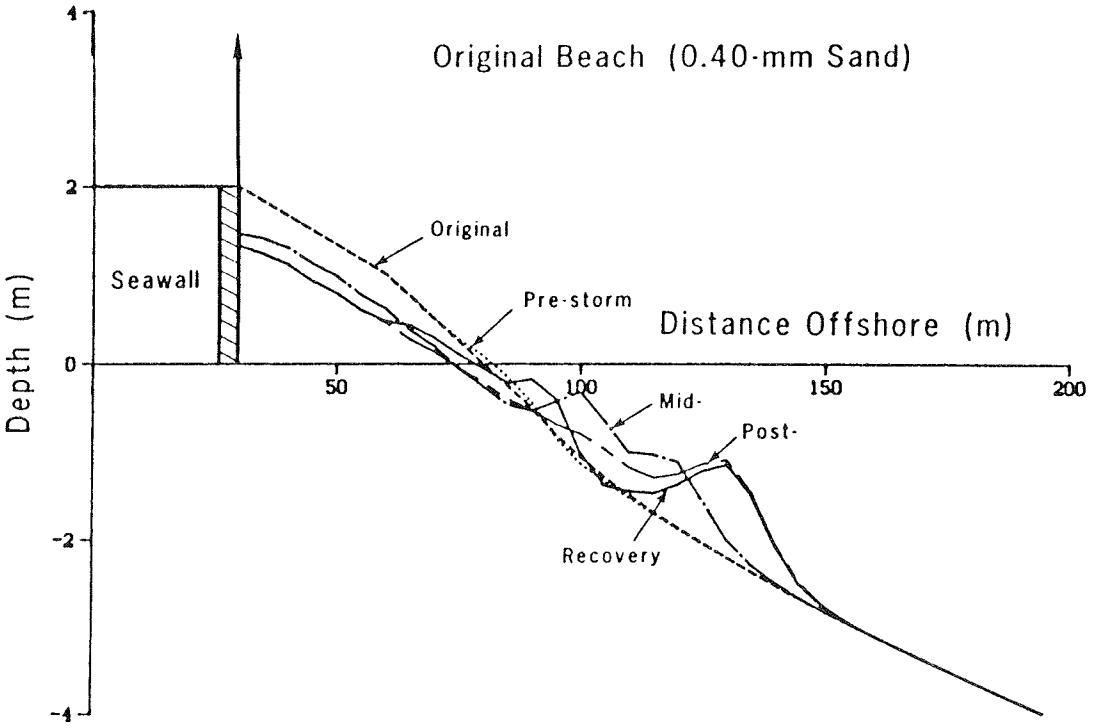

b. 0.40-mm beach

Figure 87. Response of original beach to the storm event

531. Initial wave conditions produced erosion for the 0.25-mm grain size (Figure 87a), and a small bar developed offshore with the shoreline receding somewhat. As water level increased during the storm, the beach in front of the seawall was submerged, and considerable erosion occurred. The high seawall prevented the beach from retreating. A long flat bar developed during the peak of the storm which moved offshore with the break point as the water level decreased. After the storm, the inshore portion of the profile partly recovered, producing buildup on the foreshore and a bar-like feature just below the still-water level. The main part of the bar, however, did not contribute material for the recovery process since it was located too deep and too far seaward of the breaking waves.

532. The equilibrium profile of the 0.40-mm sand was much steeper than the 0.25-mm beach (Figure 87b) because of the grain-size dependence of the A-parameter in Equation 1. Mild waves arriving during the initial part of the simulation period produced onshore transport and a small berm. During the storm surge, the amount of subaerial erosion was similar to that in the 0.25-mm profile example, but the bar did not migrate as far offshore. The recovery of the 0.40-mm beach did not produce such a marked trough seaward of the bar-like feature as did the 0.25-mm beach.

533. Artificial berm. The first type of beach fill evaluated was an artificial berm consisting of approximately 85 m^3/m of material placed on the subaerial portion of the beach. In simulations with the beach fill, it was assumed that the fill material was identical to the natural beach sand. A small bar formed before the storm, much in agreement with the case without the fill but closer to shore. During the storm, a large part of the fill eroded and was deposited offshore. Figure 88(a and b) illustrates simulation results for the 0.25- and 0.40-mm grain sizes. Although significant recovery occurred for the 0.25-mm beach, a large amount of material was trapped offshore. The eroded material from the artificial berm for the 0.40-mm beach was deposited closer to shore, and during the recovery phase the entire bar moved slightly onshore.

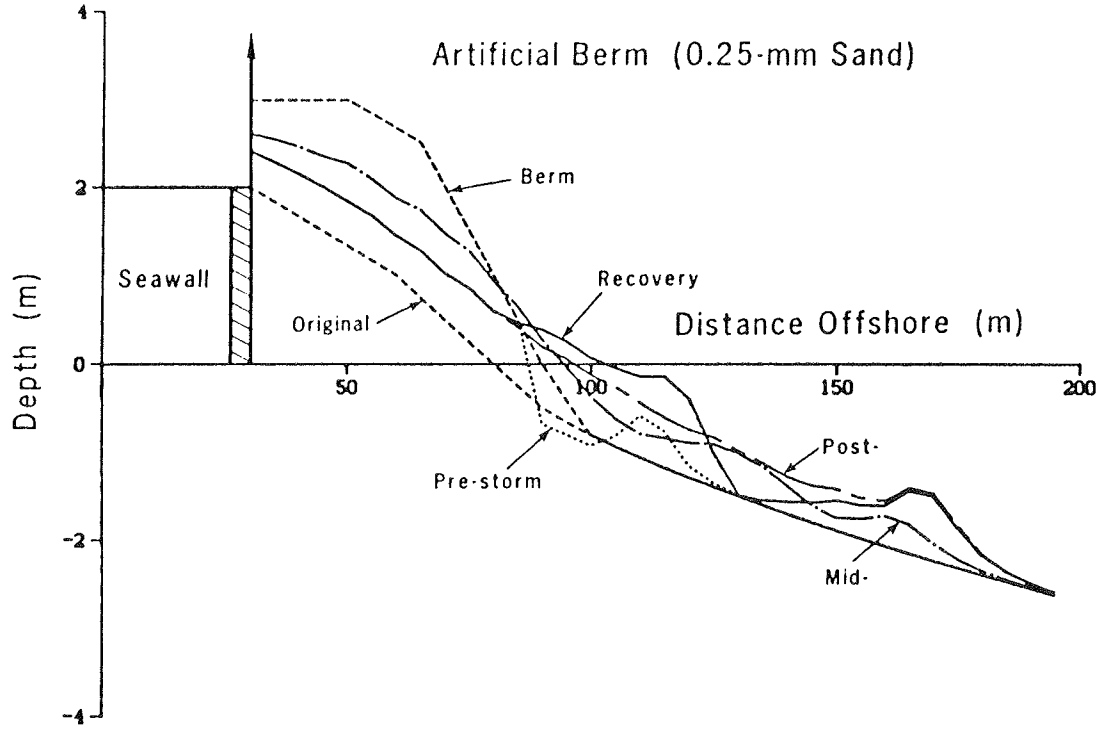

a. 0.25-mm beach

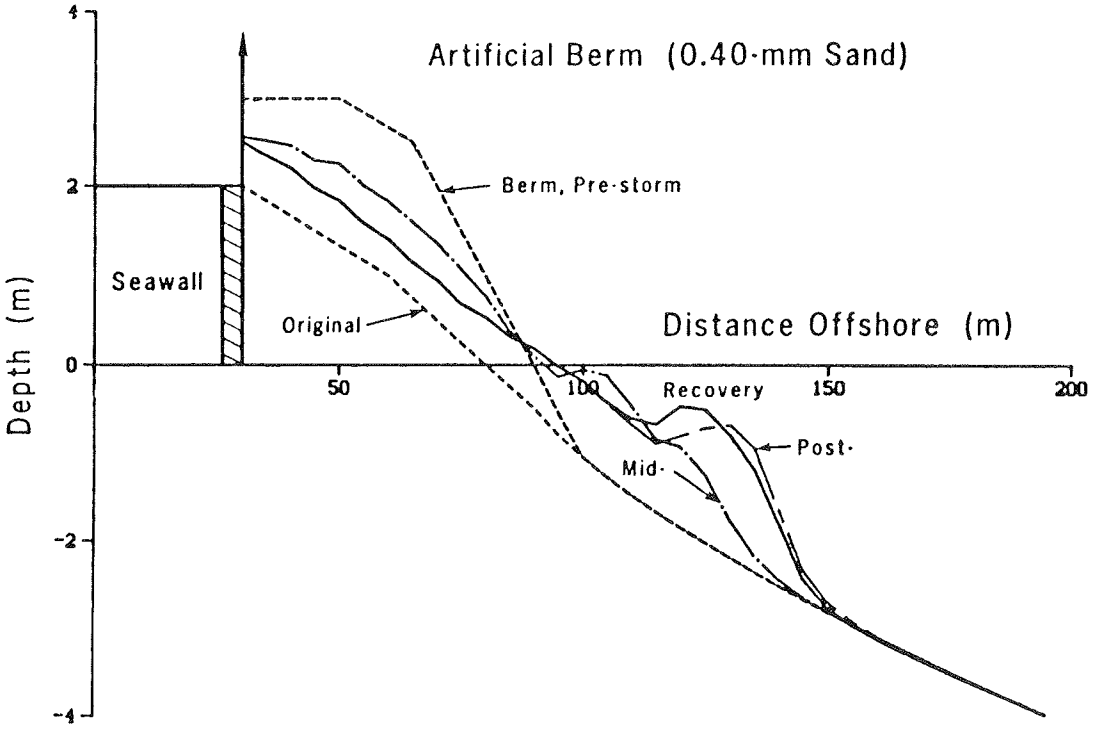

b. 0.40-mm beach

Figure 88. Response of artificial berm to the storm event

534. Bruun fill. In the second fill alternative, material was deposited mostly along the subaqueous portion of the profile in accordance with the equilibrium shape of the beach (called a Bruun beach fill). Bruun (1988) has advocated "profile nourishment," as opposed to placing fill material only on the upper part of the profile, under the concept that the beach can best resist erosive wave action in its most natural shape. The fill volume was 85 m^3/m, the same as for the artificial berm. Figure 89(a and b) shows the simulation result for the two grain sizes studied. The amount of subaerial erosion was reduced significantly even though the entire profile was submerged during much of the storm surge. Bar development was less pronounced for the 0.25-mm beach compared to the artificial berm case, whereas the 0.40-mm beach showed stronger bar formation.

535. Summary. The numerical model provided qualitatively reasonable results in calculation of the response of hypothetical beach cross sections to storm events. In the examples, the Bruun fill provided better overall protection of the subaerial beach according to the numerical model, and less material was redistributed along the profile during the storm surge compared to the artificial berm design. Examples given in this section are described further by Kraus and Larson (1988b). Larson and Kraus (in press) extend the analysis further to consider model predictions for erosion of various cross sections to a synthetic hurricane and a synthetic extratropical storm with return periods of approximately 2-5 years.

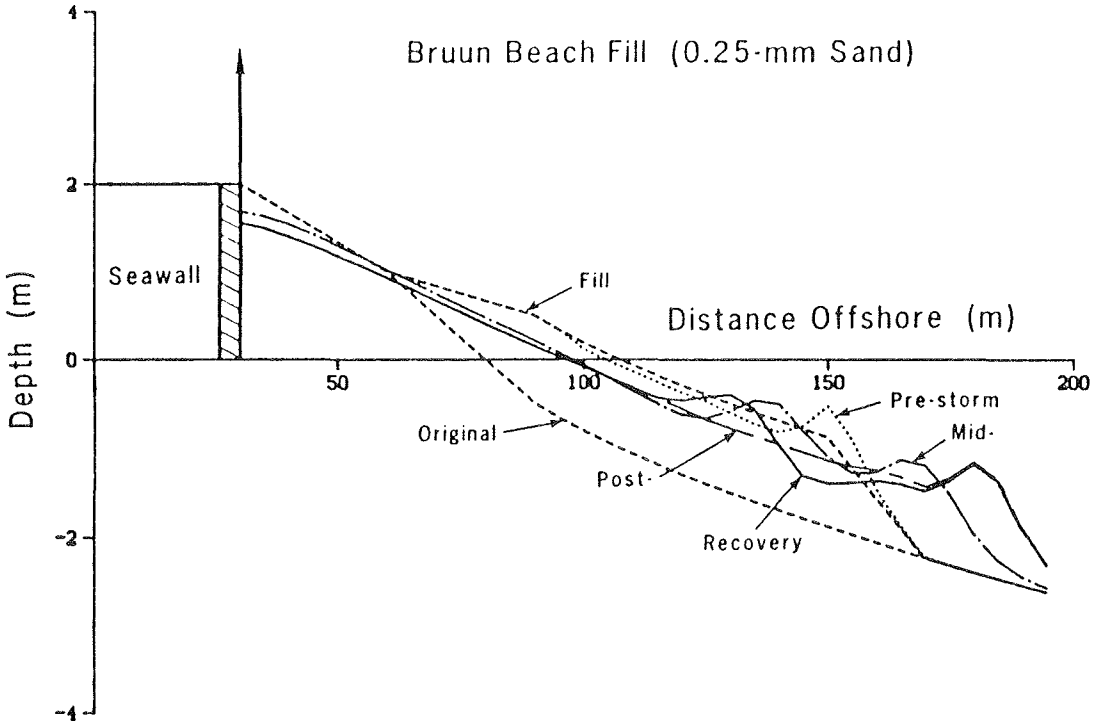

a. 0.25-mm beach

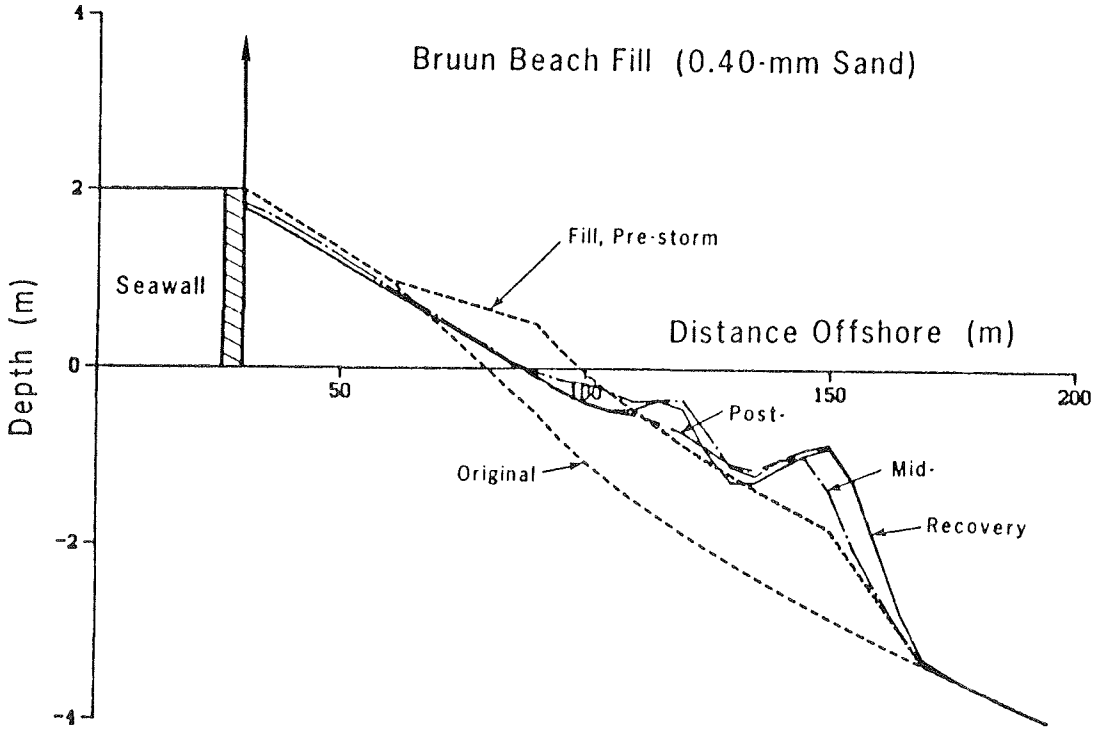

b. 0.40-mm beach

Figure 89. Response of the Bruun fill to the storm event

PART VIII: SUMMARY AND CONCLUSIONS

536. The ultimate objective of this study was to develop an engineering numerical model of beach profile change having the capability of simulating formation and movement of major morphologic features of the profile, particularly bars and berms. Beach profile response produced by severe storm or hurricane events, with large erosion and possible dune retreat, was the principal target problem of the study, although profile change occurring on longer time scales, such as adjustment of beach fill, which involves accretionary as well as erosional processes, was also of interest. A basic assumption underlying this work was that major morphologic change occurring in and around the surf zone is produced by breaking and broken waves.

537. Data from two LWT experiments were used in development of the numerical model; one experiment performed by the US Army Corps of Engineers (CE) and the other carried out by the Central Research Institute of Electric Power Industry (CRIEPI), Japan. In total, these experiments encompassed 42 cases having different values of wave height, wave period, water level, grain size, and initial profile slope or shape. The CRIEPI experiment also included measurements of wave height along the profile from prebreaking through the surf zone.

538. Extensive analysis of morphologic features of the profile was conducted to provide the foundation for the numerical model, but the analysis also produced functional relationships between geometric characteristics of the profile and wave and sand properties. Geometric properties of the profile that were quantified were bar volume, bar height, depth-to-bar crest, ratio of depth-to-bar trough and depth-to-bar crest, distance between break point and trough bottom, movement of mass center of bar, bar migration speed, bar slopes, active profile height, step and terrace slopes, berm volume, berm height, and berm slopes. This type of analysis is expected to stimulate corresponding analysis of field profiles and provide guidance for collecting analogous field data.

539. Regression relationships were established between a number of geometric characteristics of the profile and wave and sand properties. In this process, the dimensionless fall speed H_o/wT emerged as an important

parameter together with the deepwater wave steepness H_o/L_o . Quantities that could be related to either H_o/wT , H_o/L_o , or both parameters were bar volume, ratio of trough depth to crest depth, bar height, and active profile height, respectively normalized with various wave or sand properties. Distance between break point and trough bottom, normalized with deepwater wavelength, was determined to be a function of the local slope seaward of the break point and H_b/H_o . Average depth to bar crest proved to be directly proportional to the breaking wave height. Profile properties derived from the LWT data sets were found comparable to those in the field, which supported the possibility of generalizing observations from the LWT experiments to field application. The validity of the equilibrium beach profile concept was confirmed by the LWT experiments, which clearly showed a systematic decrease in profile change as time elapsed.

540. A criterion (Equation 2) was developed to delineate between formation of bar and berm profiles in terms of H_o/wT and H_o/L_o . Although several well-known criteria were evaluated using the LWT experiments, the criterion developed in the present study appeared to be the most attractive from a physical point of view and gave a good delineation between bar and berm profiles. The criterion was closely related to the predominant direction of cross-shore transport. A bar formed under mainly offshore-directed transport and a berm formed under mainly onshore-directed transport. The criterion was tested with field data and found to be valid with the same value of the empirically determined coefficient when the deepwater wave height appearing in the criterion was taken to be the mean wave height.

541. Profile slopes were analyzed for the seaward and shoreward side of the bar, seaward and shoreward side of the berm, inshore step, and terrace. Circumstantial evidence was found for the process of avalanching to occur on the shoreward bar face and on the inshore step as the slopes grew beyond a critical angle. An average estimate of this angle of initial yield was 28 deg, and the slope appeared to reach a stable value of around 20 deg. The average slope on the seaward bar face was typically in the range 8-12 deg and was, in many cases, well approximated by two linear slopes, possibly signifying the occurrence of two somewhat different sediment transport processes. Bar slopes for the LWT experiments were considerably steeper than correspond-

ing slopes found in the field, attributed to the monochromatic waves and constant water level used in the experiments. Berm face slopes were typically in the range of 6-8 deg on the seaward side and 2-4 deg on the shoreward side.

542. Properties of the cross-shore transport rate were investigated by integrating the mass conservation equation between consecutive profiles in time. This methodology provided a picture of the net average transport rate distribution between two surveys. The magnitude of the net transport rate distribution decreased with time as the profile approached an equilibrium shape and less material moved along the profile. Decrease of peak transport rates was best described by a function which showed an inverse dependence with elapsed time, not with an expected exponential decay with time. This difference was attributed to randomness of microscale processes and slight unsteadiness in forcing conditions, which produce a perturbation on the idealized mean behavior. Decrease of the peak transport rate was more rapid for accretionary profiles than erosional profiles.

543. By comparing the initial and final profile surveys, an "equilibrium transport distribution" was defined and calculated, which indicated how sand was redistributed along the profile to achieve an equilibrium configuration. Equilibrium distribution could be classified into three characteristic shapes in a majority of the experimental cases; Erosional (Type E), Accretionary (Type A), and mixed Accretionary-Erosional (Type AE). Type E distributions showed transport directed offshore along the entire profile, whereas Type A distributions showed transport directed onshore along the entire profile. Type AE distributions were characterized by a mixed response with offshore transport along the shoreward portion of the profile and onshore transport along the seaward portion of the profile.

544. The profile was divided into four different zones to interpret and quantify properties of the cross-shore transport rate distribution, in analogy with recent findings from nearshore wave dynamics. These zones were: prebreaking zone (I), breaker transition zone (II), broken wave zone (III), and swash zone (IV). For Zone I, the LWT experiments showed that the net transport rate was well approximated by an exponential decay with distance from the break point, with a spatial decay coefficient (average value of 0.18 m^{-1}) proportional to the ratio of the grain size to the breaking wave height for

erosional conditions. Exponential decay proved to be valid for onshore transport as well, but the spatial decay coefficient was almost constant, with an average value of 0.11 m^{-1}.

545. For Zone II, which extends over the narrow range from the break point to the plunge point, it was difficult to extract information on the transport characteristics from the LWT experiments. However, an exponential decay with distance offshore showed good agreement with transport rate data inferred from the small number of available cases, with a spatial decay coefficient about 0.20 of the value of the spatial decay coefficient applicable to Zone I. Zone III encompasses the main part of the surf zone, and the transport rate was demonstrated to be closely related to the energy dissipation per unit volume, based on the CRIEPI experiment results involving wave height distributions and profile change. Values of empirical coefficients in the transport equation found through regression analysis were similar to values found by other authors through more indirect numerical modeling.

546. In Zone IV, the region dominated by runup and backrush, the transport rate is governed by swash dynamics. A transport rate expressed in terms of physical quantities could not be developed for this zone due to lack of measurements of swash wave properties. However, the transport rate showed an approximately linear behavior for both offshore and onshore transport for a wide range of conditions. The extent of Zone IV decreased if the profile eroded and a step evolved, and the transport rate simultaneously decreased with time.

547. A numerical model of profile response was developed on the basis of quantitative analysis of the LWT wave and profile change data. The domain of model extends from the depth of significant net cross-shore sediment movement, located seaward of the largest breaking waves, to the limit of runup on the beach face. The model calculates the wave height distribution across-shore at each time-step with linear wave theory up to the break point, and thereafter with a breaker decay model in the surf zone. The break point is determined from an empirical criterion, derived from the CRIEPI data set, relating the breaker ratio to the surf similarity parameter defined by the deepwater wave steepness and the local slope seaward of the break point. A nonlinear shoaling theory was applied initially but found to overestimate the

breaking wave height, not producing as good agreement as linear wave theory in comparisons with the LWT data.

548. In the numerical model, the net cross-shore sediment transport rate distribution is determined by using local wave properties along the profile. The profile is divided into four zones according to findings from the LWT data sets, and the respective transport relationships are used to determine the transport magnitude. Transport direction is determined from an empirical criterion derived from the LWT data sets, which predicts bar or berm profile development. Changes in the profile are determined from the mass conservation equation. The model proved to be numerically stable over a wide range of conditions, and simulated profiles approached an equilibrium configuration if exposed to constant waves and water level.

549. The model was calibrated against seven cases from the CE and CRIEPI experiments showing foreshore erosion and bar formation. The optimal value of the empirical rate coefficient for the transport relationship applied in zones of broken waves was $1.6\ 10^{-6}\ m^4/N$. The model was then verified against two independent cases from the CE and CRIEPI experiments with the parameter values given by the calibration. Good agreement was obtained between calculated and measured profiles regarding both the amount of foreshore erosion and the movement and size of the main breakpoint bar. The bar trough was less well reproduced, and smaller features inshore of the main breakpoint bar were omitted in the simulations. The model was also tested with one CE case which included a water level variation simulating a tide, and this case was also satisfactorily reproduced.

550. A number of hypothetical cases were simulated with the numerical model to evaluate the influence of variations in incident wave height, wave period, and water level. Sensitivity analyses were performed for a large number of model parameters to establish their influence on bar formation. Simulation for a hypothetical example which included a seawall on the foreshore showed that the size of the bar was approximately the same as for simulations without the seawall, but the area immediately seaward of the seawall experienced more erosion. Simulations of beach fill adjustment for use in storm protection design were also performed as an example of the utility of the model.

551. The process of multiple bar formation was simulated and compared with one case from the CE data set where two bars developed. Multiple bars could be generated in the numerical model by allowing wave reformation and the appearance of multiple break points. Data from the LWT experiments gave little guidance about the cross-shore transport properties in zones of wave reformation. The transport rate in this zone was determined through simple functional relationships based on qualitative observations from the experiments.

552. The model was also used to simulate onshore transport and berm formation by using one CE case. The size of the berm was well reproduced; however, the model failed to adequately describe the seaward berm face slope and inshore profile shape. The seaward berm face slope is only limited by the angle of initial yield in the model because of the crude description of transport in the swash zone.

553. A comparison between the present model and the Kriebel (1982, 1986) model was conducted to evaluate how bar formation would affect beach erosion. One hypothetical case involved a variation in water level which prevented bar development; both models gave similar predictions of erosion. The description of the profile at the dune toe was more realistically described by the present model, based on experience with the LWT and other experiments, than by the Kriebel model, which distributed the eroded material more evenly over the surf zone. Another comparison case involved bar development, giving a significant difference in dune retreat, for which the Kriebel model produced a larger amount of erosion than the present model, as expected.

554. The numerical model was also used to simulate bar movement in the field at CERC's FRF in Duck, North Carolina. Four different storm events showing erosive profile response and offshore bar movement were used in the calibration, and another independent event was used for verification of the model. Some empirical model parameters determined with the LWT data had to be modified somewhat to achieve agreement with measured field profiles. In particular, the transport rate coefficient took a smaller value for the field simulation than for the LWT cases, with an overall best value in a least-square sense of $0.7\ 10^{-6}\ m^4/N$.

555. Bar movement and location of bar crest were well reproduced by the model both for the field calibration and verification runs. However, bar troughs were not pronounced enough in the model, and bar size was underestimated. Although bar face slopes produced by the model were steep for the LWT cases simulated, in agreement with the physical experiment data, model simulations for the field data with variable input waves and water level produced more gentle slopes in agreement with the field measurements. This finding supports the assumption of superposition implicit in the numerical model, whereby the effect of a random wave field can be simulated as the effect of a number of consecutive individual waves of different height and period.

556. In conclusion, this study validated the methodology of obtaining quantitative information on beach profile response in prototype-sized facilities and generalizing the information to field conditions. The developed numerical model successfully reproduced beach profile change both in large tanks and in the field. The approach of focusing on macroscale profile features such as bars and berms proved highly productive, both for providing a thorough and quantitative understanding of beach profile change to wave action and for promoting development of numerical models for simulating coastal processes aimed at engineering use.

REFERENCES

Allen, J. R. 1970. "The Avalanching of Granular Solids on Dune and Similar Slopes," Journal of Geology, Vol 78, No. 3, pp 326-351.

Aubrey, D. G. 1978. "Statistical and Dynamical Prediction of Changes in Natural Sand Beaches," unpublished Ph.D. thesis, University of California, San Diego, CA.

_____. 1979. "Seasonal Patterns of Onshore/Offshore Sediment Movement," Journal of Geophysical Research, Vol 84, No. C10, pp 6347-6354.

Aubrey, D. G., Inman, D. L., and Nordstrom, C. E. 1977. "Beach Profiles at Torrey Pines, California," Proceedings of the 15th Coastal Engineering Conference, American Society of Civil Engineers, pp 1297-1311.

Aubrey, D. G., Inman, D. L., and Winant, C. D. 1980. "The Statistical Prediction of Beach Changes in Southern California," Journal of Geophysical Research, Vol 85, No. C6, pp 3264-3276.

Aubrey, D. G., and Ross, R. M. 1985. "The Quantitative Description of Beach Cycles," Marine Geology, Vol 69, pp 155-170.

Bagnold, R. A. 1940. "Beach Formation by Waves; Some Model-Experiments in a Wave Tank," Journal of the Institution of Civil Engineers, No. 1, pp 27-52.

_____. 1963. "Mechanics of Marine Sedimentation," In: The Sea, Vol 3, ed. M. N. Hill, Interscience, NY, pp 507-528.

_____. 1966. "An Approach to the Sediment Transport Problem from General Physics," Geological Survey Professional Paper 422-I, Washington D.C.

Bailard, J. A. 1982. "An Energetics Total Load Sediment Transport Model for a Plane Sloping Beach," Naval Civil Engineering Laboratory, Report No. TN-1626, Port Hueneme, CA.

Bailard, J. A., and Inman, D. L. 1981. "An Energetics Bedload Model for a Plane Sloping Beach: Local Transport," Journal of Geophysical Research, Vol 86, No. C3, pp 2035-2043.

Balsillie, J. H. 1984. "A Multiple Shore-Breaking Wave Transformation Computer Model," Florida Department of Natural Resources, Beaches and Shores Technical and Design Memorandum No. 84-4, Tallahassee, FL.

Basco, D. R. 1985. "A Qualitative Description of Wave Breaking," Journal of Waterway, Port, Coastal and Ocean Engineering, Vol 111, No. 2, pp 171-188.

Basco, D. R., and Yamashita, T. 1987. "Toward a Simple Model of the Wave Breaking Transition Region in Surf Zones," Proceedings of the 20th Coastal Engineering Conference, American Society of Civil Engineers, pp 955-970.

Bascom, W. N. 1951. "The Relationship Between Sand Size and Beach-Face Slope," Transactions American Geophysical Union, Vol 32, No. 6, pp 866-874.

Battjes, J. A. 1975. "Surf Similarity," Proceedings of the 14th Coastal Engineering Conference, American Society of Civil Engineers, pp 466-480.

Battjes, J. A., and Janssen, J. P. F. M. 1979. "Energy Loss and Set-Up Due to Breaking of Random Waves," Proceedings of the 16th Coastal Engineering Conference, American Society of Civil Engineers, pp 569-587.

Berg, D. W., and Duane, D. B. 1968. "Effect of Particle Size and Distribution on Stability of Artificially Filled Beach, Presque Isle Peninsula, Pennsylvania," Proceedings of the 11th Conference on Great Lakes Research, International Association of Great Lakes Research, pp 161-178.

Birkemeier, W. A. 1985a. "Time Scale of Nearshore Profile Changes," Proceedings of the 19th Coastal Engineering Conference, American Society of Civil Engineers, pp 1507-1521.

_____. 1985b. "Field Data on Seaward Limit of Profile Change," Journal of Waterway, Port, Coastal and Ocean Engineering, Vol 111, No. 3, pp 598-602.

Birkemeier, W. A., Kraus, N. C., Scheffner, N. W., and Knowles, S. C. 1987. "Feasibility Study of Quantitative Erosion Models for Use by the Federal Emergency Management Agency in the Prediction of Coastal Flooding," Technical Report CERC-87-8, Coastal Engineering Research Center, US Army Engineer Waterways Experiment Station, Vicksburg, MS.

Boczar-Karakiewicz, B., and Davidson-Arnott, R. G. D. 1987. "Nearshore Bar Formation by Non-Linear Wave Processes - A Comparison of Model Results and Field Data," Marine Geology, Vol 77, pp 287-304.

Bowen, A. J. 1980. "Simple Models of Nearshore Sedimentation; Beach Profiles and Longshore Bars," In: The Coastline of Canada, ed. S. B. McCann, Geological Survey of Canada, Paper 80-10, pp 1-11.

Bruun, P. 1954. "Coast Erosion and the Development of Beach Profiles," Technical Memorandum No. 44, Beach Erosion Board, Coastal Engineering Research Center, US Army Engineer Waterways Experiment Station, Vicksburg, MS.

_____. 1962. "Sea-Level Rise as a Cause of Shore Erosion," Journal of the Waterways and Harbors Division, American Society of Civil Engineers, Vol 88, No. WW1, pp 117-130.

_____. 1988. "Profile Nourishment: Its Background and Economic Advantages," Journal of Coastal Research, Vol 4, No. 2, pp 219-228.

Buhr Hansen, J., and Svendsen, I. A. 1975. "Laboratory Generation of Waves of Constant Form," Proceedings of the 14th Coastal Engineering Conference, American Society of Civil Engineers, pp 321-339.

Caldwell, J. M. 1959. "Shore Erosion by Storm Waves," Miscellaneous Paper No. 1-59, Beach Erosion Board, Coastal Engineering Research Center, US Army Engineer Waterways Experiment Station, Vicksburg, MS.

Carter, T. G., Liu, P. L-F., and Mei, C. C. 1973. "Mass Transport by Waves and Offshore Sand Bedforms," Journal of the Waterways, Harbors and Coastal Engineering Division, American Society of Civil Engineers, Vol 99, No. WW2, pp 165-184.

Chappell, J., and Eliot, I. G. 1979. "Surf-Beach Dynamics in Time and Space - An Australian Case Study, and Elements of a Predictive Model," Marine Geology, Vol 32, pp 231-250.

Chiu, T. Y. 1977. "Beach and Dune Response to Hurricane Eloise of September 1975," Proceedings of Coastal Sediments '77, American Society of Civil Engineers, pp 116-134.

Dally, W. R. 1980. "A Numerical Model for Beach Profile Evolution," unpublished M.S. Thesis, University of Delaware, Newark, DE.

_____. 1987. "Longshore Bar Formation - Surf Beat or Undertow," Proceedings of Coastal Sediments '87, American Society of Civil Engineers, pp 71-86.

Dally, W. R., and Dean, R. G. 1984. "Suspended Sediment Transport and Beach Profile Evolution," Journal of Waterway, Port, Coastal and Ocean Engineering, Vol 110, No. 1, pp 15-33.

Dally, W. R., Dean, R. G., Dalrymple, R. A. 1985a. "Wave Height Variation Across Beaches of Arbitrary Profile," Journal of Geophysical Research, Vol 90, No. C6, pp 11917-11927.

_____. 1985b. "A Model for Breaker Decay on Beaches," Proceedings of the 19th Coastal Engineering Conference, American Society of Civil Engineers, pp 82-98.

Dalrymple, R. A., and Thompson, W. W. 1977. "Study of Equilibrium Beach Profiles," Proceedings of the 15th Coastal Engineering Conference, American Society of Civil Engineers, pp 1277-1296.

Davidson-Arnott, R. G. D. 1975. "Form, Movement and Sedimentological Characteristics of Wave-Formed Bars - A Study of their Role in Nearshore Equilibrium," unpublished Ph.D. thesis, Department of Geography, University of Toronto, Toronto, Canada.

_____. 1981. "Computer Simulation of Nearshore Bar Formation," Earth Surface Processes and Landforms, Vol 6, pp 23-34.

Davidson-Arnott, R. G. D., and Pember, G. F. 1980. "Morphology and Sedimentology of Multiple Parallel Bar Systems, Southern Georgian Bay, Ontario," In: The Coastline of Canada, ed. S. B. McCann, Geological Survey of Canada, Paper 80-10, pp 417-428.

Davidson-Arnott, R. G. D., and Randall, D. C. 1984. "Spatial and Temporal Variations in Spectra of Storm Waves Across a Barred Nearshore," Marine Geology, Vol 60, pp 15-30.

Davis, R. A., and Fox, W. T. 1972. "Coastal Processes and Nearshore Sand Bars," Journal of Sedimentary Petrology, Vol 42, No. 2, pp 401-412.

Davis, R. A., Fox, W. T., Hayes, M. O., and Boothroyd, J. C. 1972. "Comparison of Ridge and Runnel Systems in Tidal and Non-Tidal Environments," Journal of Sedimentary Petrology, Vol 42, No. 2, pp 413-421.

Dean, R. G. 1973. "Heuristic Models of Sand Transport in the Surf Zone," Proceedings of the Conference on Engineering Dynamics in the Surf Zone, Sydney, Australia, pp 208-214.

_____. 1976. "Beach Erosion: Causes, Processes, and Remedial Measures," CRC Reviews in Environmental Control, CRC Press Inc., Vol 6, Issue 3, pp 259-296.

_____. 1977. "Equilibrium Beach Profiles: U.S. Atlantic and Gulf Coasts," Department of Civil Engineering, Ocean Engineering Report No. 12, University of Delaware, Newark, DE.

_____. 1984. "Applications of Equilibrium Beach Profile Concepts," Coastal Engineering Abstracts, American Society of Civil Engineers, pp 140-141.

_____. 1987. "Coastal Sediment Processes: Toward Engineering Solutions," Proceedings of Coastal Sediments '87, American Society of Civil Engineers, pp 1-24.

De Best, A., and Bijker, E. W. 1971. "Scouring of a Sand Bed in Front of a Vertical Breakwater," Report No. 71-1, Department of Civil Engineering, Delft University of Technology, The Netherlands.

Deguchi, I., and Sawaragi, T. 1985. "Calculation of the Rate of Net On-Offshore Sediment Transport on the Basis of Flux Concept," Proceedings of the 19th Coastal Engineering Conference, American Society of Civil Engineers, pp 1325-1341.

Dette, H. H. 1986. "Untersuchungen über Dünenabbrüche und Stranderosion im Grossen Wellenkanal," Die Küste, Heft 43, pp 247-282.

Dette, H. H., and Uliczka, K. 1987a. "Prototype Investigation on Time-Dependent Dune Recession and Beach Erosion," Proceedings of Coastal Sediments '87, American Society of Civil Engineers, pp 1430-1444.

_____. 1987b. "Velocity and Sediment Concentration Fields Across Surf Zones," Proceedings of the 20th Coastal Engineering Conference, American Society of Civil Engineers, pp 1062-1076.

Dingler, J. R., and Inman, D. L. 1977. "Wave-Formed Ripples in Nearshore Sands," Proceedings of the 15th Coastal Engineering Conference, American Society of Civil Engineers, pp 2109-2126.

Dolan, T. J. 1983. "Wave Mechanics for the Formation of Multiple Longshore Bars with Emphasis on the Chesapeake Bay," unpublished M.S. thesis, University of Delaware, Newark, DE.

Dolan, T. J., and Dean, R. G. 1984. "Multiple Longshore Sand Bars in the Upper Chesapeake Bay," Estuarine Coastal and Shelf Science, Vol 21, No. 5, pp 727-743.

Dyhr-Nielsen, M., and Sørensen, T. 1971 "Some Sand Transport Phenomena on Coasts with Bars," Proceedings of the 12th Coastal Engineering Conference, American Society of Civil Engineers, pp 855-865.

Eagleson, P. S., Glenne, B., and Dracup, J. A. 1963. "Equilibrium Characteristics of Sand Beaches," Journal of the Hydraulics Division, American Society of Civil Engineers, Vol 89, No. 1, pp 35-57.

Ebersole, B. A. 1987. "Measurements and Prediction of Wave Height Decay in the Surf Zone," Proceedings of Coastal Hydrodynamics, American Society of Civil Engineers, pp 1-16.

Edelman, T. 1969. "Dune Erosion During Storm Conditions," Proceedings of the 11th Coastal Engineering Conference, American Society of Civil Engineers, pp 719-722.

_____. 1973. "Dune Erosion During Storm Conditions," Proceedings of the 13th Coastal Engineering Conference, American Society of Civil Engineers, pp 1305-1311.

Evans, O. F. 1940. "The Low and Ball of the Eastern Shore of Lake Michigan," Journal of Geology, Vol 48, No. 5, pp 476-511.

Exon, N. F. 1975. "An Extensive Offshore Sand Bar Field in the Western Baltic Sea," Marine Geology, Vol 18, pp 197-212.

Fairchild, J. C. 1973. "Longshore Transport of Suspended Sand," Proceedings of the 13th Coastal Engineering Conference, American Society of Civil Engineers, pp 1062-1088.

Fenaish, T. A., Overton, M. F., and Fisher, J. S. 1988. "Dune Erosion and Sediment Profile Due to Wave Uprush," Coastal Engineering Abstracts, American Society of Civil Engineers, pp 283-284.

Felder, W. N. 1978. "Simulation Modeling of Offshore Bars," Department of Environmental Sciences, unpublished Ph.D. thesis, University of Virginia, Charlottesville, VA.

Felder, W. N., and Fisher, J. S. 1980. "Simulation Model Analysis of Seasonal Beach Cycles," Coastal Engineering, Vol 3, pp 269-282.

Fox, W. T., and Davis, R. A. 1973. "Simulation Model for Storm Cycles and Beach Erosion on Lake Michigan," Geological Society of America Bulletin, Vol 84, pp 1769-1790.

Galvin, C. J. 1969. "Breaker Travel and Choice of Design Wave Height," Journal of Waterways and Harbors Division, American Society of Civil Engineers, Vol 95, No. 2, pp 175-200.

_____. 1972. "Wave Breaking in Shallow Water," In: Waves on Beaches and Resulting Sediment Transport, ed. R. E. Meyer, Academic Press, pp 413-456.

Gourlay, M. R. 1968. "Beach and Dune Erosion Tests I," Report No. M 935/M 936, Delft Hydraulics Laboratory, Delft, The Netherlands.

_____. 1981. "Beaches: Profiles, Processes and Permeability," Proceedings of the 17th Coastal Engineering Conference, American Society of Civil Engineers, pp 1320-1339.

_____. 1985. "Beaches: States, Sediments and Set-Up," Preprints of the Australasian Conference on Coastal and Ocean Engineering, Vol 1, pp 347-356.

Greenwood, B., and Davidson-Arnott, R. G. D. 1972. "Textural Variation in Sub-Environments of the Shallow-Water Wave Zone, Kouchibouguac Bay, New Brunswick, Canadian Journal of Earth Sciences, Vol 9, No. 6, pp 679-687.

_____. 1975. "Marine Bars and Nearshore Sedimentary Processes, Kouchibouguac Bay, New Brunswick," In: Nearshore Sediment Dynamics and Sedimentation, An Interdisciplinary Review, John Wiley and Sons, New York, pp 123-150.

_____. 1979. "Sedimentation and Equilibrium in Wave-Formed Bars: A Review and Case Study," Canadian Journal of Earth Sciences, Vol 16, No. 2, pp 312-332.

Greenwood, B., and Mittler, P. R. 1979. "Structural Indices of Sediment Transport in a Straight, Wave-Formed, Nearshore Bar," Marine Geology, Vol 32, pp 191-203.

_____. 1984. "Sediment Flux and Equilibrium Slopes in a Barred Nearshore," Marine Geology, Vol 60, pp 79-98.

Guza, R. T., and Bowen, A. J. 1977. "Resonant Interaction for Waves Breaking on a Beach," Proceedings of the 15th Coastal Engineering Conference, American Society of Civil Engineers, pp 560-579.

Guza, R. T., and Thornton, E. B. 1982. "Swash Oscillations on a Natural Beach," Journal of Geophysical Research, Vol 87, No. C1, pp 483-491.

Hallermeier, R. J. 1979. "Uses for a Calculated Limit Depth to Beach Erosion," Proceedings of the 16th Coastal Engineering Conference, American Society of Civil Engineers, pp 1493-1512.

Hallermeier, R. J. 1981. "Terminal Settling Velocity of Commonly Occurring Sand Grains," Sedimentology, Vol 28.

_____. 1982. "Oscillatory Bedload Transport: Data Review and Simple Formulation," Continental Shelf Research, Vol 1, pp 159-190.

_____. 1984. "Wave Cuts in Sand Slopes Applied to Coastal Models," Journal of Waterway, Port, Coastal and Ocean Engineering, Vol 110, No. 1, pp 34-49.

_____. 1987. "Applying Large Replicas of Shore Erosion by Storms," Proceedings of Coastal Sediments '87, American Society of Civil Engineers, pp 1415-1429.

Hands, E. B. 1976. "Observations of Barred Coastal Profiles under the Influence of Rising Water Levels, Eastern Lake Michigan, 1967-71," Technical Report 76-1, Coastal Engineering Research Center, US Army Engineer Waterways Experiment Station, Vicksburg, MS.

Hartnack, W. 1924. "Über Sandriffe," Jahrbuch der Geografischen Gesellschaft zu Greifswald, Band XL/XLII, pp 47-70.

Hashimoto, H., and Uda, T. 1980. "An Application of an Empirical Prediction Model of Beach Profile Change to the Ogawara Coast," Coastal Engineering in Japan, Vol 23, pp 191-204.

Hattori, M. 1982. "Field Study on Onshore-Offshore Sediment Transport," Proceedings of the 18th Coastal Engineering Conference, American Society of Civil Engineers, pp 923-940.

Hattori, M., and Kawamata, R. 1979. "Restoration of Sandy Beaches Fronting Seawalls," Proceedings of Coastal Structures '79, American Society of Civil Engineers, pp 388-404.

_____. 1981. "Onshore-Offshore Transport and Beach Profile Change," Proceedings of the 17th Coastal Engineering Conference, American Society of Civil Engineers, pp 1175-1193.

Hayden, B., Felder, W., Fisher, J., Resio, D., Vincent, L., and Dolan, R. 1975. "Systematic Variations in Inshore Bathymetry," Department of Environmental Sciences, Technical Report No. 10, University of Virginia, Charlottesville, VA.

Hayes, M. O., and Boothroyd, J. C. 1969. "Storms as Modifying Agents in the Coastal Environment," Coastal Environments, Northeast Massachusetts and New Hampshire, Eastern Section, Society of Economic Paleontologists and Mineralogists, Field Guide. Reprinted in Davis, R. A. ed., 1987, Beach and Nearshore Sediments and Processes, SEPM Reprint Series Number 12, SEPM, Tulsa, OK, pp 25-39.

Holman, R. A. 1986. "Extreme Value Statistics for Wave Run-Up on a Natural Beach," Coastal Engineering, Vol 9, pp 527-544.

Holman, R. A., and Bowen, A. J. 1982. "Bars, Bumps, and Holes: Models for the Generation of Complex Beach Topography," Journal of Geophysical Research, Vol 87, pp 457-468.

Holman, R. A., and Sallenger, A. H. 1985. "Set-up and Swash on a Natural Beach," Journal of Geophysical Research, Vol 81, pp 6441-6449.

Horikawa, K., and Kuo, C. 1967. "A Study on Wave Transformation Inside the Surf Zone," Proceedings of the 10th Coastal Engineering Conference, American Society of Civil Engineers, pp 217-233.

Howd, P. A., and Birkemeier, W. A. 1987. "Beach and Nearshore Survey Data: 1981-1984 CERC Field Research Facility," Technical Report CERC-87-9, Coastal Engineering Research Center, US Army Engineer Waterways Experiment Station, Vicksburg, MS.

Hughes, S. A. 1983. "Movable-Bed Modeling Law for Coastal Dune Erosion," Journal of Waterway, Port, Coastal and Ocean Engineering, American Society of Civil Engineers, Vol 109, No. 2, pp 164-179.

_____. 1984. "Movable-Bed Modeling Law for Coastal Dune Erosion," Journal of Waterway, Port, Coastal and Ocean Engineering, Closure, Vol 110, No. 4, pp 504-507.

Hughes, S. A., and Chiu, T. Y. 1981. "Beach and Dune Erosion During Severe Storms," Report UFL/COEL-TR/043, Coastal and Oceanographic Engineering Department, University of Florida, Gainesville, FL.

Hughes, M. G., and Cowell, P. J. 1987. "Adjustment of Reflective Beaches to Waves," Journal of Coastal Research, Vol 3, No. 2, pp 153-167.

Hunt, I. A. 1959. "Design of Seawalls and Breakwaters," Journal of Waterways and Harbors Division, Vol 85, pp 123-152.

Hunter, R. E., Clifton, H. E., and Phillips, R. L. 1979. "Depositional Processes, Sedimentary Structures, and Predicted Vertical Sequences in Barred Nearshore Systems, Southern Oregon Coast," Journal of Sedimentary Petrology, Vol 49, No. 3, pp 711-726.

Inman, D. L. 1957. "Wave Generated Ripples in Nearshore Sand," Technical Memorandum No. 100, Beach Erosion Board, Coastal Engineering Research Center, US Army Engineer Waterways Experiment Station, Vicksburg, MS.

Inman, D. L., and Bagnold, R. A. 1963. "Littoral Processes," In: The Sea, Vol 3, ed. M. N. Hill, Interscience, New York, pp 529-553.

Ippen, A. I., and Eagleson, P. S. 1955. "A Study of Sediment Sorting by Waves Shoaling on a Plane Beach," Technical Memorandum No. 63, Beach Erosion Board, US Army Engineer Waterways Experiment Station, Vicksburg, MS.

Iwagaki, Y., and Noda, H. 1963. "Laboratory Studies of Scale Effects in Two-Dimensional Beach Processes," Proceedings of the 8th Coastal Engineering Conference, American Society of Civil Engineers, pp 194-210.

Jaffe, B. E., Sternberg, R. W., and Sallenger, A. H. 1985. "The Role of Suspended Sediment in Shore-Normal Beach Profile Changes," Proceedings of the 19th Coastal Engineering Conference, American Society of Civil Engineers, pp 1983-1996.

Jansen, P. C. M. 1986. "Laboratory Observations of the Kinematics in the Aerated Region of Breaking Waves," Coastal Engineering, Vol 9, pp 453-477.

Johnson, J. W. 1949. "Scale Effects in Hydraulic Models Involving Wave Motion," Transactions of the American Geophysical Union, Vol 30, No. 4, pp 517-525.

Kajima, R., Shimizu, T., Maruyama, K., and Saito, S. 1983a. "Experiments of Beach Profile Change with a Large Wave Flume," Proceedings of the 18th Coastal Engineering Conference, American Society of Civil Engineers, pp 1385-1404.

Kajima, R., Saito, S., Shimizu, T., Maruyama, K., Hasegawa, H., and Sakakiyama, T. 1983b. "Sand Transport Experiments Performed by Using a Large Water Wave Tank," Data Report No. 4-1, Central Research Institute for Electric Power Industry, Civil Engineering Division. (in Japanese)

Kamphuis, J. W., and Bridgeman, S. G. 1975. "Placing Artificial Beach Nourishment," Proceedings of Coastal Engineering in the Oceans III, American Society of Civil Engineers, pp 197-216.

Kana, T. W. 1977. "Suspended Sediment Transport at Price Inlet, S. C.," Proceedings of Coastal Sediments '77, American Society of Civil Engineers, pp 366-382.

Kemp, P. H. 1961. "The Relationship Between Wave Action and Beach Profile Characteristics," Proceedings of the 7th Conference on Coastal Engineering, American Society of Civil Engineers, pp 262-277.

Keulegan, G. H. 1945. "Depths of Offshore Bars," Engineering Notes No. 8, Beach Erosion Board, Coastal Engineering Research Center, US Army Engineer Waterways Experiment Station, Vicksburg, MS.

_____. 1948. "An Experimental Study of Submarine Sand Bars," Technical Report No. 3, Beach Erosion Board, Coastal Engineering Research Center, US Army Engineer Waterways Experiment Station, Vicksburg, MS.

King, C. A. M., and Williams, W. W. 1949. "The Formation and Movement of Sand Bars by Wave Action," Geological Journal, Vol 113, pp 70-85.

Kobayashi, N. 1987. "Analytical Solutions for Dune Erosion by Storms," Journal of Waterway, Port, Coastal and Ocean Engineering, Vol 113, No. 4, pp 401-418.

Komar, P. D., and Gaughan, M. K. 1973. "Airy Wave Theory and Breaker Height Prediction," Proceedings of the 13th Coastal Engineering Conference, American Society of Civil Engineers, pp 405-418.

Kraus, N. C. 1987. "The Effects of Seawalls on the Beach: A Literature Review," Proceedings of Coastal Sediments '87, American Society of Civil Engineers, pp 945-960.

_____. 1988. "The Effects of Seawalls on the Beach: An Extended Review," In: The Effects of Seawalls on the Beach, eds. N. C. Kraus and O. H. Pilkey, Journal of Coastal Research, pp 1-28.

Kraus, N. C., and Dean, J. L. 1987. "Longshore Sediment Transport Rate Distributions Measured by Trap," Proceedings of Coastal Sediments '87, American Society of Civil Engineers, pp 881-896.

Kraus, N. C., Gingerich, K. J., and Rosati, J. D. 1989. "Toward an Improved Empirical Formula for Longshore Sand Transport," Proceedings of the 21st Coastal Engineering Conference, American Society of Civil Engineers, pp 1182-1196.

Kraus, N. C., and Horikawa, K. in press. "Nearshore Sediment Transport," In: The Sea, Vol 9, eds. B. LeMehaute and D. Hanes, John Wiley and Sons, New York, NY.

Kraus, N. C., and Larson, M. 1988a. "Beach Profile Change Measured in the Tank for Large Waves, 1956-1957 and 1962," Technical Report CERC-88-6, Coastal Engineering Research Center, US Army Engineer Waterways Experiment Station, Vicksburg, MS.

_____. 1988b. "Prediction of Initial Profile Adjustment on Nourished Beaches to Wave Action," Proceedings of Beach Technology '88, Florida Shore and Beach Preservation Association, pp 125-137.

Kraus, N. C., Scheffner, N. W., Hanson, H., Chou, L. W., Cialone, M. A., Smith, J. M., and Hardy, T. A. 1988. "Coastal Processes at Sea Bright to Ocean Township, New Jersey, Volume I: Main Text and Appendix A," Miscellaneous Paper CERC-88-12, Coastal Engineering Research Center, US Army Engineer Waterways Experiment Station, Vicksburg, MS.

Kriebel, D. L. 1982. "Beach and Dune Response to Hurricanes," unpublished M.S. Thesis, University of Delaware, Newark, DE.

_____. 1986. "Verification Study of a Dune Erosion Model," Shore and Beach, Vol 54, No. 3, pp 13-21.

_____. 1987. "Beach Recovery Following Hurricane Elena," Proceedings of Coastal Sediments '87, American Society of Civil Engineers, pp 990-1005.

Kriebel, D. L., and Dean, R. G. 1984. "Beach and Dune Response to Severe Storms," Proceedings of the 19th Coastal Engineering Conference, American Society of Civil Engineers, pp 1584-1599.

_____. 1985a. "Numerical Simulation of Time-Dependent Beach and Dune Erosion," Coastal Engineering, Vol 9, pp 221-245.

_____. 1985b. "Estimates of Erosion and Mitigation Requirements under Various Scenarios of Sea Level Rise and Storm Frequency for Ocean City, Maryland," Preliminary Report, Coastal and Oceanographic Department, University of Florida, Gainesville, FL.

Kriebel, D. L., Dally, W. R., and Dean, R. G. 1986. "Beach Profile Response Following Severe Erosion Events," Report UFL/COEL-86/016, Coastal and Oceanographic Department, University of Florida, Gainesville, FL.

_____. 1987. "Undistorted Froude Model for Surf Zone Sediment Transport," Proceedings of the 20th Coastal Engineering Conference, American Society of Civil Engineers, pp 1296-1310.

Larson, M., and Kraus, N. C. In press. "Prediction of Beach Fill Response to Varying Waves and Water Level," Proceedings of Coastal Zone '89, American Society of Civil Engineers.

Larson, M., Kraus, N. C., and Byrnes, M. R. In prep. "SBEACH: Numerical Model for Simulating Storm-Induced Beach Change," Report 2, Numerical Formulation and Model Test, Technical Report, Coastal Engineering Research Center, US Army Engineer Waterways Experiment Station, Vicksburg, MS.

Lau, J., and Travis, B. 1973. "Slowly Varying Stokes Waves and Submarine Longshore Bars," Journal of Geophysical Research, Vol 78, pp 4489-4497.

Lehmann, F. W. P. 1884. "Das Küstengebiet Hinterpommerns," Zeitschrift das Gesellschaft für Erdkunde zu Berlin, Band XIX.

Longuet-Higgins, M. S. 1952. "On the Statistical Distribution of the Heights of Sea Waves," Journal of Marine Research, Vol 11, pp 245-266.

Longuet-Higgins, M. S., and Stewart, R. W. 1963. "A Note on Wave Set-up," Journal of Marine Research, Vol 21, pp 4-10.

Madsen, O. S., and Grant, W. D. 1977. "Quantitative Description of Sediment Transport by Waves," Proceedings of the 15th Coastal Engineering Conference, American Society of Civil Engineers, pp 1093-1112.

Mason, C., Sallenger, A. H., Holman, R. A., and Birkemeier, W. A. 1985. "DUCK82 - a Coastal Storm Processes Experiment," Proceedings of the 19th Coastal Engineering Conference, American Society of Civil Engineers, pp 1913-1927.

McKee, E. D., and Sterrett, T. S. 1961. "Laboratory Experiments on Form and Structure of Longshore Bars and Beaches," In: Geometry of Sandstone Bodies, eds. Peterson, J. A., and Osmond, J. C., American Association of Petroleum Geologists, pp 13-28.

Mei, C. C. 1985. "Resonant Reflection of Surface Water Waves by Periodic Sandbars," Journal of Fluid Mechanics, Vol 152, pp 315-335.

Meyer, R. D. 1936. "A Model Study of Wave Action on Beaches," unpublished M.S. Thesis, Department of Civil Engineering, University of California, Berkeley, CA.

Miller, R. L. 1976. "Role of Vortices in Surf Zone Prediction: Sedimentation and Wave Forces," In: Beach and Nearshore Sedimentation, eds. R. A. Davis and R. I. Ethington, Society of Economic Paleontologists and Mineralogists, Special Publication No. 24, pp 92-114.

Mimura, N., Otsuka, Y., and Watanabe, A. 1987. "Laboratory Study on Two-Dimensional Beach Transformation Due to Irregular Waves," Proceedings of the 20th Coastal Engineering Conference, American Society of Civil Engineers, pp 1393-1406.

Mizuguchi, M. 1981. "An Heuristic Model of Wave Height Distribution in Surf Zone," Proceedings of the 17th Coastal Engineering Conference, American Society of Civil Engineers, pp 278-289.

Moore, B. D., 1982. "Beach Profile Evolution in Response to Changes in Water Level and Wave Height," unpublished M.S. thesis, University of Delaware, Newark, DE.

Möller, J. P., and Swart D. H. 1988. "Extreme Erosion Event on an Artificially-Nourished Beach," Coastal Engineering Abstracts, American Society of Civil Engineers, pp 244-245.

Mothersill, J. S. 1970. "Relationship of Grain-Size Modes to Nearshore Sedimentary Environments, Lake Superior, Ontario," Canadian Journal of Earth Sciences, Vol 7, pp 522-527.

Nairn, R. B. 1988. "Prediction of Wave Height and Mean Return Flow in Cross Shore Sediment Transport Modelling," Symposium on Mathematical Modelling of Sediment Transport in the Coastal Zone, International Association of Hydraulic Research, Copenhagen, Denmark, pp 193-202.

Nayak, I. V. 1970. "Equilibrium Profiles of Model Beaches," Hydraulic Engineering Laboratory, Technical Report HEL-2-25, University of California, Berkeley, CA.

_____. 1971. "Equilibrium Profiles of Model Beaches," Proceedings of the 12th Coastal Engineering Conference, American Society of Civil Engineers, pp 1321-1340.

Nielsen, P. 1979. "Some Basic Concepts of Wave Sediment Transport," Paper No. 20, Technical University of Denmark, Lyngby, Denmark.

Nilsson, H. D. 1979. "Multiple Longshore Sand Bars: Environments of Deposition and a Model for their Generation and Maintenance," unpublished Ph.D. thesis, University of Massachusetts, Amherst, MA.

Nishimura, H., and Sunamura, T. 1987. "Numerical Simulation of Beach Profile Changes," Proceedings of the 20th Coastal Engineering Conference, American Society of Civil Engineers, pp 1444-1455.

Ostle, B., and Mensing, R. W. 1975. Statistics in Research, The Iowa State University Press, Ames, IA.

Otto, T. 1911 "Der Darss und Zingst," Jahrbuch der Geografischen Gesellschaft zu Greifswald, Band XIII, pp 393-403.

Owens, E. H. 1977. "Temporal Variations in Beach and Nearshore Dynamics," Journal of Sedimentary Petrology, Vol 47, No 1, pp 168-190.

Overton, M. F., and Fisher, J. S. 1988. "Simulation Modeling of Dune Erosion," Coastal Engineering Abstracts, American Society of Civil Engineers, pp 287-288.

Raynor, A. C., and Simmons, G. W. 1964. "Summary of Capabilities," Miscellaneous Paper No. 3-64, Coastal Engineering Research Center, US Army Engineer Waterways Experiment Station, Vicksburg, MS.

Rector, R. L. 1954. "Laboratory Study of Equilibrium Profiles of Beaches," Technical Memorandum No. 41, Beach Erosion Board, Coastal Engineering Research Center, US Army Engineer Waterways Experiment Station, Vicksburg, MS.

Rushu, R., and Liang, W. 1986. "Investigation on Two-Dimensional Transformation of Sandy Beach under Wave Action," Proceedings of the 3rd International Symposium on River Sedimentation, The University of Mississippi, pp 378-387.

Sallenger, A. S., Holman, R. A., and Birkemeier, W. A. 1985. "Storm-Induced Response of a Nearshore-Bar System," Marine Geology, 64, pp 237-257.

Sasaki, T. 1983. "Three-Dimensional Topographic Changes on the Foreshore Zone of Sandy Beaches," Science Report, Institute of Geoscience, University of Tsukuba, Section A, Vol 4, pp 69-95.

Sato, S., and Horikawa, K. 1987. "Laboratory Study on Sand Transport over Ripples Due to Asymmetric Oscillatory Flows," Proceedings of the 17th Coastal Engineering Conference, American Society of Civil Engineers, pp 1481-1495.

Savage, R. P. 1959. "Notes on the Formation of Beach Ridges," Annual Bulletin, Beach Erosion Board, Coastal Engineering Research Center, US Army Engineer Waterways Experiment Station, Vicksburg, MS.

Saville, T. 1957. "Scale Effects in Two Dimensional Beach Studies," Transactions from the 7th General Meeting of the International Association of Hydraulic Research, Vol 1, pp A3-1-A3-10.

Sawaragi, T., and Deguchi, I. 1981. "On-Offshore Sediment Transport Rate in the Surf Zone," Proceedings of the 17th Coastal Engineering Conference, American Society of Civil Engineers, pp 1194-1214.

Sayao, O. S. F. J. 1984. "Movable-Bed Modeling Law for Coastal Dune Erosion," Journal of Waterway, Port, Coastal and Ocean Engineering, Discussion, Vol 110, No. 4, pp 493-495.

Saylor, J. H., and Hands, E. B. 1971. "Properties of Longshore Bars in the Great Lakes," Proceedings of the 12th Coastal Engineering Conference, American Society of Civil Engineers, pp 839-853.

Scott, T. 1954. "Sand Movement by Waves," Technical Memorandum No. 48, Beach Erosion Board, Coastal Engineering Research Center, US Army Engineer Waterways Experiment Station, Vicksburg, MS.

Seelig, W. N. 1983. "Understanding Beach Erosion and Accretion," Journal of Waterway, Port, Coastal and Ocean Engineering, American Society of Civil Engineers, Vol 49, No. 4, pp 490-494.

Seymour, R. J. 1985. "Results of Cross-shore Transport Experiments," Journal of Waterway, Port, Coastal, and Ocean Engineering, Vol 112, No. 1, pp 168-173.

_____. 1986. "Results of Cross-Shore Transport Experiments," Journal of Waterway, Port, Coastal and Ocean Engineering, Vol 112, No. 1, pp 168-173.

_____. 1987. "An Assessment of NSTS," Proceedings of Coastal Sediments '87, American Society of Civil Engineers, pp 642-651.

Seymour, R. J., and Castel D. 1988. "Validation of Cross-Shore Transport Formulations," Coastal Engineering Abstracts, American Society of Civil Engineers, pp 273-274.

Seymour, R. J., and King, D. B. 1982. "Field Comparisons of Cross-shore Transport Models," Journal of Waterway, Port, Coastal, and Ocean Engineering, Vol 108, No. WW2, pp 163-179.

Shepard, F. P. 1950. "Longshore-Bars and Longshore-Troughs," Technical Memorandum No. 15, Beach Erosion Board, Coastal Engineering Research Center, US Army Engineer Waterways Experiment Station, Vicksburg, MS.

Shibayama, T. 1984. "Sediment Transport Mechanism and Two-Dimensional Beach Transformation Due to Waves," unpublished Ph.D. thesis, University of Tokyo, Tokyo, Japan.

Shibayama, T., and Horikawa, K. 1980a. "Bed Load Measurement and Prediction of Two-Dimensional Beach Transformation Due to Waves," Coastal Engineering in Japan, Vol 23, pp 179-190.

_____. 1980b. "Laboratory Study on Sediment Transport Mechanism Due to Wave Action," Proceedings of the Japanese Society of Civil Engineers, No. 296, April, pp 131-141.

Shimizu, T., Saito, S., Maruyama, K., Hasegawa, H., and Kajima, R. 1985. "Modeling of Onshore-Offshore Sand Transport Rate Distribution Based on the Large Wave Flume Experiments," Civil Engineering Laboratory Report No. 384028, Abiko City, Japan. (in Japanese)

Shore Protection Manual. 1984. 4th ed., 2 vols, US Army Engineer Waterways Experiment Station, Coastal Engineering Research Center, US Government Printing Office, Washington, DC.

Short, A. D. 1975a. "Offshore Bars Along the Alaskan Arctic Coast," Journal of Geology, Vol 83, pp 209-221.

_____. 1975b. "Multiple Offshore Bars and Standing Waves," Journal of Geophysical Research, Vol 80, No. 27, pp 3838-3840.

_____. 1979. "Three Dimensional Beach-Stage Model," Journal of Geology, Vol 87, pp 553-571.

Shuto, N. 1974. "Nonlinear Long Waves in a Channel of Variable Section," Coastal Engineering in Japan, Vol 17, pp 1-12.

Singamsetti, S. R., and Wind, H. G. 1980. "Breaking Waves: Characteristics of Shoaling and Breaking Periodic Waves Normally Incident to Plane Beaches of Constant Slope," Delft Hydraulics Laboratory, Report M 1371, Delft, The Netherlands.

Skjelbreia, J. E. 1987. "Observations of Breaking Waves on Sloping Bottoms by Use of Laser Doppler Velocimetry," Report No. KH-R-48, Division of Engineering and Applied Science, California Institute of Technology, Pasadena, CA.

Smith, J., and Kraus, N. C. 1988. "An Analytical Model of Wave-Induced Longshore Current Based on Power Law Wave Height Decay," Miscellaneous Paper CERC-88-3, Coastal Engineering Research Center, US Army Engineer Waterways Experiment Station, Vicksburg, MS.

Sonu, C. J. 1969. "Collective Movement of Sediment in Littoral Environment," Proceedings of the 11th Coastal Engineering Conference, American Society of Civil Engineers, pp 373-400.

_____. 1970. "Beach Changes by Extraordinary Waves Caused by Hurricane Camille," Coastal Studies Institute, Technical Report 77, Louisiana State University, Baton Rouge, LA, pp 33-45.

Stive, M. J. F. 1987. "A Model for Cross-Shore Sediment Transport," Proceedings of the 20th Coastal Engineering Conference, American Society of Civil Engineers, pp 1550-1564.

Stive, M. J. F., and Battjes, J. A. 1985. "A Model for Offshore Sediment Transport," Proceedings of the 19th Coastal Engineering Conference, American Society of Civil Engineers, pp 1420-1436.

Sunamura, T. 1975. "A Study of Beach Ridge Formation in Laboratory," Geographical Review of Japan, 48-11, pp 761-767.

_____. 1980. "Parameters for Delimiting Erosion and Accretion of Natural Beaches," Annual Report of the Institute of Geoscience, University of Tsukuba, No. 6, pp 51-54.

_____. 1981a. "Bedforms Generated in a Laboratory Wave Tank," Science Reports of the Institute of Geoscience, University of Tsukuba, Section A, Vol 2, pp 31-43.

_____. 1981b. "A Laboratory Study of Offshore Transport of Sediment and a Model for Eroding Beaches," Proceedings of the 17th Coastal Engineering Conference, American Society of Civil Engineers, pp 1051-1070.

_____. 1983. "A Predictive Model for Shoreline Changes on Natural Beaches Caused by Storm and Post-Storm Waves," Transactions of the Japanese Geomorphological Union, Vol 4, pp 1-10.

_____. 1984a. "On-Offshore Sediment Transport Rate in the Swash Zone of Laboratory Beaches," Coastal Engineering in Japan, Vol 27, pp 205-212.

_____. 1984b. "Quantitative Predictions of Beach-Face Slopes," Geological Society of America Bulletin, Vol 95, pp 242-245.

_____. In press. "Sandy Beach Geomorphology as Elucidated by Laboratory Modeling," In: Coastal Modeling: Techniques and Application, Elsevier, Amsterdam, The Netherlands.

Sunamura, T., and Horikawa, K. 1975. "Two-Dimensional Beach Transformation Due to Waves," Proceedings of the 14th Coastal Engineering Conference, American Society of Civil Engineers, pp 920-938.

Sunamura, T. and Maruyama, K. 1987. "Wave-Induced Geomorphic Response of Eroding Beaches - with Special Reference to Seaward Migrating Bars," Proceedings of Coastal Sediments '87, American Society of Civil Engineers, pp 884-900.

Sunamura, T., and Takeda, I. 1984. "Landward Migration of Inner Bars," Marine Geology, 60, pp 63-78.

Svendsen, I. A. 1984. "Wave Heights and Set-Up in a Surf Zone," Coastal Engineering, Vol 8, pp 303-329.

_____. 1987. "Analysis of Surf Zone Turbulence," Journal of Geophysical Research, Vol 92, No. C5, pp 5115-5124.

Svendsen, I. A., Madsen, P. A., and Buhr Hansen, J. 1979. "Wave Characteristics in the Surf Zone," Proceedings of the 14th Coastal Engineering Conference, American Society of Civil Engineers, pp 520-539.

Swart, D. H. 1975. "A Schematization of Onshore-Offshore Transport," Proceedings of the 14th Coastal Engineering Conference, American Society of Civil Engineers, pp 884-900.

_____. 1977. "Predictive Equations Regarding Coastal Transport," Proceedings of the 15th Coastal Engineering Conference, American Society of Civil Engineers, pp 1113-1132.

Takeda, I. 1984. "Beach Changes by Waves," Science Report, Institute of Geoscience, University of Tsukuba, Japan, Sect A, Vol 5, pp 29-63.

Takeda, I., and Sunamura, T. 1987. "Beach Changes by Storm waves," Proceedings of the 20th Coastal Engineering Conference, American Society of Civil Engineers, pp 1612-1622.

Thomas, K. V., and Baba, M. 1986. "Berm Development on a Monsoon-Influenced Microtidal Beach," Sedimentology, Vol 33, pp 537-546.

Uliczka, K., and Dette, H. H. 1987. "About the Effect of Monochromatic and Irregular Waves on Beach and Dune Profiles," Proceedings of Seminar on Hydrologie und Küsteningenieurwesen, Hannover, Germany.

University of California. 1982. "Surface Water Temperatures at Shore Stations, United States West Coast," Scripps Institution of Oceanography, La Jolla, CA.

van de Graaff, J. 1983. "Probabilistic Design of Dunes," Proceedings of Coastal Structures '83, American Society of Civil Engineers, pp 820-831.

van Hijum, E. 1975. "Equilibrium Profiles of Coarse Material Under Wave Attack," Proceedings of the 14th Coastal Engineering Conference, American Society of Civil Engineers, pp 939-957.

_____. 1977. "Equilibrium Profiles and Longshore Transport of Coarse Material Under Oblique Wave Attack," Proceedings of the 15th Coastal Engineering Conference, American Society of Civil Engineers, pp 1258-1276.

van Hijum, E., and Pilarczyk, K. W. 1982. "Gravel Beaches - Equilibrium Profile and Longshore Transport of Coarse Material under Regular and Irregular Wave Attack," Delft Hydraulics Laboratory, Publication No. 274, Delft, The Netherlands.

Vellinga, P. 1982. "Beach and Dune Erosion During Storm Surges," Publication No. 276, Delft Hydraulics Laboratory, Delft, The Netherlands.

_____. 1983. "Predictive Computational Model for Beach and Dune Erosion During Storm Surges," Proceedings of Coastal Structures '83, American Society of Civil Engineers, pp 806-819.

_____. 1984. "Movable-Bed Modeling Law for Coastal Dune Erosion," Journal of Waterway, Port, Coastal and Ocean Engineering, Discussion, Vol 110, No. 4, pp 495-504.

_____. 1986. "Beach and Dune Erosion During Storm Surges," Delft Hydraulics Communication No. 372, Delft Hydraulics Laboratory, Delft, The Netherlands.

Verhagen, H. J. 1985. "Guideline for the Judgement of Safety of Dunes as Coastal Defense," Ministerie van Verkeer en Waterstaat, Amsterdam, The Netherlands.

Visser, C. 1983. "Design of Dunes as Coastal Protection in the Delta Area of the Netherlands," Proceedings of Coastal Structures '83, American Society of Civil Engineers, pp 792-805.

Wang, H., Dalrymple, R. A., and Shiau, J. C. 1975. "Computer Simulation of Beach Erosion and Profile Modification Due to Waves," Proceedings of the Symposium on Modeling Techniques, American Society of Civil Engineers, pp 1369-1384.

Watanabe, A. 1982. "Numerical Models of Nearshore Currents and Beach Deformation," Coastal Engineering in Japan, Vol 25, pp 147-161.

_____. 1985. "Three-Dimensional Predictive Model of Beach Evolution Around a Structure," Proceedings of International Symposium on Water Wave Research, University of Hannover, Germany, pp 121-142.

Watanabe, A., Riho, Y., and Horikawa, K. 1981. "Beach Profiles and On-Offshore Sediment Transport," Proceedings of the 17th Coastal Engineering Conference, American Society of Civil Engineers, pp 1106-1121.

Waters, C. H. 1939. "Equilibrium Slopes of Sea Beaches," unpublished M.S. thesis, University of California, Berkeley, CA.

Watts, G. M. 1953. "A Study of Sand Movement at South Lake Worth Inlet, Florida," Technical Memorandum No. 42, Beach Erosion Board, Coastal Engineering Research Center, US Army Engineer Waterways Experiment Station, Vicksburg, MS.

_____. 1954. "Laboratory Study of Effect of Varying Wave Periods on Beach Profiles," Technical Memorandum No. 53, Beach Erosion Board, Coastal Engineering Research Center, US Army Engineer Waterways Experiment Station, Vicksburg, MS.

Watts, G. M., and Dearduff, R. F. 1954. "Laboratory Studies of Effect of Tidal Action on Wave-Formed Beach Profiles," Technical Memorandum No. 52, Beach Erosion Board, Coastal Engineering Research Center, US Army Engineer Waterways Experiment Station, Vicksburg, MS.

Weggel, R. J. 1972. "Maximum Breaker Height," Journal of the Waterways, Harbors and Coastal Engineering Division, American Society of Civil Engineers, Vol 98, No. 1, pp 529-547.

Wells, D. R. 1967. "Beach Equilibrium and Second-Order Wave Theory," Journal of Geophysical Research, Vol 72, No. 2, pp 497-504.

Winant, C. D., Inman, D. L., and Nordstrom, C. E. 1975. "Description of Seasonal Beach Changes Using Empirical Eigenfunctions," Journal of Geophysical Research, Vol 80, No. 15, pp 1979-1986.

Wood, W. L., and Weishar, L. L., 1985. "Beach Response to Long Period Lake-Level Variation," Proceedings of the 19th Coastal Engineering Conference, American Society of Civil Engineers, pp 1571-1583.

Wright, L. D., Chappel, J., Thom, B. G., Bradshaw, M. P., and Cowell, P. 1979. "Morphodynamics of Reflective and Dissipative Beach and Inshore Systems: Southeastern Australia," Marine Geology, Vol 32, pp 105-140.

Wright, L. D., Nielsen, P., Shi, N. C., and List, J. H. 1986. "Morphodynamics of a Bar-Trough Surf Zone," Marine Geology, Vol 70, pp 251-285.

Wright, L. D., and Short, A. D. 1984. "Morphodynamic Variability of Surf Zones and Beaches: a Synthesis," Marine Geology, Vol 56, pp 93-118.

Wright, L. D., Short, A. D., and Green, M. O. 1985. "Short-Term Change in the Morphodynamic State of Beaches and Surf Zones: An Empirical Predictive Model," Marine Geology, Vol 62, pp 339-364.

Wright, L. D., Short, A. D., Boon, J. D., Hayden, B., Kimball, S., and List, J. H. 1987. "Morphodynamic Responses of an Energetic Beach to Temporal Variations in Wave Steepness, Tide Range, and Incident Wave Groupiness," Marine Geology, Vol 74, pp 1-20.

Zenkovich, V. P. 1967. "Submarine Sand Bars and Related Formations," In: Processes of Coastal Development, ed. J. A. Steers, Oliver and Boyd Ltd, New York, NY, pp 219-236.

APPENDIX A: CORRELATION AND REGRESSION ANALYSIS

1. Correlation and regression analysis deals with the investigation and inference of dependencies between variables as derived solely from statistical techniques. Even if a high degree of association between variables is found by this method, the resultant relation does not necessarily have, and usually will not have, a clear physical basis. However, these statistical methods can provide an indication of possible relationships to be accepted or rejected after physical considerations. Information in this appendix may be obtained from any textbook on regression analysis, e.g., Ostle and Mensing (1975)*, and is included here to facilitate understanding of the statistical techniques and terminology extensively employed in the data analyses presented in the main text of this report.

Correlation Coefficient

2. The correlation coefficient r expresses the degree of linearity between variables. For a set of discrete data, r is defined as:

$$r = \frac{s_{xy}}{s_x s_y} \tag{A1}$$

where

$$s_{xy} = \frac{1}{n-1} \sum_{i=1}^{n} (x_i - \bar{x})(y_i - \bar{y}) \tag{A2}$$

$$s_x^2 = \frac{1}{n-1} \sum_{i=1}^{n} (x_i - \bar{x})^2 \tag{A3}$$

---

* References cited in the Appendix can be found in the Reference list at the end of the main text.

$$s_y^2 = \frac{1}{n-1} \sum_{i=1}^{n} (y_i - \bar{y})^2 \qquad (A4)$$

in which

s_{xy} = covariance between x and y

n = number of values in the data set

x_i, y_i = corresponding values from the data sets to be correlated

$\bar{x}$, $\bar{y}$ = mean values for the respective data sets

s_x^2 = variance of x

s_y^2 = variance of y

3. Values of the correlation coefficient are in the domain $-1 \leq r \leq 1$. A value of $r = 1$ implies a perfect linear relationship between the studied variables, $r = -1$ indicates an inverse linear dependence, and $r = 0$ means no linear dependence.

Coefficient of Determination

4. In regression analysis, the parameters of a chosen functional relationship are estimated in an optimal way to provide the best fit with the measured data according to a predetermined criterion. The criterion typically used to optimize the parameter values is a minimization of the sum of the squares of the difference between predicted and measured values of the dependent variable. For example, if y is considered a function of the m variables $x_1, x_2, \ldots, x_m$, the parameters in the function $y(x_1, x_2, \ldots, x_m)$ should be estimated to minimize the function R, defined as:

$$R = \sum_{i=1}^{n} (y_i^p - y_i^m)^2 \qquad (A5)$$

where

y_i^p = value predicted with a regression equation

y_i^m = measured value

5. To find the optimal estimate, the partial derivative of R is taken with respect to each parameter contained in the regression equation. The equations thus obtained are set equal to zero to obtain an extremum (minimum) for R. For the case of a linear regression equation involving m independent variables, a linear set of m equations is obtained and may be solved directly by matrix theory. If the system of equations has a nonlinear form, the solution can be obtained numerically, usually by iteration.

6. A nonlinear regression equation can sometimes be reduced to linear form by an appropriate transformation of variables. For example, exponential or power equations can be transformed to linear form by taking the logarithm. However, this manipulation involves a modification of the original problem since the minimization is carried out with respect to the logarithmic values and not the original untransformed values. The difference is usually small but can be significant if the measured values vary over a large range.

7. A quantity expressing the ratio between the explained variation by the regression model and the total variation in the data, denoted as the coefficient of determination r^2, is defined as

$$r^2 = \frac{\sum_{i=1}^{n} (y_i^p - \bar{y})^2}{\sum_{i=1}^{n} (y_i^m - \bar{y})^2} \qquad \text{(A6)}$$

The equation for the coefficient of determination may be rewritten in a slightly different form to more easily allow interpretation:

$$r^2 = \frac{\sum_{i=1}^{n} (y_i^m - \bar{y})^2 - \sum_{i=1}^{n} (y_i^p - y_i^m)^2}{\sum_{i=1}^{n} (y_i^m - \bar{y})^2} = 1 - \frac{\sum_{i=1}^{n} (y_i^p - y_i^m)^2}{\sum_{i=1}^{n} (y_i^m - \bar{y})^2} \qquad \text{(A7)}$$

8. The last term on the right side of this equation can be interpreted as expressing the variation in the data not explained by the regression model (Equation A5 normalized with the total variation in the data). Thus, if the regression model fits the data perfectly, the second term will be zero, and $r^2 = 1$. It is also recognized that the coefficient of determination varies between 0 and 1 since the sum of squares of the difference between measured and predicted values is normalized by the total variation.

Use in Present Study

9. In the data analysis conducted in this study, correlation and regression techniques were extensively used to investigate dependencies and establish empirical relationships between variables. A correlation analysis was first carried out irrespective of physical dimensions to identify variables which had marked influence on the quantity being studied. From this information on dependencies, supplemented by physical considerations, regression equations involving pertinent variables were derived, in most cases consisting of dimensionless groups formed by the studied variables.

10. In some cases, nonlinear equations were used to develop functional relationships between variables when it was not possible to transform the equations to a linear form. A special computer solution procedure was developed to obtain the optimal parameter values for these cases. Even if it was possible to transform some regression equations to linear form, results from the original nonlinear equation were used if an appreciable difference in the optimal parameter estimates occurred. Also, to evaluate the performance of the numerical model, coefficients of determination based on the difference between calculated values and measured values were frequently used.

APPENDIX B: NOTATION

A	Shape parameter for equilibrium beach profile, $m^{1/3}$
D	Median grain size of beach sand, m
$\mathcal{D}$	Wave energy dissipation per unit water volume, $Nm/m^3/sec$
$\mathcal{D}_{eq}$	Equilibrium energy dissipation per unit water volume, $Nm/m^3/sec$
E	Wave energy density, Nm/m^2
F	Wave energy flux, Nm/m/sec
F_s	Stable wave energy flux, Nm/m/sec
g	Acceleration due to gravity, m/sec^2
h	Water depth, m
h_c	Depth-to-bar crest, m
h_i^c	Calculated profile depth at grid point i, m
h_i^m	Measured profile depth at grid point i, m
h_t	Depth-to-bar trough, m
H	Wave height, m
$\bar{H}$	Mean wave height, m
H_{mo}	Energy-based wave height, m
H_{rms}	Root mean square wave height, m
H_{so}	Significant wave height, m
i	Integer number
k	Integer number
K	Transport rate coefficient, m^4/N
ℓ_b	Berm length, m
ℓ_B	Bar length, m
ℓ_p	Plunge distance, m
ℓ_R	Runup length, m
ℓ_t	Trough length, m
ℓ_{tc}	Distance between break point and bar trough, m
L	Wavelength, m
n	Exponent determining spatial decay of transport rate in wave reformation zones
N	Number of cells where avalanching occurs
q	Cross-shore sand transport rate, $m^3/m/sec$

q_b	Transport rate at break point, $m^3/m/sec$
q_m	Peak transport rate, $m^3/m/sec$
q_{mo}	Peak transport rate at time t=0, $m^3/m/sec$
q_r	Transport rate at wave reformation point, $m^3/m/sec$
Q_A	Average absolute transport rate, $m^3/m/sec$
r	Correlation coefficient
r^2	Coefficient of determination
R	Sum of squares of difference between measured and calculated beach profile, m^2
S	Specific gravity of sand
S_{xx}	Radiation stress component directed onshore, N/m
t	Time, sec
T	Wave period, sec
U	Ursell number
V	Bar or berm volume, m^3/m
w	Sand fall velocity, m/sec
x	Cross-shore coordinate, m
x_1	Seaward location of no profile change, m
x_m	Location of minimum transport rate in wave reformation zone, m
x_o	Shoreward location of no profile change, m
x_r	Location of wave reformation point, m
x_{CM}	Location of bar mass center, m
z	Depth coordinate
Z_b	Maximum berm height, m
Z_B	Maximum bar height, m
Z_R	Height of active subaerial profile, m
α	Temporal rate coefficient, sec^{-1}
β	Beach slope
β_1	First seaward bar slope
β_2	Second seaward bar slope
β_3	Shoreward bar slope
β_4	Terrace slope
β_5	Step slope
γ	Ratio between wave height and water depth at breaking

Γ	Stable wave height coefficient
Δ	Change in quantity
ϵ	Slope-related transport rate coefficient, m^2/sec
η	Wave setup or setdown, m
κ	Wave decay coefficient
λ	Spatial decay coefficient, m^{-1}
ν	Spatial decay coefficient, m^{-1}
ρ	Density of water, kg/m^3
ϕ_1	Shoreward berm slope
ϕ_2	Seaward berm slope

Subscripts and Superscripts:

b	Breaking condition
eq	Equilibrium condition
i	Specific value of a variable
m	Measured quantity
o	Deepwater condition
p	Predicted quantity
1,2	Specific value of a variable
k	Specific value of a variable